POLITECNICO DI MILANO

School of Civil Engineering

Master of Science in Civil Engineering

Computational Homogenization of Syntactic Foams & Material Response Subjected to Extreme Loads

Supervisor:

Prof. Stefano Mariani

Co-Advisor:

Prof. Marco Di prisco

Master of Science Thesis by:

Bahman Bahmani Ghajar

Matricola: 749454

Table of Contents

Table of Figures

Part-1 – Computational Modeling of Syntactic Foams for Deriving the Homogenized Properties

Abstract

Owing to the important role of Syntactic Foam composite materials in various industrial applications, having applicable information about its mechanical (constitutive) properties are of high level of efficiency for analysis and design purposes. This work aims at deriving the bounds of the overall properties of a specific type of syntactic foam-hollow sphere glass-polymer resin- composite material. Focusing on the overall mechanical parameters of the composite material, such as; the Young modulus and the Poisson's ratio, the investigation is centered on a computational homogenization scheme over a vast range of Representative Volume Elements (RVE) types. Several computational models of RVEs are created using a commercial code finite element analysis code, to investigate the effects of independent material manufacturing parameters, such as; inclusion particles-hollow sphere glass- membrane thickness, volume fraction and size and distribution patterns. The computational modeling procedure is arranged with a hierarchical trend, starting from simple ones, in order to assure results reliability. Furthermore, experimental results and analytic tools-MATLAB code for Voigt-Reuss bounds- are used as benchmarks to validate and compare the derived results.

1. Introduction and Research Outline

A great variety of Structural Engineering applications such as marine and aerospace ones strive for low density materials having high strength, modulus, and damage tolerance [1]. A class of closed-cell foams, synthesized by dispersing rigid hollow particles in a matrix material, has shown considerable promise for such applications [2][3][4]. These foams, called syntactic foams, possess considerably superior mechanical properties, making it possible to use them for load bearing structural applications. Additionally, the presence of porosity inside the hollow particles, called microballoons, leads to lower moisture absorption and lower thermal expansion, resulting in better dimensional stability [2][3]. The size and distribution of porosity can be controlled in these foams by means of volume fraction and wall thickness of the microballoon [4][5] and other independent parameters, such as inclusions spread pattern in the matrix for one fabrication method and inclusions diameter distribution in a specific production category.

The research procedure has almost followed the same scientific trend of M.Profiri and N. Gupta [7-10]. In the research activities by M.Profiri et al. [7-10], apart from experimental studies, theoretical models that relate mechanical properties with composition of syntactic foams are also available [7] [8]. A thorough overview of modeling efforts for particulate composites has been presented by Pal [11]. The Hashin's technique [12] has been extended to syntactic foams by Lee and Westmann [13] to obtain a single equation for the bulk modulus and bounds for the shear modulus. Huang and Gibson estimated the elastic moduli by computing the change in strain energy due to a single hollow sphere in an infinite matrix material [14]. The differential scheme has been applied to derive expressions for Young's modulus and Poisson's ratio of syntactic foams containing high volume fraction of microballoons. [15] First, the elastic properties in the case of an infinitely dilute dispersion of hollow inclusions are determined. A differential scheme is then used to extrapolate the effective properties of syntactic foams for a broad range of microballoon volume fractions.

Having such experimental and analytic results, the current research adds computational models of every kind of composite material RVE with such characteristics. The concept of homogenization technique is explained in Chapter-3.

Other than introductory and concluding parts, the research body contains sessions on the independent input parameters which affect the RVE homogenization results, as follows:

1. Inclusion Area Fraction
2. Inclusion Volume Dispersion
3. Inclusion Membrane Thickness ratio
4. Inclusion Size Distribution pattern

Every input parameter with its domain and trend of influence is thoroughly explained through the relevant session and the results are compared with the available benchmarks. In general the target parameters are Young Modulus and Poisson's ratio of different RVE models.

Analytic models are calculated using MATLAB code *Voigt-Reuss bounds* [15] with its concept explained in Appendix-A and its code text given in Appendix-B. These analytic results are benchmarks to validate computational ones of target parameters lest having solutions totally off the expected scale.

2. Composite Materials

Principles of Composite material are discussed in this chapter. In sections 2.1 an introduction on composite materials and their features are presented. In sections 2.3.1 and 2.3.2 different types of composite materials and their constituting parts are briefly covered.

2.1 Introduction

The “composite” concept is not a human invention. Wood is a natural composite material consisting of one type of polymer – cellulose fibers with good strength and stiffness- in a resinous matrix of another polymer, the polysaccharide lignin. Bone, teeth and mollusk shells are other natural composites, combining hard ceramic reinforcing phases in natural organic polymer matrices [16]. Although man was familiar with composite materials during the history, it is only in the last half century that science and technology of composite materials have developed to provide the engineering with a novel class of materials, and the necessary tools to enable us to use them properly
[16].

Figure-1 gives an idea of the most familiar composite materials. Within each group of materials- metallic, ceramic and polymeric- there are certain familiar materials which can be described as composites. Steels, ceramics and concrete all are classic examples of composite materials. These materials are well known and their mechanical properties are controlled by the form and the distribution of their micro-structures.

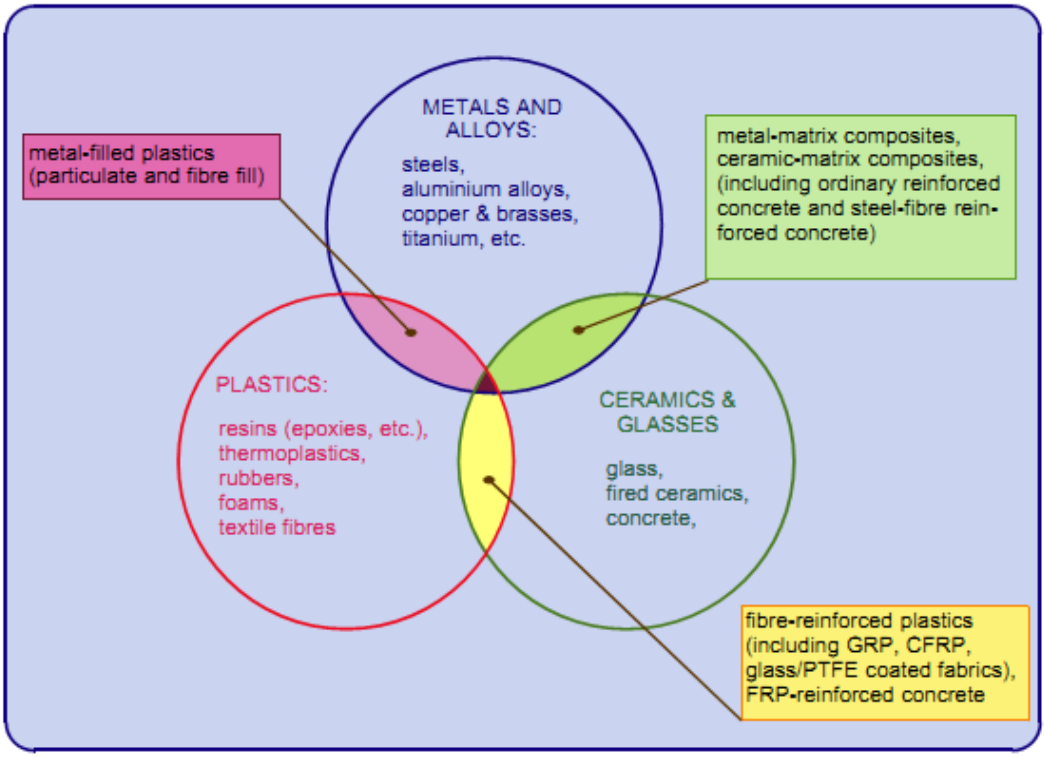

Figure 1- Three main classes of engineering materials, whose combination provides Composite Materials [16]

2.2 Properties of composite materials

These are the summary of advantages proposed by composite materials related to their mechanical properties and applications [16]:

- High resistance to fatigue and corrosion
- High strength or stiffness to weight ratio; Weight savings are significant respect to the weight of conventional metallic designs.
- Improved dent resistance.
- High resistance to impact damage
- Dimensional stability; Having low thermal conductivity and low coefficient of thermal expansion and can be tailored to comply with a broad range of thermal expansion design requirements to minimize thermal stresses.
- Less need of materials, since composite parts and structures are frequently built to shape rather than machined to the required configuration, as is common with metals.
- Excellent heat sink properties, especially carbon-carbon, combined with their lightweight have extended their use for aircraft brakes.
- Improved friction and wear properties
- Some of the disadvantages of composite materials are as follows:
- High cost of raw materials and fabrication.
- Possible weak transverse properties, since usually composites expected to provide a high strength along a special direction like the direction of fibers.
- Reuse and disposal may be difficult.
- Difficult structural and health monitoring inspections

New technologies have provided a variety of reinforcing fibers and matrices that can be combined to form composites having a wide range of properties.
Since the composites are capable of providing structural efficiency at lower weight, as compared to equivalent metallic structures, they have emerged as the primary materials for future use such as marine and aerospace applications [17, 18].

2.3 Composite material classification

Composite materials can be classified according to the type of reinforcement used. Two broad classes of composites are the fibrous and the particulate ones.
Each one also can be subdivided into specific categories, as discussed below [20].

2.3.1. Fibrous composites

A fibrous composite consists of either continuous or chopped fibers, suspended in a matrix material. Schematics of both types of fibrous composites are shown in Figure-2

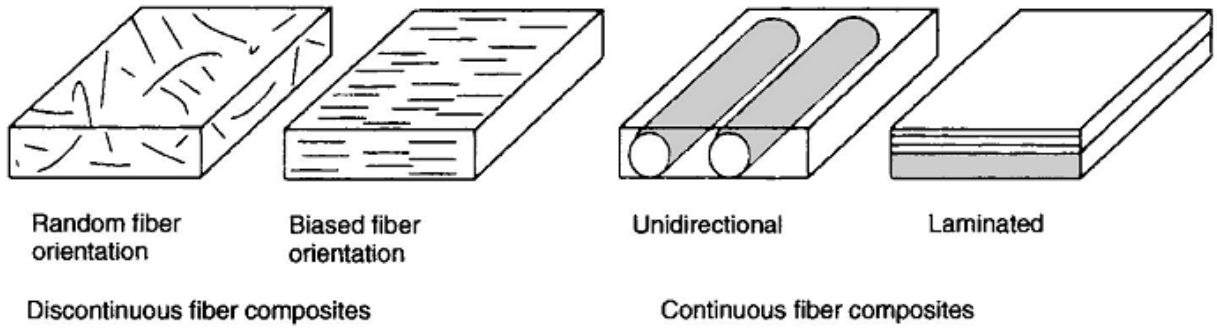

Figure 2- Schematic representations of fibrous composites [16]

Continuous fibers are characterized as having a very high length to diameter ratio. They are generally stronger and stiffer than bulk materials [19].
Composites, in which the reinforcements are discontinuous fibers, can be produced to have either random or biased orientation. The discontinuities can produce a material response that is anisotropic. Moreover, continuous fibers may be either single or multilayered ones. The single layer continuous fiber composites can be either unidirectional or woven and multilayered composites are generally referred to as laminates.

A very good example of fibrous composite materials could be Fiber Reinforced Concrete (FRC). In fact the fiber itself could be from a vast category of materials ranging from synthetic plastics to steel, etc. However the most common type is SFRC which stands for Steel Fiber Reinforced Concrete. This material has proven to have several advantages compared to traditional Reinforced Concrete and concrete paste. The addition of fibers to the concrete which is a particulate composite itself – due to presence of aggregates in the cement paste – gives an additional tensile stiffness and strength to the material in a rather homogeneous pattern with respect to its spread over the casting volume.

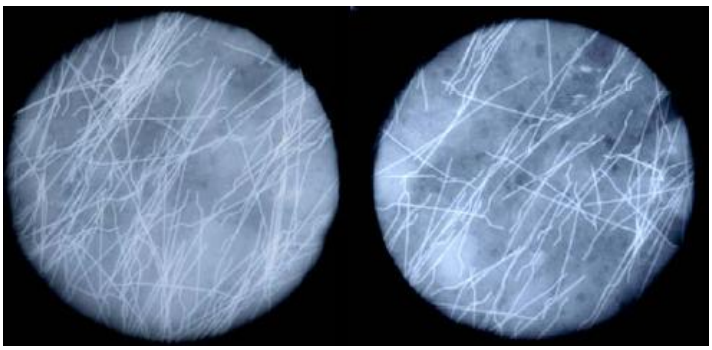

Figure 3- The spreading pattern of fibers in two different cylindrical samples

2.3.2 Particulate composites

A particulate composite is characterized as being composed of particles suspected in a matrix. Particles can have virtually any shape, size or configuration. An example of well-known particulate composites is concrete. A schematic of several types of particulate composites is shown in Figure -4. There are two categories of particulates: flake and filled/skeletal.

A flake composite is generally composed of flakes with large ratio of platform area to thickness, suspended in a matrix material. A filled/skeletal composite is composed of a continuous skeletal matrix filled by a second material. The response of a particulate composite can be either anisotropic or orthotropic.

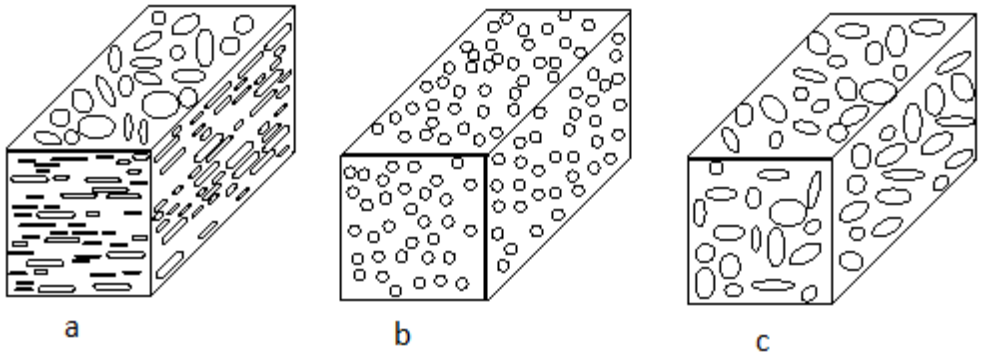

Figure 4- Schematic representation of particulate composites, a) flake composite, b) general particulate composite, c) filler composite [11]

In fact Syntactic foams which are the subject of the current research are categorized as particulate composites which are synthesized by dispersing hollow microspheres, called microballoons, in a matrix material [21]. In the coming chapter the effects of several microbaloon properties on the overall properties of a particulate composite material – syntactic foam- is investigated by computational method.

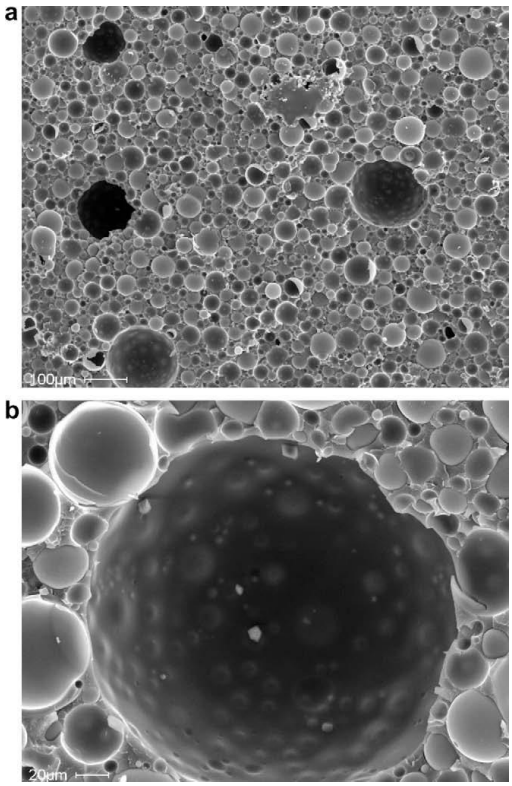

Figure 5-Micrographs of syntactic foams [10]

3. Homogenization

3.1. Introduction

A composite is a heterogeneous material whose properties vary from point to point on a length scale 'l', called microscale, which is much smaller than both the scale of variation of the loading conditions and the overall body dimensions which are characterized by the length 'L' defining the macroscale. At the macroscale level the composite can be regarded as a continuum medium characterized by uniform properties; such properties will be in the following equivalently referred to as effective, or homogenized, or overall, or macroscopic [23]. Any region occupied by material over which the composite properties are constant at the microscale level will be called phase; therefore, a composite material is a continuum in which a number of discrete homogeneous continua are bonded together. Any region of the heterogeneous body characterized by a length scale 'L' such that $l/L \ll 1$, which is then macroscopically seen as homogeneous, is called ***Representative Volume Element*** hereafter shortened in **RVE** [23].

One fundamental step in both the design and the analysis of syntactic foams concerns the evaluation of their ***linear elastic behavior***. The computation of the so-called effective (i.e., macroscopic) elastic moduli of syntactic foams can be tackled by means of homogenization techniques [23].

In the current research, in order to estimate the overall properties of syntactic foams made of glass sphere (as inclusion) and vinyl ester (as matrix), computational models of various geometrical properties are created to represent each material RVE with its corresponding characteristics. On the other hand there are analytic methods which are introduced in the following.

In the following, the material properties of the Sphere-Glass and Matrix Vinyl Ester are assumed as Figure - 6:

Composite Phase	Young Modulus (GPa)	Poisson's Ratio
Vinyl Ester	3.21	0.3
Sphere Glass	60	0.21

Table 6 - Composite Phase Material Properties

3.1.1 Analytic Procedure

There is a wide range of analytic methods which are in fact mathematical models with various assumptions based on the composite materials structure and properties. Eshelby solution [23][24], Dilute approximation[23][24], Voigt and Reuss bounds[25] and Hashin–Shtrikman bounds [26][27] as four methods in order to derive the overall properties of composite material RVE for a linear elastic constitutive behavior assumption [23]. While M.Profiri [7] takes a combination of the methods of Lee and Westmann [13] besides Dilute approximation [23][24] and Hashin's technique as introduced by Torquato [12].

In this thesis a simple technique based on Voigt and Reuss Bounds is presented in order to set benchmarks as a comparing tool for the computational results, besides the experimental results.

Voigt and Reuss approaches respectively assume the state of strain or stress to be uniform inside the RVE [22]. They are known to provide bilateral bounding for the elastic moduli of multiphase systems, even though bounds are not tight. Analytical results furnished by the two approaches are here used to validate the numerical results. The mathematical procedure is explained in Appendix-A and the MATLAB code is given in Appendix –B.

3.1.2 Computational Procedure

The computational procedure of the homogenization is a combination of finite element analysis and a numerical procedure which uses the outcomes. RVE is assumed a square shape with its phases of different materials. The RVE boundary condition is described under plane stress conditions. No assumption of an isotropic behavior is valid a prior to the homogenization. Considering the plane stress condition, the RVE is subjected to unit stresses on its boundary and afterwards strains over the area of RVE finite elements are derived and averaged. Having three different elements in a 2D stress vector, three equations are created which results in Young Modulus and the Poisson's ratio in two directions. Applying the strains on boundary conditions and calculating the stress values over the RVE gives another set of results for Young Modulus and the Poisson's ratio. The two sets of results provide the bounds by which the RVE overall constitutive properties are constrained.

3.2 Independent Parameters

The computational tool used for modeling the explained problem is a non-commercial code called ***MEMSYS***. The following parameters effects have been investigated on the composite material overall mechanical parameters:

1. ***Inclusion Area Fraction***: The *Volume Fraction of Inclusion Particles* that constitute the composite material. This means the volume ratio of present inclusions with respect to the material overall volume. In this case as the analysis is done using 2D models, ***Inclusion Area Fraction*** is considered as the independent parameter. Inclusion area corresponds to the inclusion circle area including the void and not merely to the solid part.

2. ***Inclusion Dispersion Model:*** This parameter explains the morphology of the inclusions dispersion in matrix material with respect to each other. Considering a 2D plane, there might be one equal dispersion of the inclusions in the material resulting in equal distances between inclusion particles in longitudinal and transverse directions or a kind of dispersion that results in larger distances between inclusion particles in longitudinal direction compared with transverse one or vice-the-versa.

3. ***Inclusion Membrane Thickness Ratio:*** Hollow spheres are used as inclusions in the currently investigated material; the membrane thickness of these hollow spheres is a key parameter to the deriving Syntactic Foam overall mechanical properties. Considering the substitution of circles with spheres due to the 2D nature of the modeling tool.

4. ***Inclusion Size Distribution Pattern:*** In a real manufacturing procedure, controlling a bulk mass of inclusion material (glass sphere), it can be seen that glass spheres don't have a precise and unique size; rather there's a distribution of sizes in the bulk mass of a product category with a defining nominal average and variance for the sphere diameter. Considering a discrete distribution to convert the problem for a computational modeling procedure, a series of inclusion distribution types are compared with each other to control the effect of the inclusion particles diameter size distribution on the overall mechanical properties of the corresponding composite material.

In the following ‘E’ stands for Young Modulus and ‘ni’ for Poisson’s Ratio. The indices “1” and “2” beside ‘E’ and ‘ni’ show the corresponding parameter in the horizontal and vertical directions of the RVE plane respectively.

3.2.1.1. Modeling tool (MEMSYS) validation; Homogenous RVE

In this section the capacity of MEMSYS code and the created models are checked for single material models by comparing *physically equal models* with *mathematically and computationally different inputs*.

The whole trial procedure is divided into four parts as follows:

1. Primarily a square RVE model (L=200 μm) is created, the material properties of Vinyl ester is assigned to the single part model.
2. The previous model is created with a single inclusion whose mechanical properties are the same of the matrix. (R=18 μm)

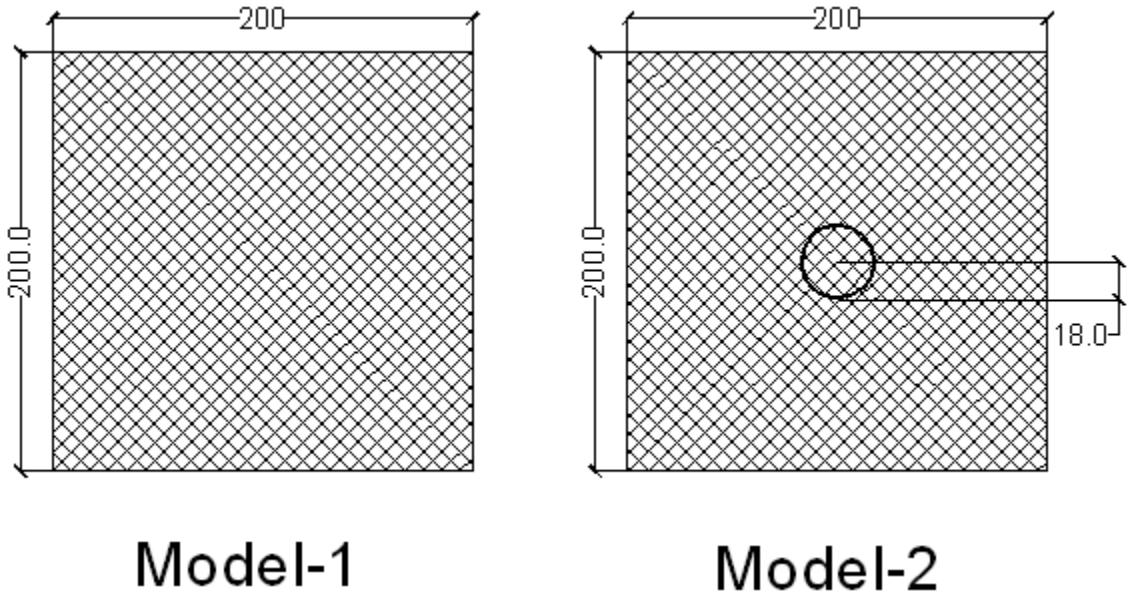

Figure-7- Equivalent Pure Vinyl Ester RVE models

*Models which are created in the third and fourth steps must have the same overall properties.

3. The model of the second step is created with a single difference of omitting the partitioned circle to create a hole instead of the circular part. (R=18 μm)
4. The model of third step is created with the only difference of partitioning a circular annulus around the circular hole. (Rext=20 μm)

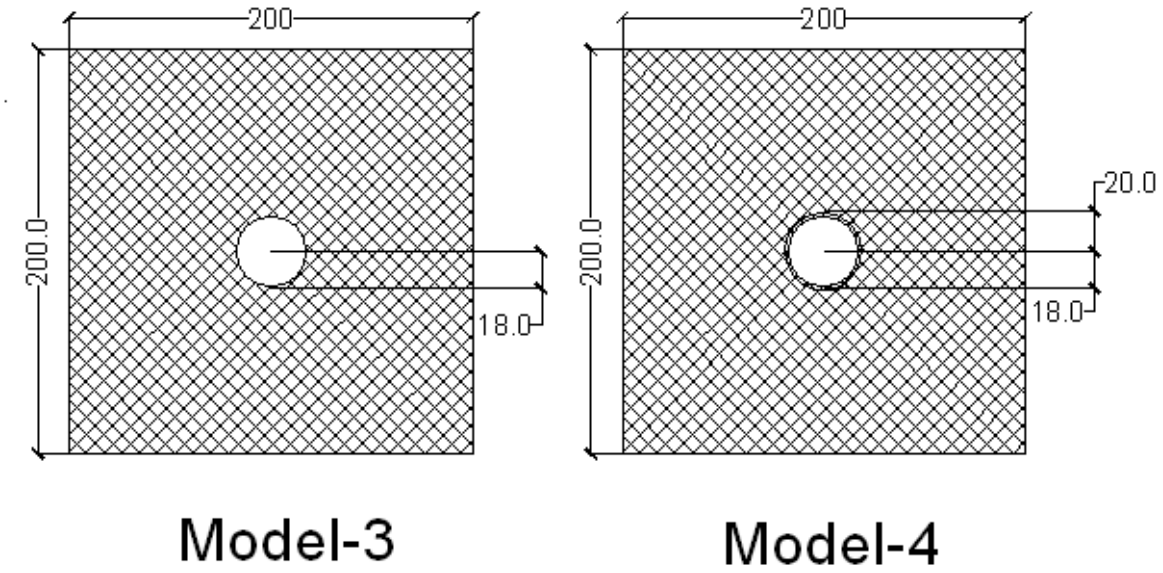

Figure 8- Equivalent Vinyl Ester RVE models with void

*Models which are created in the third and fourth steps must have the same overall properties.

Results are as follows:

RVE size 200 μ.m		*Reuss*			
Model	***Model code***	***E1(GPa)***	***ni1***	***E2(GPa)***	***ni2***
Simple Rectangle	1	3.21	0.3	3.21	0.3
Rectangle with filled-in inclusion	2	3.21	0.3	3.21	0.299999999
Rectangle with hole inside (R hole = 18μ.m)	3	3.209422	0.3000079	3.209422	0.3000079
Rectangle with hollow inclusion (R int = 18μ.m)	4	3.209423	0.3000079	3.209423	0.3000079
Model		*Voigt*			
Simple Rectangle	1	3.21	0.3	3.21	0.3
Rectangle with filled-in inclusion	2	3.21	0.3	3.21	0.3
Rectangle with hole inside (R hole = 18μ.m)	3	2.984525	0.30087	2.984525	0.30087
Rectangle with hollow inclusion (R int = 18μ.m)	4	2.98451	0.3008729	2.98451	0.3008729

Table 9 - Pure Vinyl Ester RVE model results

As it's evident in the Table-9 the corresponding values of Young Modulus and Poisson's Ratio are very close to one another. Results model codes 1 and 2, which are representing a square volume element of the Vinyl Ester, could be considered as totally equal in two procedures. Comparing the results of the model codes 3 and 4, again the values match up to the forth decimal digit.

3.2.1.2. Single Inclusion RVE Modeling with different Inclusion Area Fractions

In this step, the real case RVE models are created using one single inclusion. The inclusion area fraction of the composite material is modeled by assigning various values to the dimension length of the square shape RVE.

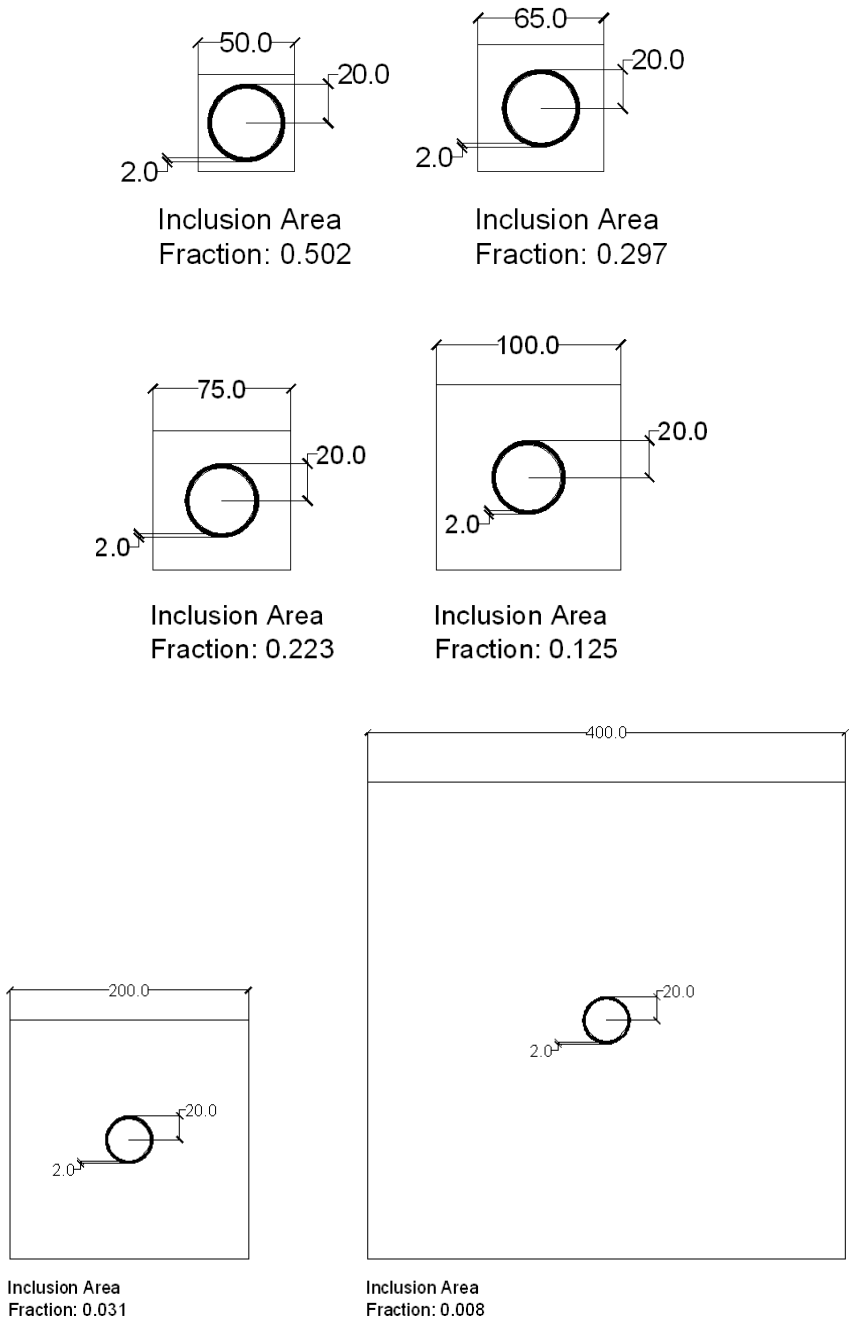

Figure 10 - RVEs with various inclusion volume fraction

**As stated before an analytic method is used as a reference for the computational results.*

The following charts compare the Young modulus and Poisson's ratio of RVE models with different inclusion volume fractions.

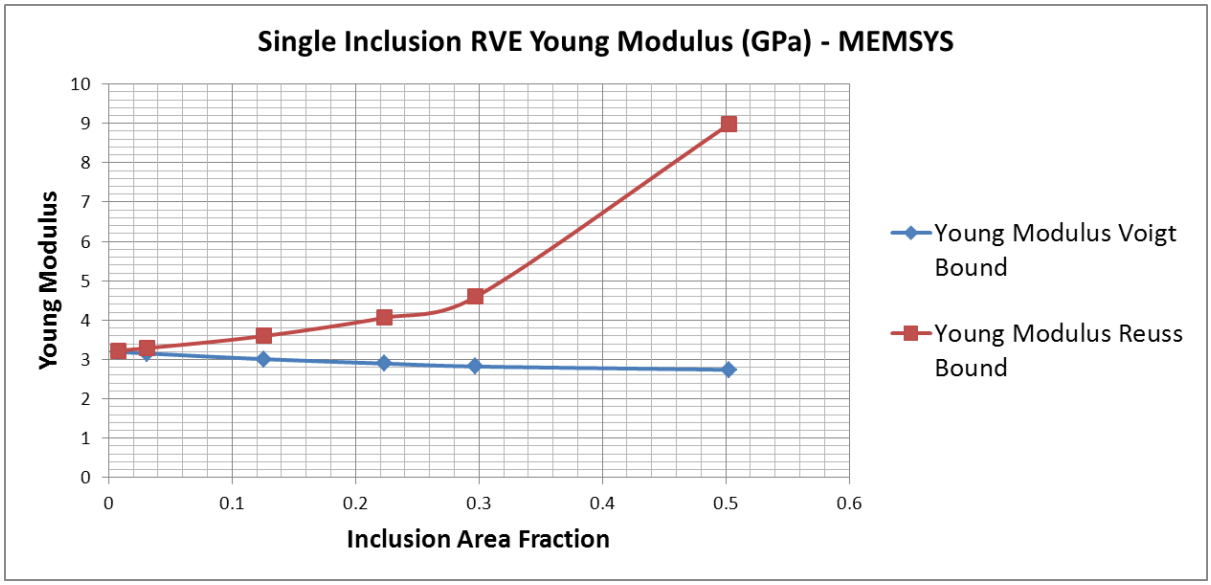

Diagram 11 – Single Inclusion RVE Young Modulus - MEMSYS

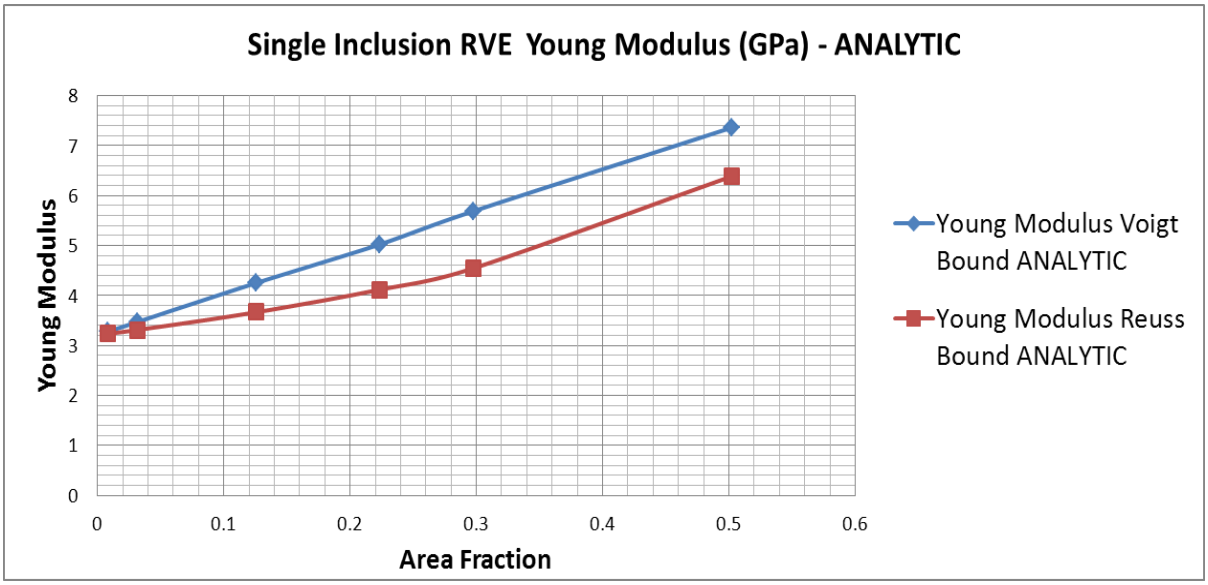

Diagram 12 - Single Inclusion RVE Young Modulus - ANALYTIC

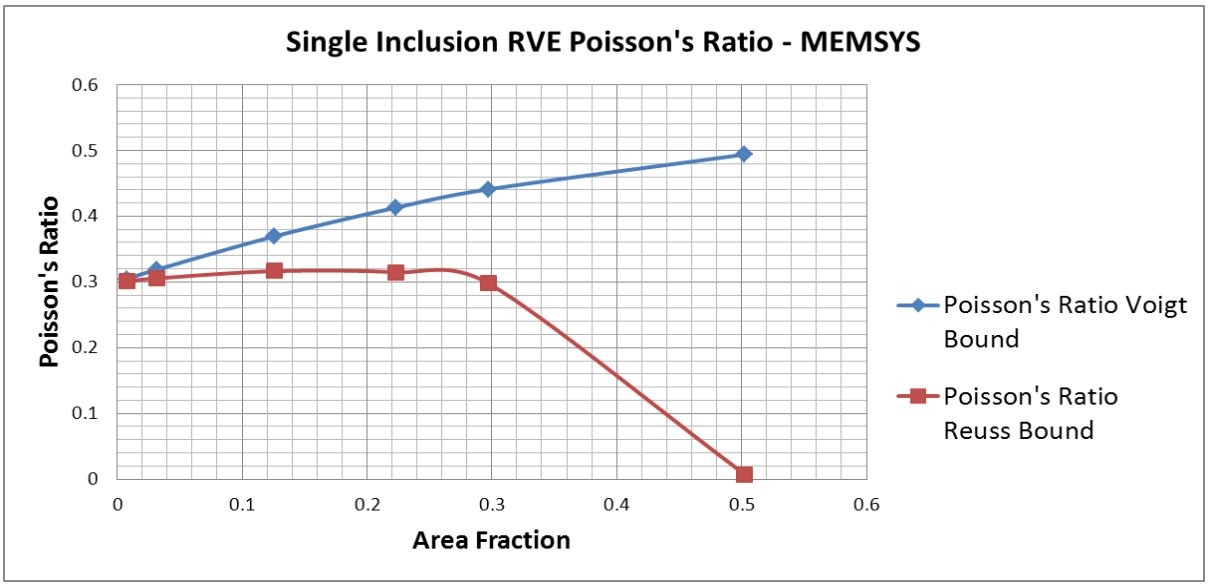

Diagram 13 – Single Inclusion RVE Poisson's Ratio - MEMSYS

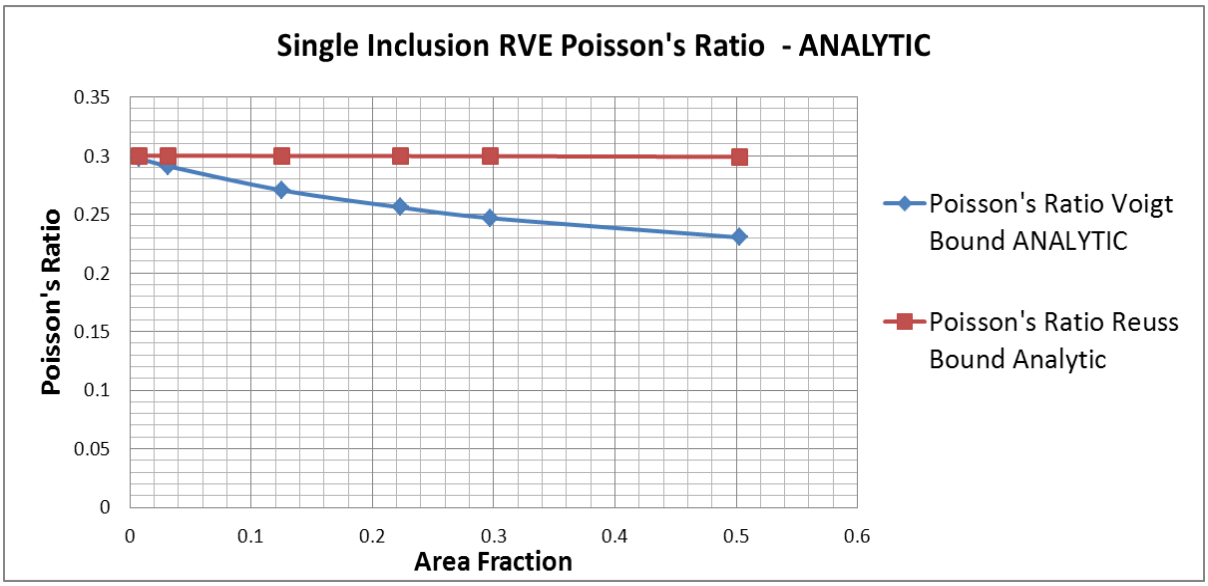

Diagram 14 – Single Inclusion RVE Poisson's Ratio - ANALYTIC

The average value of the MEMSYS bounds is calculated and shown in the diagram using the ***"avg"*** index.

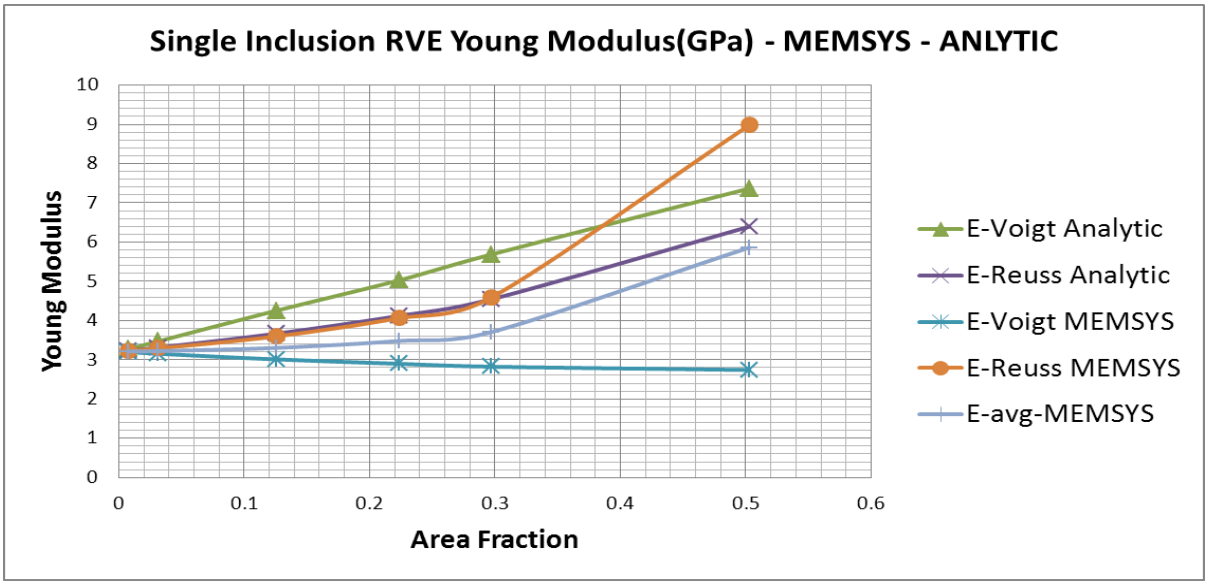

Diagram 15 – Single Inclusion RVE Young Modulus – MEMSYS - ANALYTIC

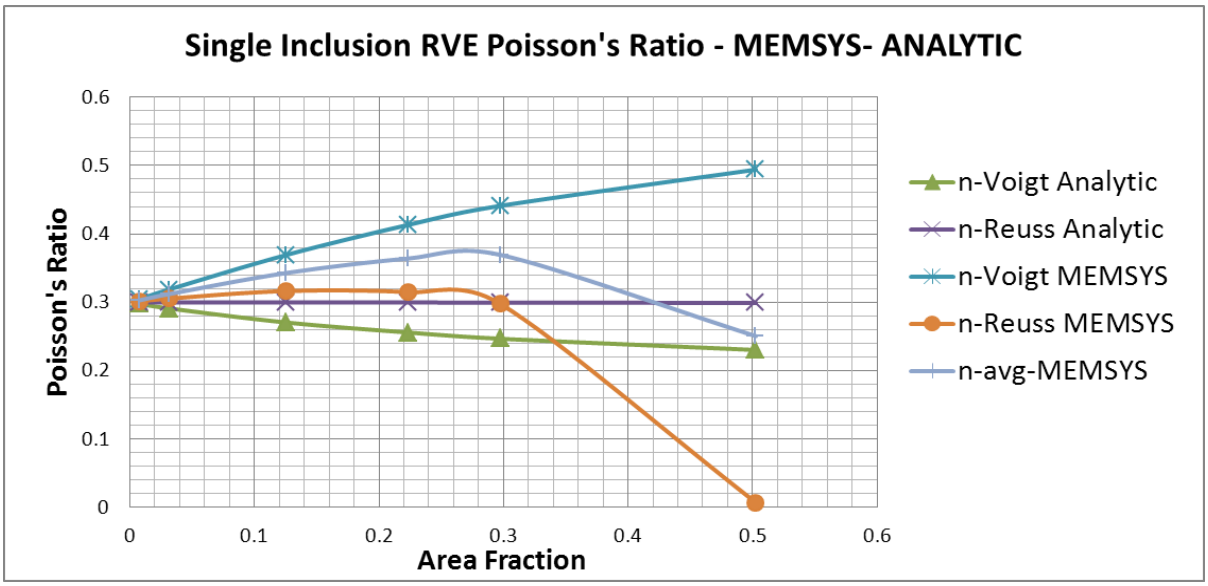

Diagram 16 - Single Inclusion RVE Poisson's Ratio – MEMSYS - ANALYTIC

Referring to the results diagrams; for area fractions between 0 to 0.3, as a result of inclusions area fraction increase; all the charts show an increasing trend in the Young Modulus expect the MEMSYS Voigt bound which has a decreasing trend with a low inclination with respect to the other trends. While the average computational results

which are shown as E-avg shows an increasing trend again. For area Fraction equal to 0.5 the results show unpredictable divergences. This could be explained by the fact that in these models the ratio between phase material dimension and the RVE length is large so that the limits of an acceptable RVE is breached, this is well explained by Nemat-Nasser [22], where a ratio between is defined as, the maximum phase material entity size over the RVE length, this ratio shall be bound by a maximum value in order to have a meaningful volume which can represent the accepted concept of a RVE. This is the reason why Multi-Inclusion RVE models better function in homogenization procedure to result the overall values of RVEs with such inclusion fraction ratios.

Figure-17 shows the results of an investigation [9] where the inclusion volume fraction of the material has been changed and the tensile modulus of the material is investigated through a series of experiments. In the computational homogenization procedure by MEMSYS the applied unit stress and strains are positive, therefore the parameter to be compared with its results is the tensile modulus, while compressive modulus changing trend with respect to volume fraction variation is shown in the referred article [9].

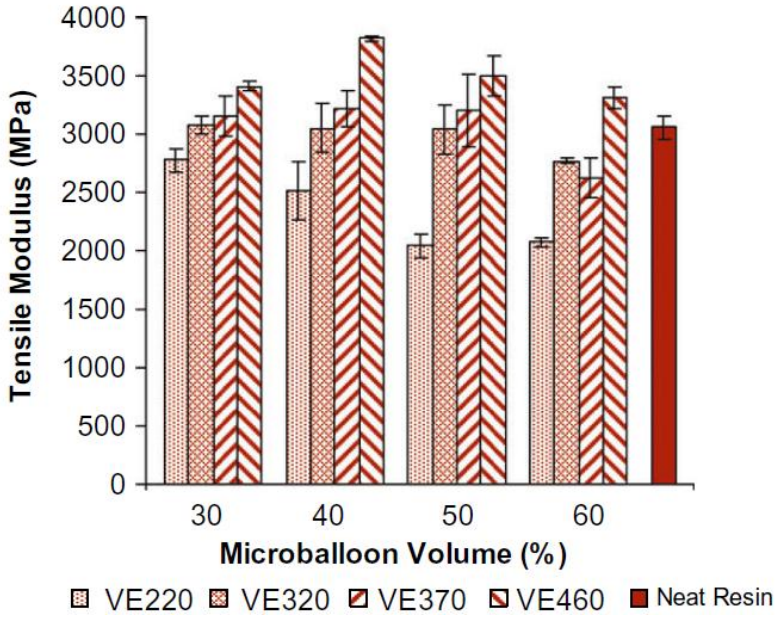

Figure 17 – Composite Materials Tensile Modulus [9]

The results in figure-17 are for area fractions which this thesis does not include a specific range of them. In fact the current research is based on 2D RVE models with a circular inclusion which could also be considered as 3D RVE models with a cylindrical inclusion. For a 2D computational model geometry of a particulate single-inclusion composite material RVE, there is a physical allowance of maximum inclusion diameter equal or less

than the RVE size, which leads to a maximum area or volume fraction of 78%. While in the numerical results [9] volume fraction refers to ratio which consists of the volume of spherical inclusions divided to the overall volume (3D RVE with spherical inclusion). In order to find the equivalent geometries between 2D and 3D RVEs, considering equal volumes of inclusion material between a 3D RVE with a spherical inclusion and a 3D RVE with a cylindrical inclusion, Table-18 is created. The external radius of the 3D RVE with spherical inclusion is the dependent parameter which is derived as a result of RVE parameters:

Equivalent RVE Models							
RVE 3D - Spherical Inclusion				RVE 2D - Cylindric Inclusion			
L	Rext	Volume Fraction		L	Rext	Volume Fraction	
50.00	24.65	0.50		50.00	20.00	0.50	
65.00	26.91	0.30		65.00	20.00	0.30	
75.00	28.22	0.22		75.00	20.00	0.22	
100.00	31.06	0.13		100.00	20.00	0.13	
150.00	35.56	0.06		150.00	20.00	0.06	
200.00	39.13	0.03		200.00	20.00	0.03	
400.00	49.31	0.01		400.00	20.00	0.01	

Table - 18 – 2D and 3D Equivalent RVE models

The Alphanumeric codes VE220, VE320, VE370, VE460 stands for different composite materials with respect to the inclusion type density. This parameter is in fact a function of the hollow inclusion membrane thickness which varies from 5 μm to 25 μm in practic.

Properties of microballoons used in fabricating syntactic foam specimens.

Microballoon type[a]	Density[c] (kg/m^3)	Mean particle size[a] (μm)	Wall thickness[b] (μm)	Radius ratio[b] (η)	Pressure for 80% survival[c] (MPa)
S22	220	35	0.521	0.970	2.76
S32	320	40	0.878	0.956	13.8
K37	370	40	1.052	0.947	27.6
K46	460	40	1.289	0.936	41.4

[a] Manufacturer's code.
[b] Calculated value.
[c] Manufacturer's data sheet.

Table 19 – Microbaloons Properties used in Syntactic Foams

Including the theoretically used inclusion type which is used in the current chapter, with a VE710 code, the following table is created:

Rext (μm)	Thickness(μm)	Real Density (kg/cm3)	Nominal Density (kg/cm3)
35	0.521	219.978	220
40	0.878	322.076	320
40	1.052	384.216	370
40	1.289	467.966	460
40	2	713.125	710

Table 20 – Microbaloons Dimensional Properties used in Syntactic Foams

Considering the volume (area) fraction range from 0.3 to 0.5; the experimental results [9] in the figure-17 and the MEMSYS results shown in Figure - 12 could be compared. All the results vary within an acceptable meaningful range, while there's an absolute mismatch between their variation trend; the trend in the experimental results of the Figure-14 show a decreasing inclination while the average MEMSYS bounds results show an increase. This could be due to the fact that the MEMSYS models for area fractions over 30% shall not be reliable as explained before based on Nemat Nasser [22] indications about the ratio between phase size with respect to RVE size and also because of the assumed constitutive model in the homogenization procedure which does not consider fractal and plastic behaviors. It is noteworthy that for volume fractions over 40%, the probability of direct contact between inclusions are relatively high and this might also change the modeling basic assumptions completely considers a complete interaction between inclusions and matrix. In the coming chapter where the stochastic dispersion of inclusions through Multi-Inclusion RVE models is described, a corrected version of the diagrams investigating the effect of the inclusion area fraction is rendered. This correction is specifically applied for the range between 30% and 50% inclusion area fraction.

3.2.1.3. Asymmetric Rectangular RVE Modeling

In this step rectangular RVE models are created instead of former square models, in case of an uneven dispersion of the inclusions in the matrix in a regular way, such arrangements of RVE models could be resulted in the real case manufactured material.

On the other hand, by comparing the overall parameters (Young modulus and Poisson's ratio) of these models with the corresponding square ones the validity of the models and the computational tool (MEMSYS) could be certified.

Two different categories of models are created for this case:

1. Rectangular RVE models with constant length
2. Rectangular RVE models with constact inclusion area fraction

3.2.1.3.1-Constant Length RVE Models

In these models, the RVE width is changing in every model and the effect of uneven dispersion of the inclusion particles in main perpendicular axes are investigated, regardless of the composite material inclusion particles area fraction.

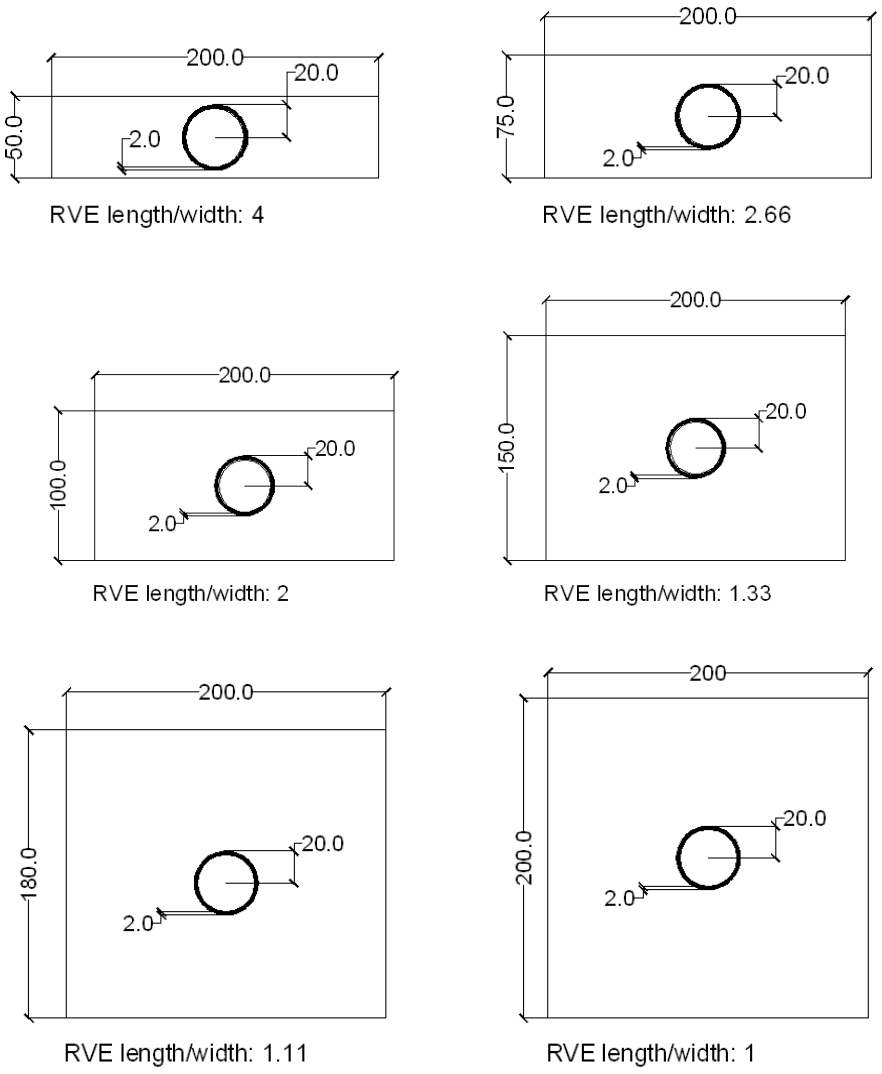

Figure 21 - Asymmetric RVE models with constant length

The results are as follows:

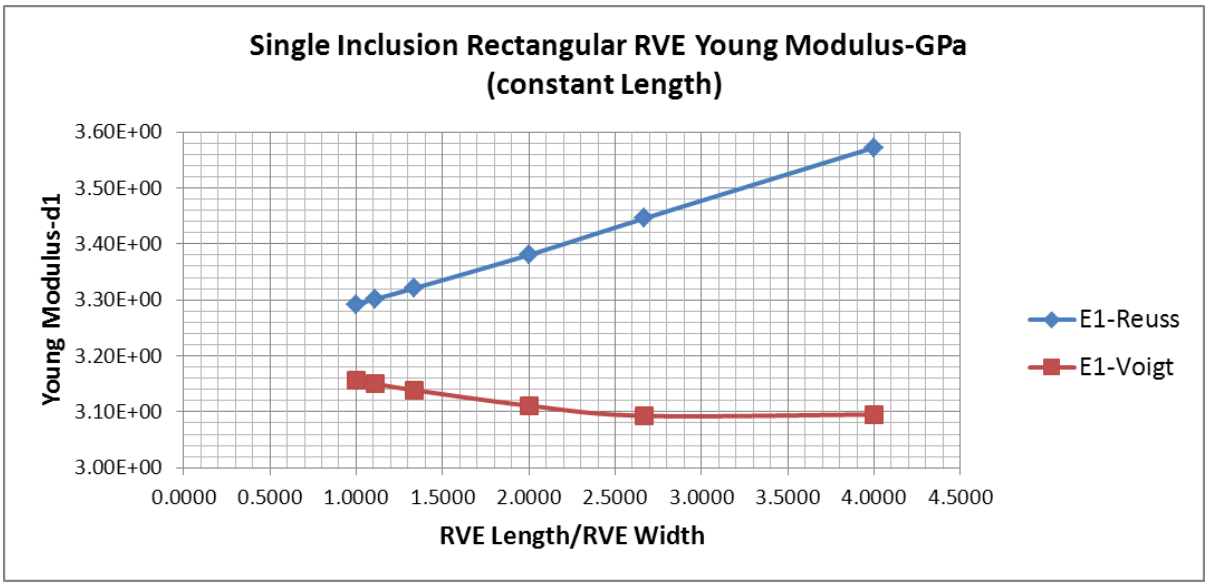

Diagram 22 – Single Inclusion Rectangular RVE Young Modulus – Constant Length

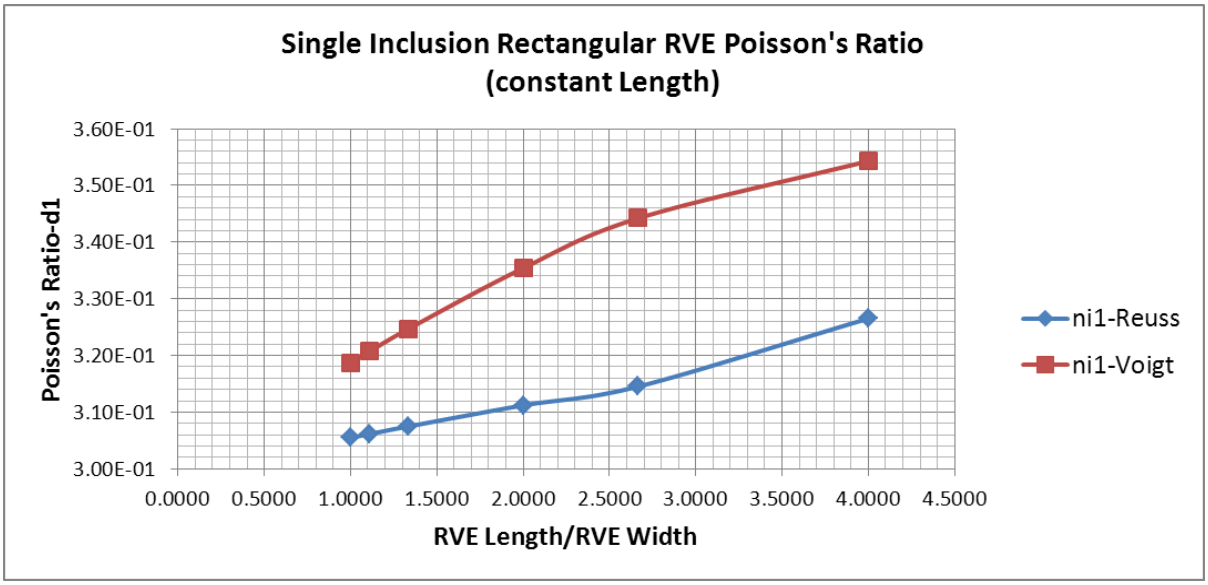

Diagram 23 - Single Inclusion Rectangular RVE Poisson's Ratio – Constant Length

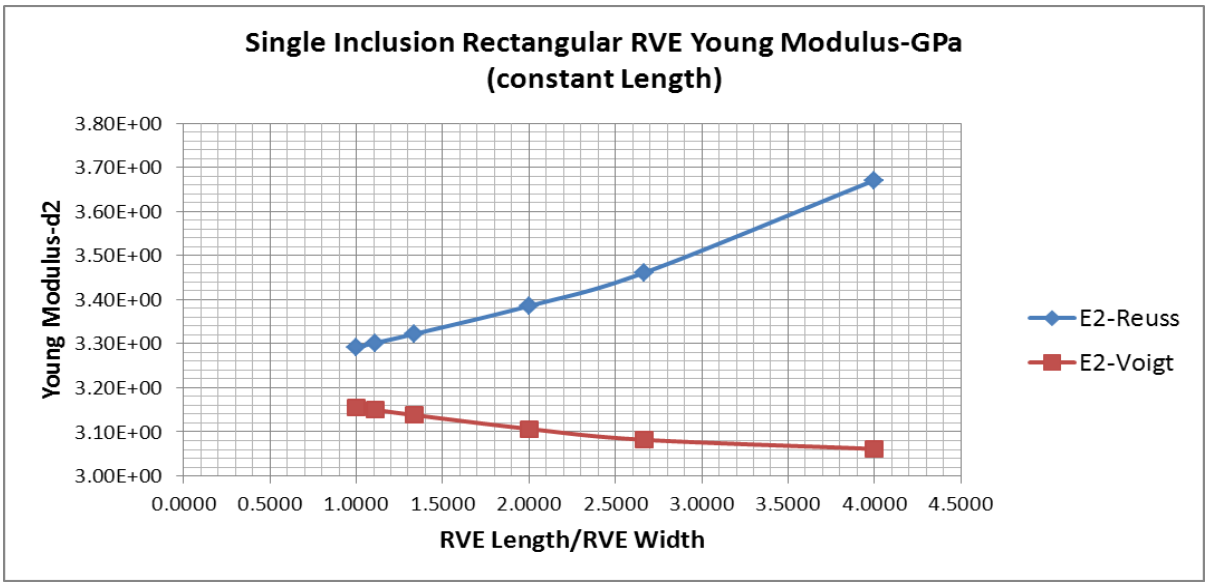

Diagram 24 - Single Inclusion Rectangular RVE Young Modulus – Constant Length

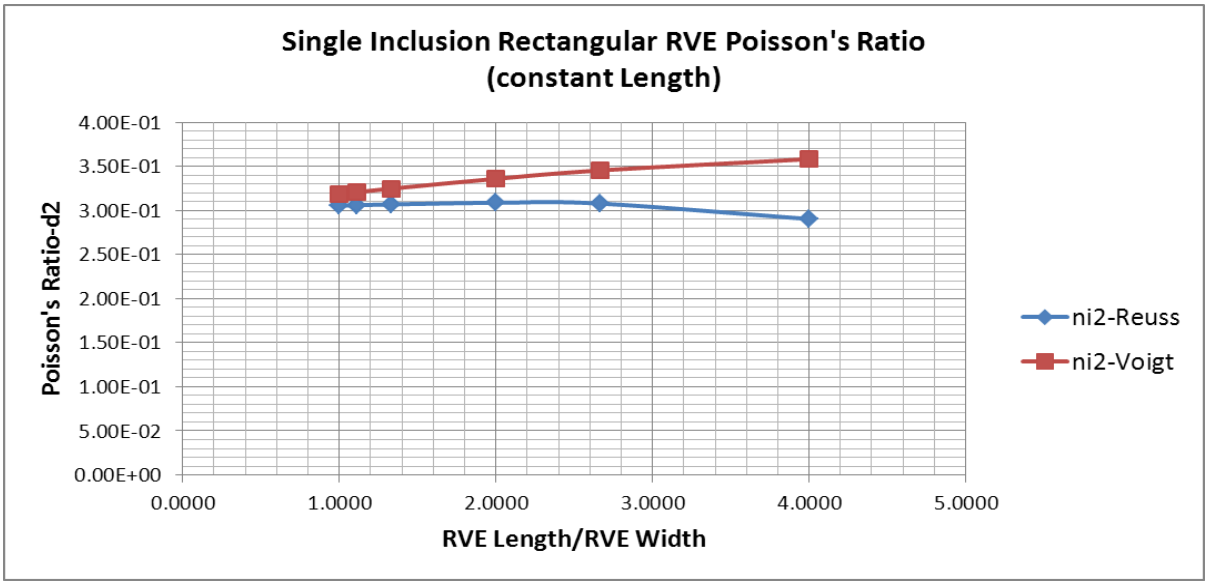

Diagram 25 - Single Inclusion Rectangular RVE Poisson's Ratio – Constant Length

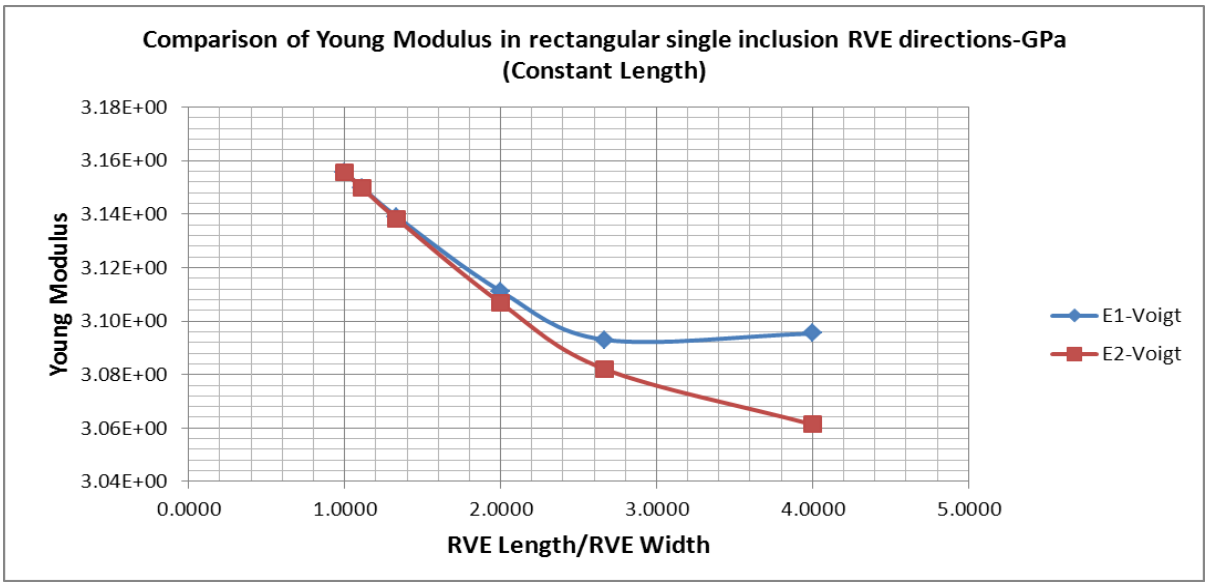

Diagram 26 – Comparison of RVE Young Modulus in different directions – Voigt Bound

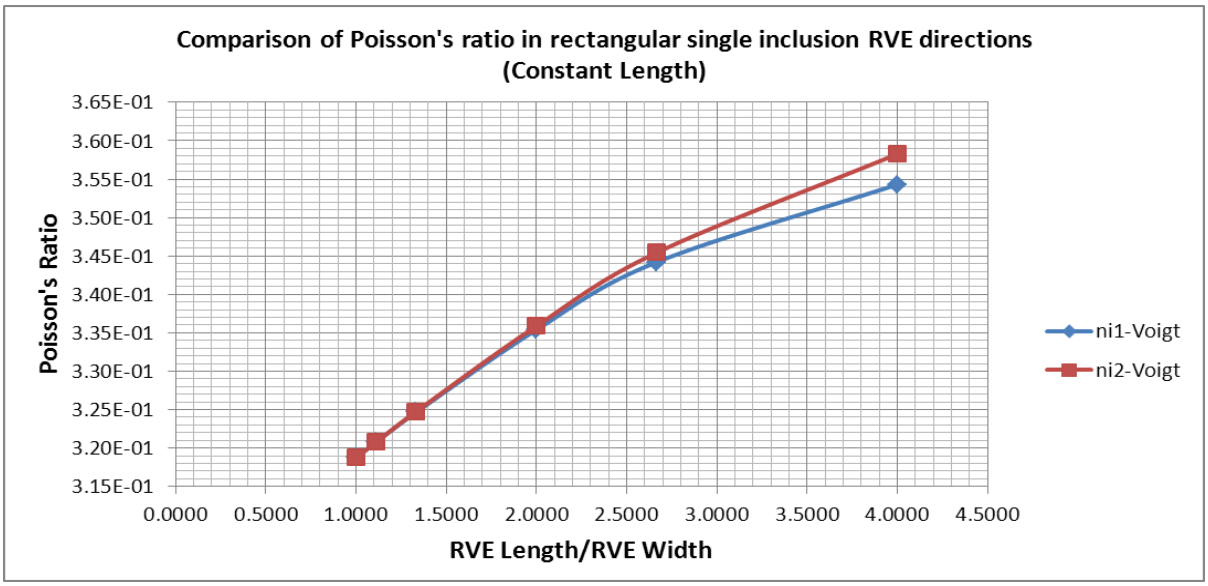

Diagram 27 - Comparison of RVE Poisson's Ratio in different directions – Voigt Bound

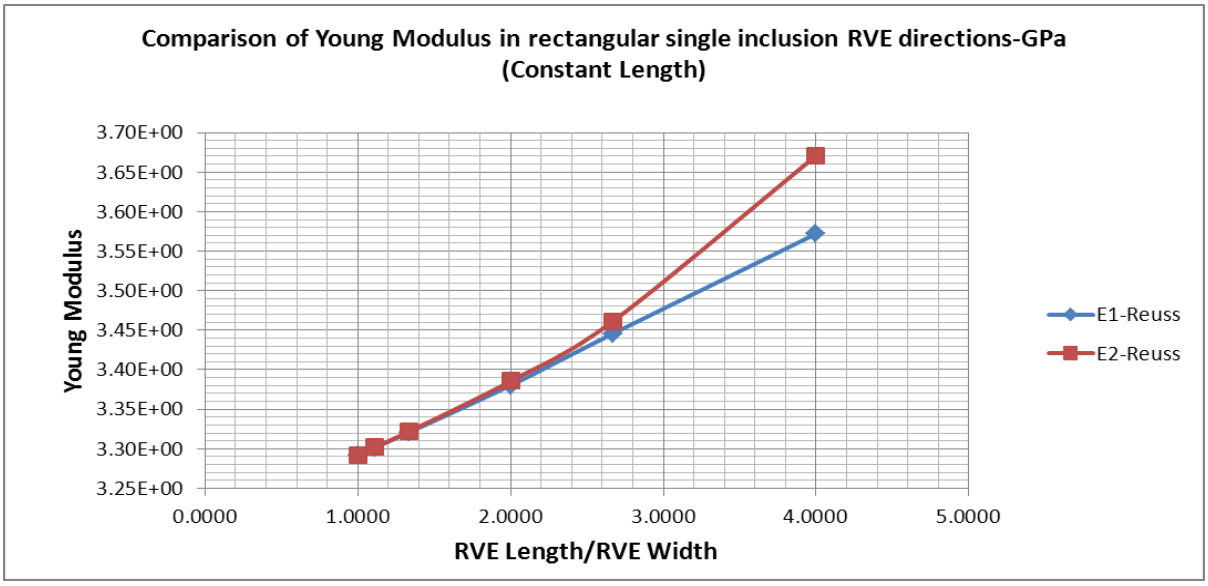

Diagram - 28 - Comparison of RVE Young Modulus in different directions – Reuss Bound

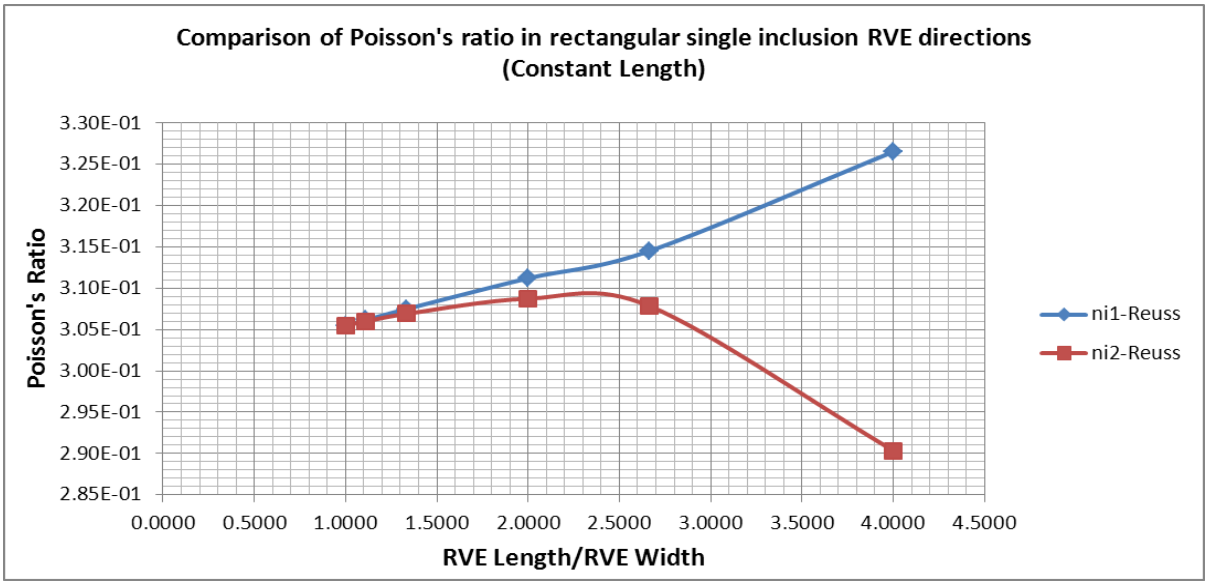

Diagram - 29 - Comparison of RVE Poisson's Ratio in different directions – Reuss Bound

The increase of the ratio of RVE length to its width means the decrease of inclusion area fraction which its results are already obtained, while the constant length of the RVE model gives the opportunity to investigate the effects of an uneven dispersion of the inclusions.

3.2.1.3.2. Constant Area Fraction RVE models

In these models the effect of uneven dispersion of the inclusion particles are investigated, considering a unique inclusion particle area fraction for every model, in other words the area fraction of models are set to be unchanged and the rectangular model width and length are changed to maintain the RVE area.

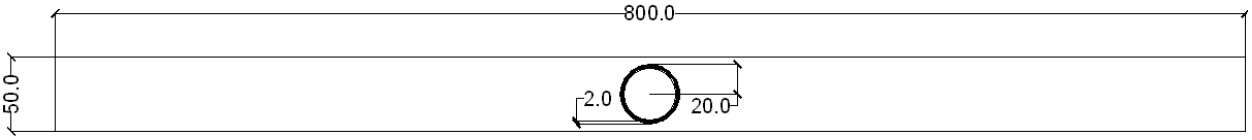

RVE length/width: 16

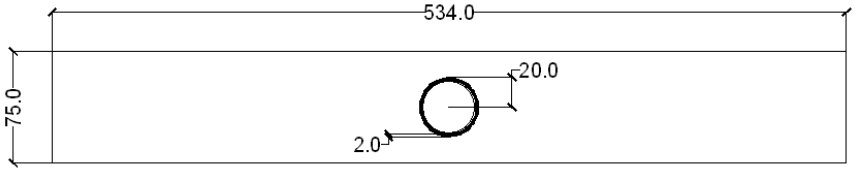

RVE length/width: 7.12

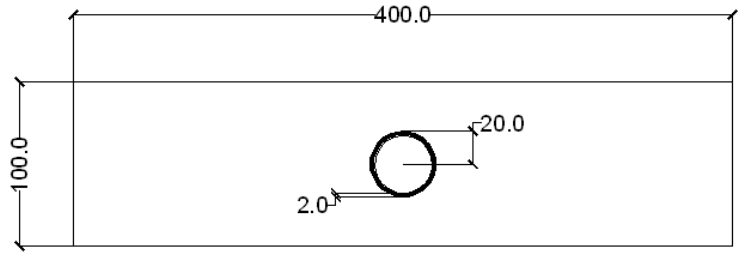

RVE length/width: 4

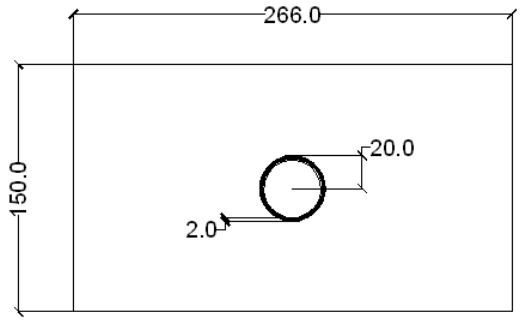

RVE length/width: 1.77

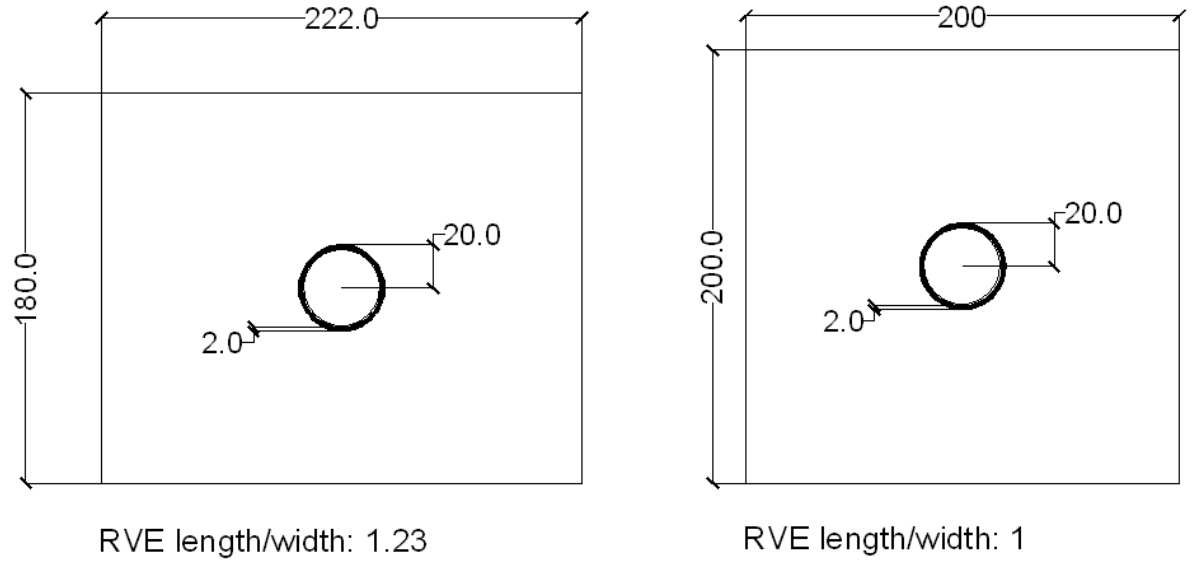

Figure 30 - Asymmetric RVEs with constant volume fraction

Diagrams 31 to 38 compare the Young modulus and Poisson's ratio of various models of the same main direction which are shown using d-1 and d-2 on the chart vertical axis; d-1 refers to the longitudinal axis and d-2 to the transverse one.

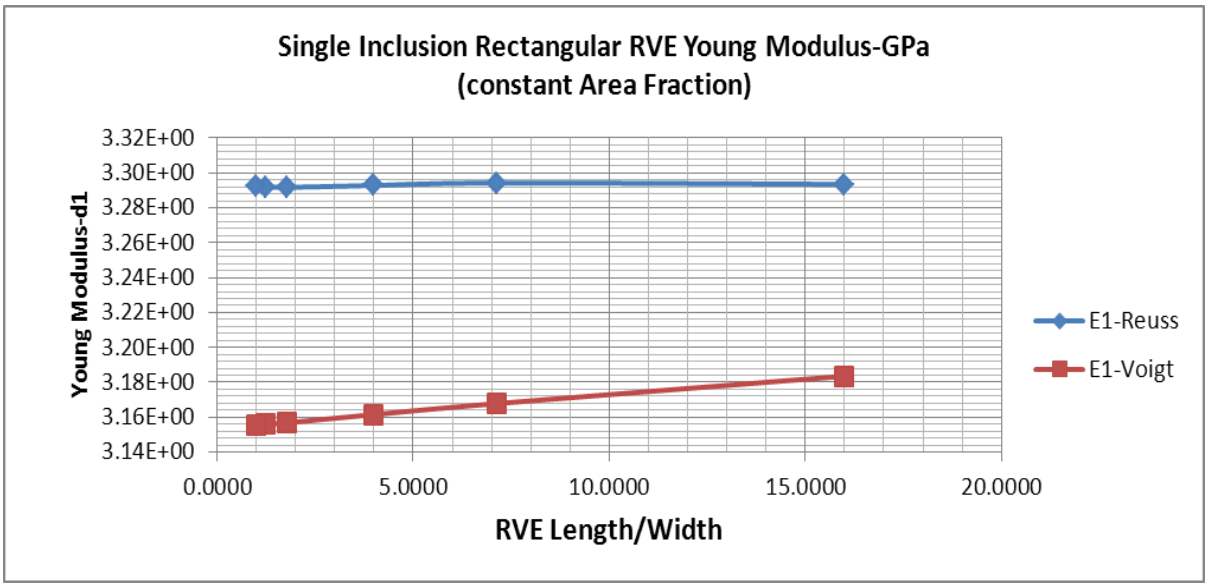

Diagram 31 – Single Inclusion Rectangular RVE Young Modulus – Constant Area Fraction

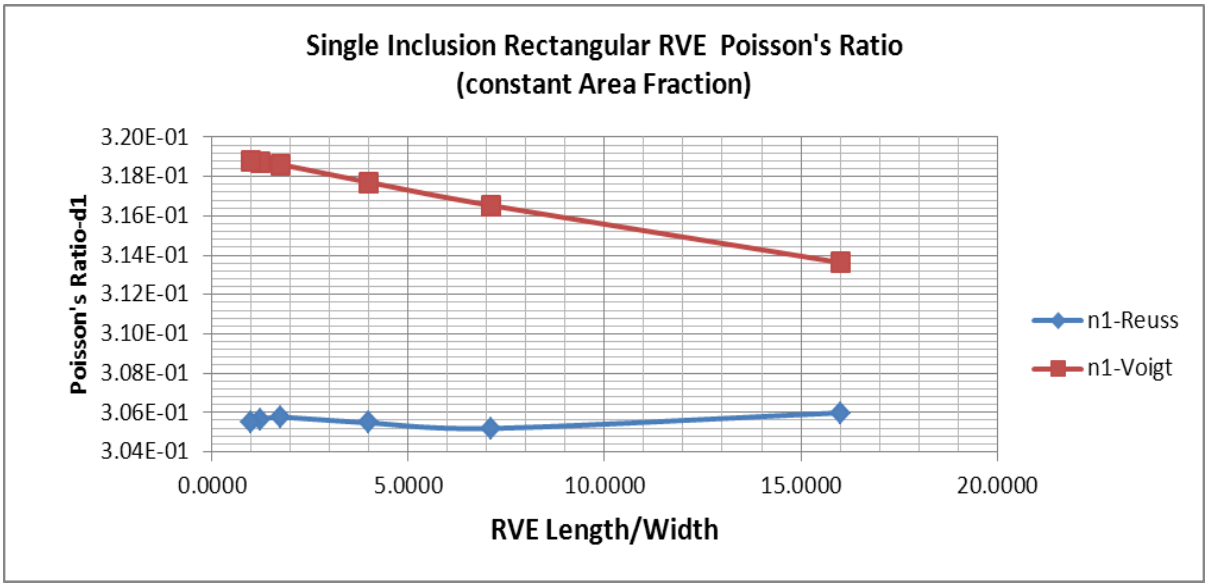

Diagram - 32 Single Inclusion Rectangular RVE Poisson's Ratio – Constant Area Fraction

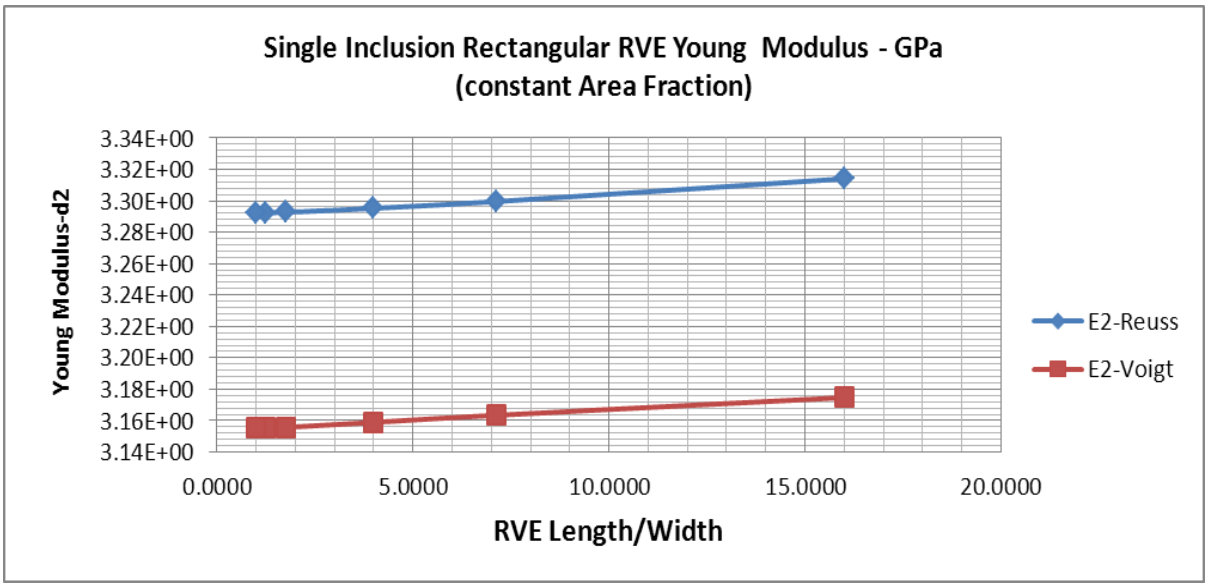

Diagram 33 - Single Inclusion Rectangular RVE Young Modulus – Constant Area Fraction

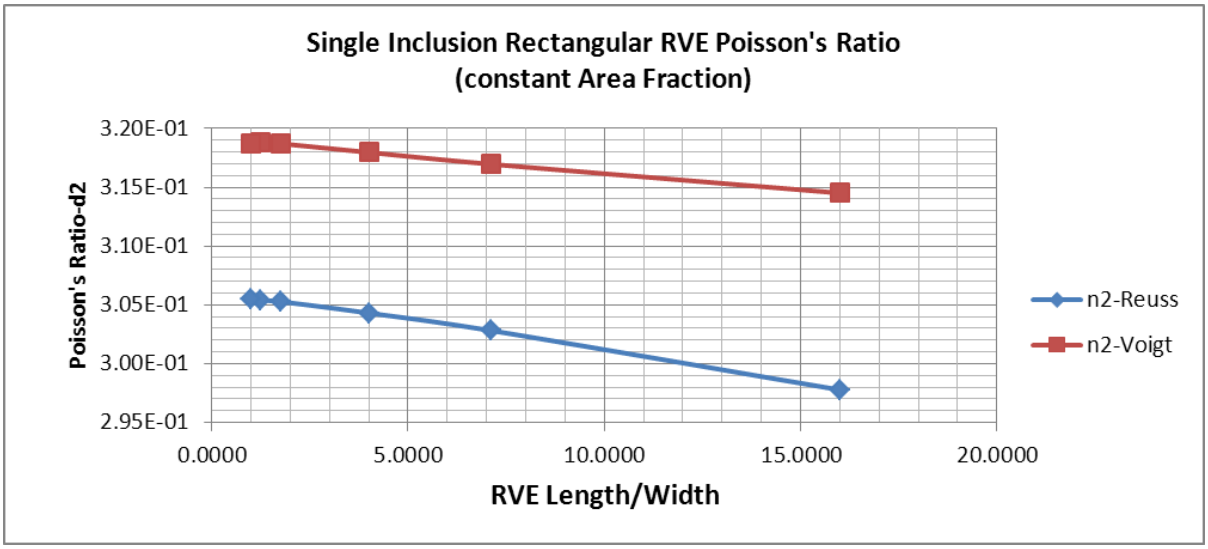

Diagram 34 - Single Inclusion Rectangular RVE Poisson's Ratio – Constant Area Fraction

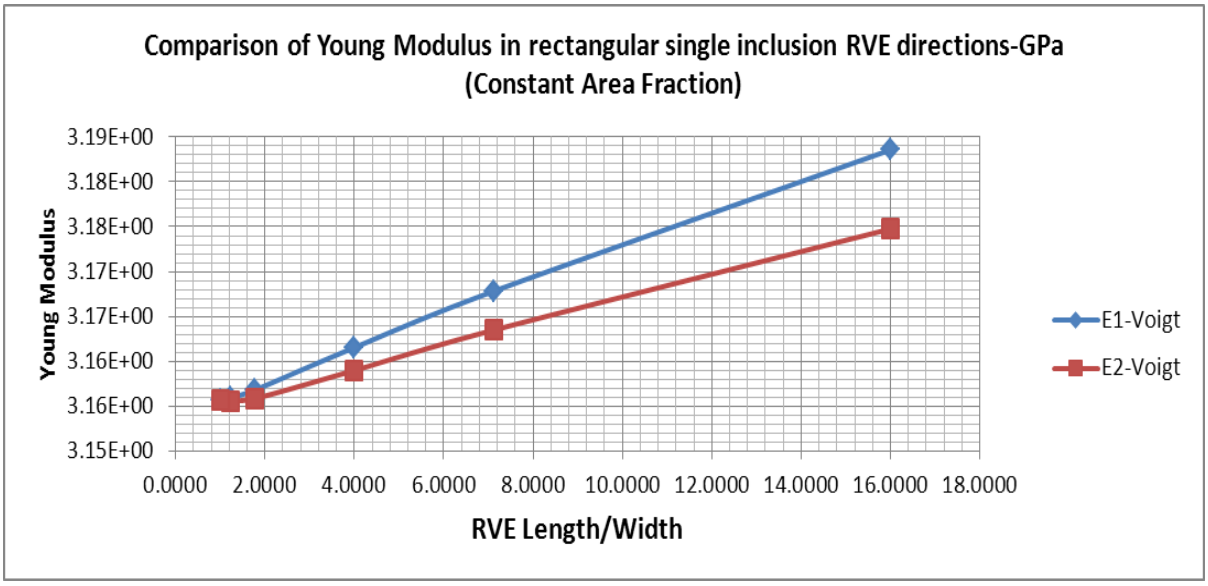

Diagram - 35 – Comparison of Asymmetric RVE Young Modulus – Constant Area Fraction – Voigt Bound

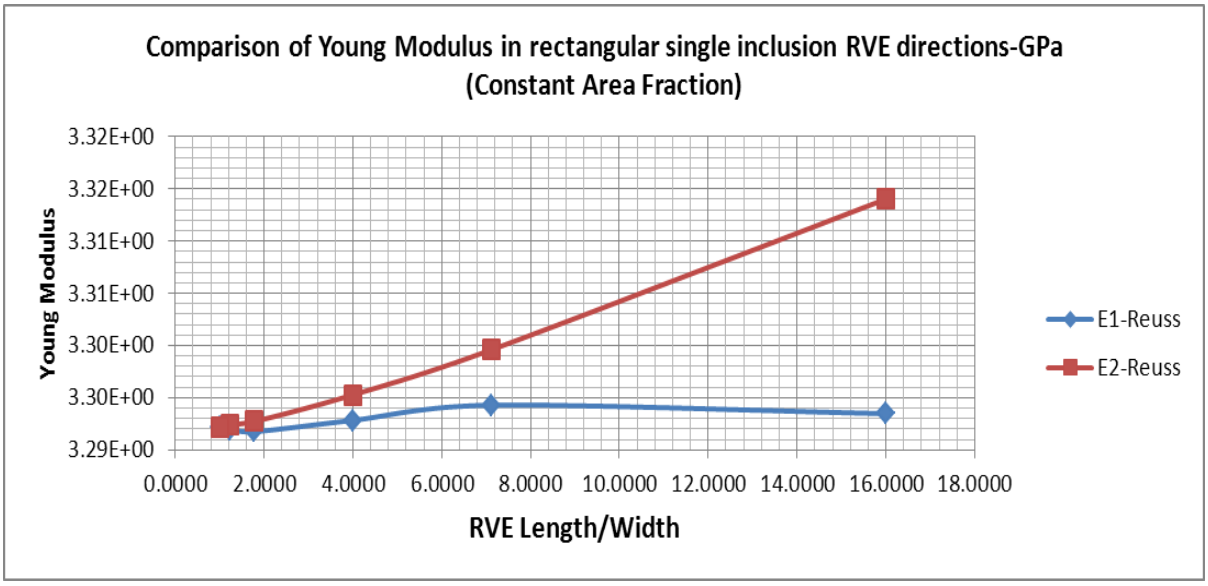

Diagram 36 - Comparison of Asymmetric RVE Young Modulus – Constant Area Fraction – Reuss Bound

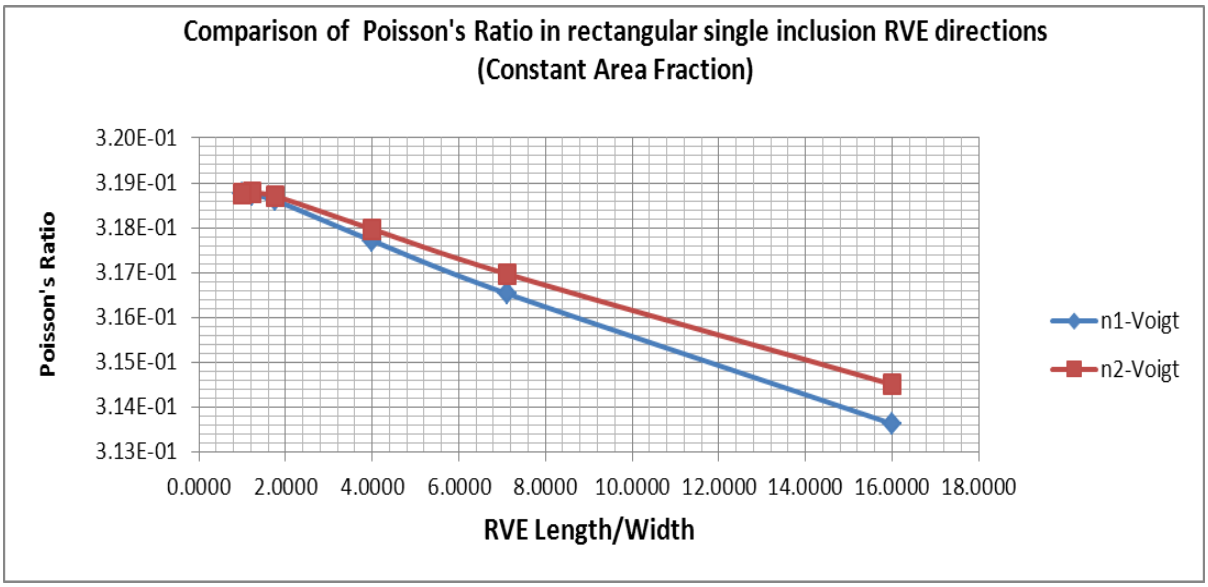

Diagram 37 - Comparison of Asymmetric RVE Poisson's Ratio – Constant Area Fraction – Voigt Bound

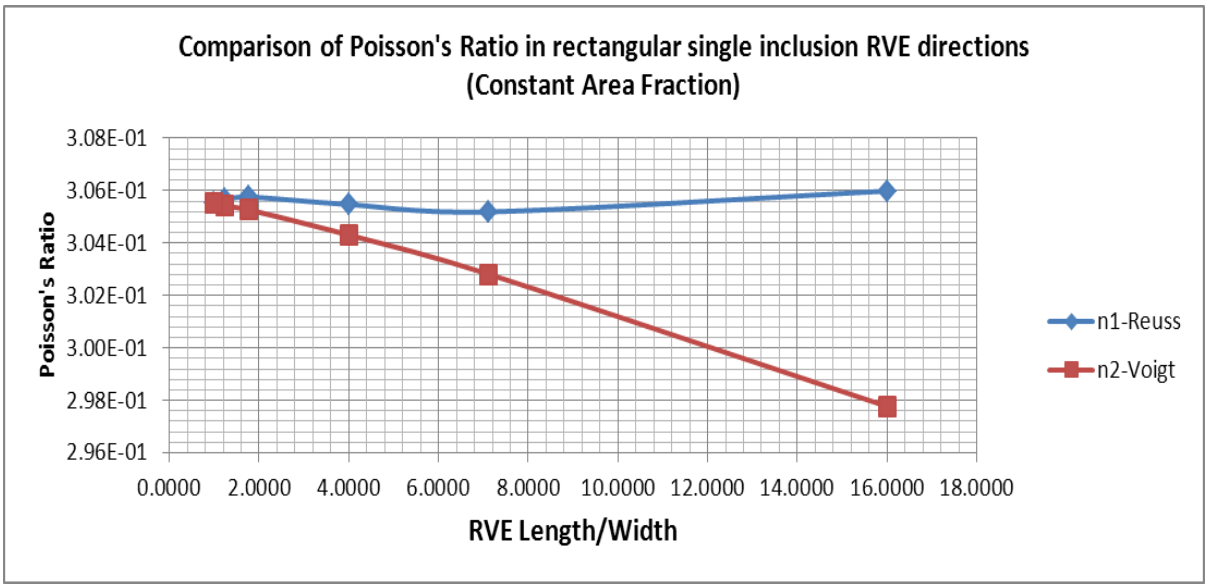

Diagram - 38 - Comparison of Asymmetric RVE Poisson's Ratio – Constant Area Fraction

The results show that, for a constant volume (area) fraction of inclusions, having larger ratios of RVE length to width or in practice larger distances between inclusions in their spreading model, the Young Modulus of the material is increased in both directions and the Poisson's Ratio is decreased in both directions. However the difference is quite negligible.

3.2.1.4. Multi-Inclusion RVE modeling

In this step RVE models are created with two or more inclusions. The RVE shape is squared and the inclusions spacing with respect to each other is precisely equal.

Two models are created, using two and four inclusions in a horizontal row.

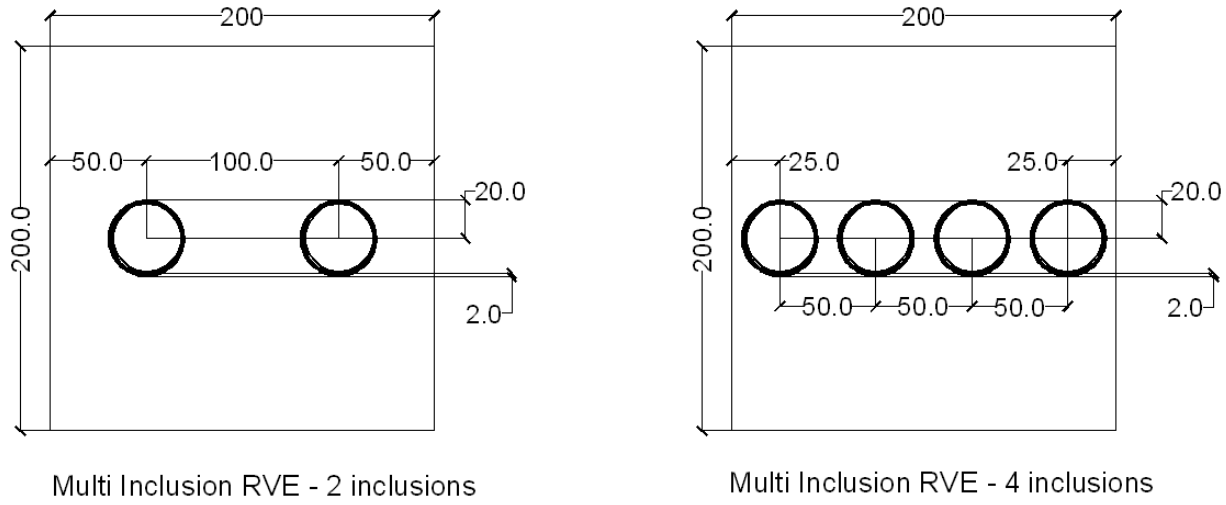

Figure 39 - Multi - Inclusion RVE Models

The results are given and used in the next step to validate the code results in case of multi material models.

3.2.1.5. Modeling tool (MEMSYS) validation; Multi-inclusion RVE - Asymmetric RVE

In the Tables 40 and 41 two groups of RVE models – each consisting of two RVE models – overall mechanical properties are shown. Each color shows one RVE group and every row of the Table 40 and 41 corresponds to the properties of one composite material. It can be seen that the area fraction of RVE models of the same group are equal. Based on the fundamental analytic definition of the overall mechanical properties of an RVE

model, the validity of MEMSYS results and the code functionality is verified up to a precise extent, in the next paragraph.

RVE			MEMSYS Voigt			
Length	Width/Length	Number of inclusions	*E1*	*E2*	*ni1*	*ni2*
200	1	4	3.0500E+00	3.0828E+00	3.5991E-01	3.5605E-01
200	0.25	1	3.0954E+00	3.0613E+00	3.5431E-01	3.5828E-01
200	1	2	3.1063E+00	3.1104E+00	3.3599E-01	3.3555E-01
200	0.5	1	3.1112E+00	3.1068E+00	3.3542E-01	3.3591E-01
RVE			**MEMSYS Reuss**			
Length	Width/Length	Number of inclusions	*E1*	*E2*	*ni1*	*ni2*
200	1	4	3.5380E+00	3.5548E+00	3.3034E-01	3.1883E-01
200	0.25	1	3.5722E+00	3.6709E+00	3.2653E-01	2.9035E-01
200	1	2	3.3789E+00	3.3775E+00	3.1077E-01	3.1134E-01
200	0.5	1	3.3803E+00	3.3856E+00	3.1122E-01	3.0875E-01

Table 40 - Multi Inclusion RVE overall properties

Considering the geometries of RVE models, the overall properties of the Multi-inclusion RVE in direction-2 (Vertical axis of RVE) should be equal to the overall properties of the asymmetric Single-inclusion RVE in direction-1 (Horizontal axis of RVE). The corresponding values are given below:

RVE			MEMSYS Voigt			
Length	Width/Length	Number of inclusions	*E1*	*E2*	*ni1*	*ni2*
200	1	4	3.0500E+00	3.0828E+00	3.5991E-01	3.5605E-01
200	0.25	1	3.0954E+00	3.0613E+00	3.5431E-01	3.5828E-01
200	1	2	3.1063E+00	3.1104E+00	3.3599E-01	3.3555E-01
200	0.5	1	3.1112E+00	3.1068E+00	3.3542E-01	3.3591E-01
RVE			**MEMSYS Reuss**			
Length	Width/Length	Number of inclusions	*E1*	*E2*	*ni1*	*ni2*
200	1	4	3.5380E+00	3.5548E+00	3.3034E-01	3.1883E-01
200	0.25	1	3.5722E+00	3.6709E+00	3.2653E-01	2.9035E-01
200	1	2	3.3789E+00	3.3775E+00	3.1077E-01	3.1134E-01
200	0.5	1	3.3803E+00	3.3856E+00	3.1122E-01	3.0875E-01

Table 41 - Multi Inclusion RVE overall Properties - Equivalent Models

In each table the results shown in the same color must match, as it is evident the Voigt results match perfectly while there are some minor differences for some of the Reuss bound results. This mismatch could be explained based on the error due to small ratio between the RVE length (width) and phase material element size as explained before. In the RVE model with its length equal to 200 μm and its width equal to 50 μm, this ratio is large and this results in results without desired precision. The remedy to avoid such results from these types of models is using Multi-Inclusion RVE models, in fact RVE length is increased and the geometry of such RVE models includes inclusions with their rather smaller sizes with respect to the RVE length. Thus the target ratio between the phase material size and the RVE length is reduced. To elaborate the concept more thoroughly, referring to the explanations regarding the computational procedure of homogenization [23] a composite material is a continuum in which a number of discrete homogeneous continua are bonded together. Considering length scale 'l' as microscale and any region of the heterogeneous body characterized by a length scale 'L' such that $l/L \ll 1$, which is then macroscopically seen as homogeneous [23]. The RVE length in investigated models in figure-39 stand for the length 'L' and the phase material size correspond to 'l'. The smaller is l/L ratio, the homogeneity of the macroscopic scale is more preserved and thus the homogenization results are expected to be more precise.

3.2.2. Models Inclusion Dispersion

Syntactic foams are fabricated by dispersing hollow microspheres in a matrix material with a twofold purpose: to embed closed cell porosity in the matrix, thus reducing the material density while controlling the size and distribution of the porosity; and to reinforce the matrix phase by using particles of a material stiffer than the matrix [8]. The "dispersion" of the inclusions in the matrix for manufacturing purposes gives a stochastic nature to the inclusions arrangement at its RVE scale level.

In this section such a stochastic dispersion is modeled in the computational approach using multi-Inclusion RVEs.

Figure-42 shows the stated randomness. The micrographs [9] show the presence of entrapped air or voids which are not considered in the current computational models by MEMSYS.

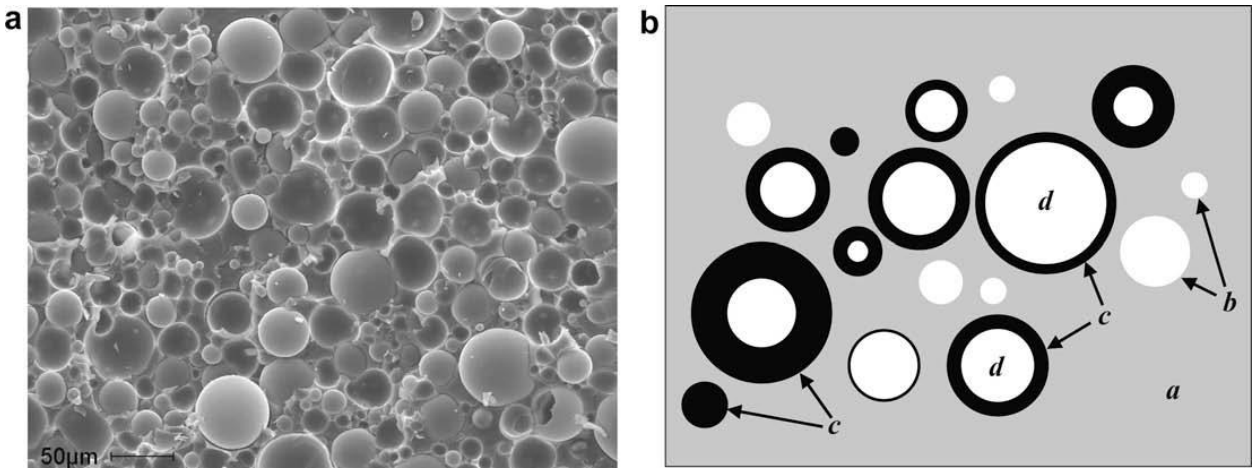

Figure 42 - (a) Micrograph and (b) schematic representation of the microstructure of typical syntactic foam. In (b), the different phases are shown, including 'a' matrix, 'b' voids, 'c' particles, and 'd' porosity enclosed inside the particle shell [8]

3.2.2.1 Multi-Inclusion RVE modeling with stochastic arrangement of inclusions

In this section, in order to represent a more realistic model of the composite material the arrangement of inclusion particle is assumed to be randomly chosen.

Considering the 4 inclusion model which was discussed the previous chapter, the coordination of each inclusion particle is randomly assigned by computational code. In the first step, the vertical coordinate is a random number and the horizontal one of the inclusion particle is as same as the 4 inclusion model shown in figure-38.

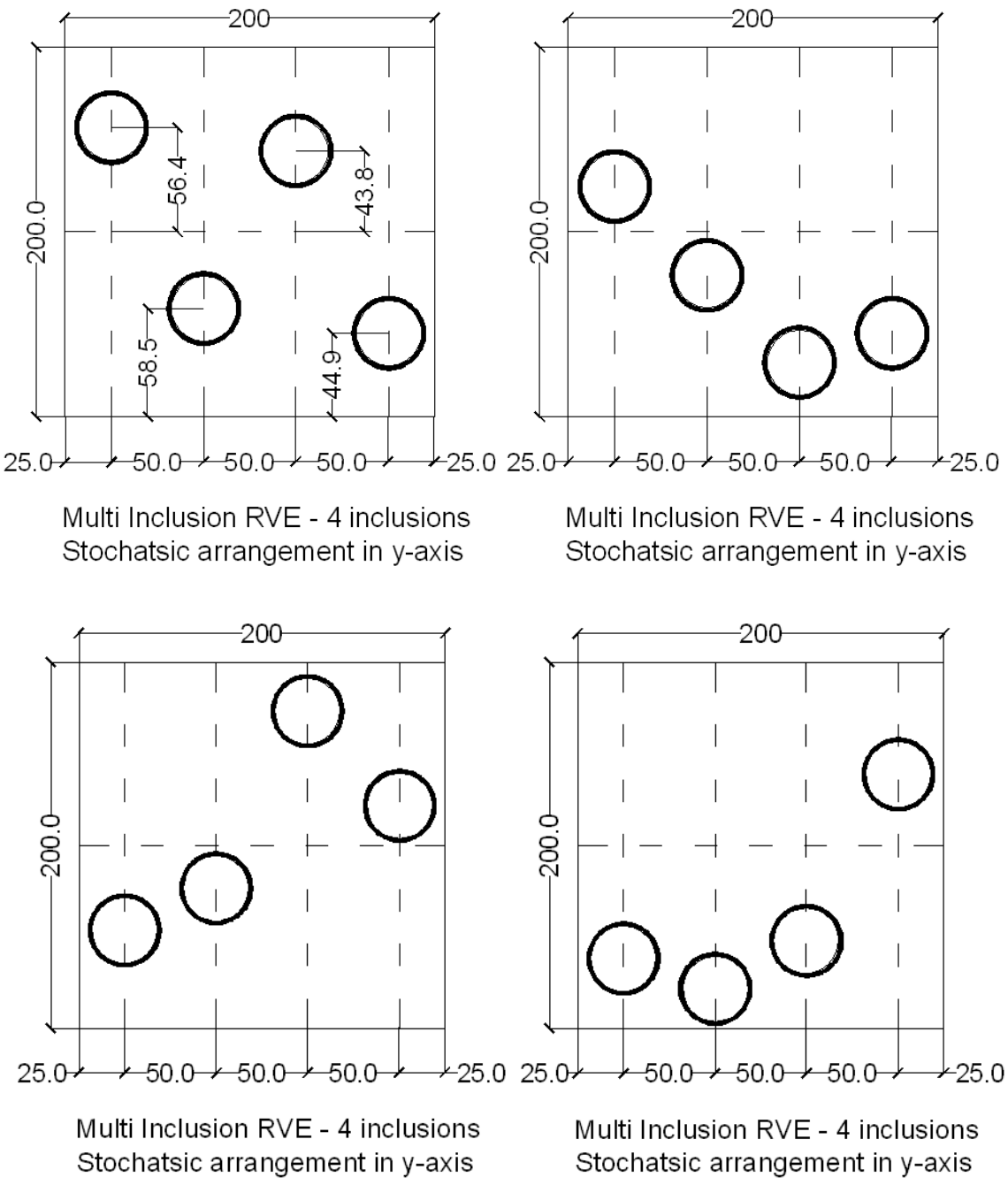

Figure 43 - RVE with stochastic arrangement of inclusions in y-axis

For sake of having an acceptable random field, 100 stochastic models are created and the results are categorized in 4 groups of 25 models, in order to compare the probabilistic values of each group instead of 100 models results and facilitate making conclusions. The overall properties of each model are derived using MEMSYS. Applying the probabilistic

calculations over the overall mechanical results of each group of 25 models, the average and standard deviation of every group is calculated, comparing the results of four groups in the Table-44 and Diagrams 46 and 47; it can be deduced the random dispersion of inclusions in the matrix doesn't affect its overall mechanical properties significantly.

Voigt	E1		E2		ni12		ni21	
N	Average	STdv	Average	STdv	Average	STdv	Average	STdv
1--25	3.01199	0.009325	3.027173	0.012336	0.368851	0.002031	0.36699	0.002402
26--50	3.007553	0.008359	3.020688	0.010297	0.369882	0.001766	0.368263	0.002012
51--75	3.011085	0.012123	3.023448	0.016823	0.369173	0.002731	0.367659	0.003293
75--100	3.012803	0.009662	3.025059	0.013604	0.368825	0.002122	0.367323	0.002608
Total	3.010858	0.010017	3.024092	0.013481	0.369183	0.0022	0.367558	0.002623
Reuss	**E1**		**E2**		**ni12**		**ni21**	
N	Average	STdv	Average	STdv	Average	STdv	Average	STdv
1--25	3.586401	0.011111	3.58069	0.007866	0.317655	0.002906	0.317967	0.001723
26--50	3.591666	0.009259	3.582789	0.006296	0.31617	0.002526	0.318095	0.001193
51--75	3.589919	0.015406	3.582681	0.010056	0.316713	0.004021	0.317933	0.001667
75--100	3.589019	0.010077	3.58118	0.006891	0.316722	0.002766	0.31825	0.001884
Total	3.589251	0.011684	3.581835	0.007841	0.316815	0.003107	0.318061	0.001617

Table 44 - Probabilistic Results of overall Properties of RVE Models with Stochastic Arrangement of Inclusions

**All the models have the same area fraction and inclusion properties, the changing parameters are the inclusions coordination in vertical direction.*

The models are categorized in groups with numeric codes as shown the Table –

Group	N
1	1--25
2	26--50
3	51--75
4	75--100

Figure 45 - Group Codes of RVE models with Stochastic Inclusion Arrangement

The following diagrams show the overall Young Modulus of the RVE in the horizontal direction (d1).

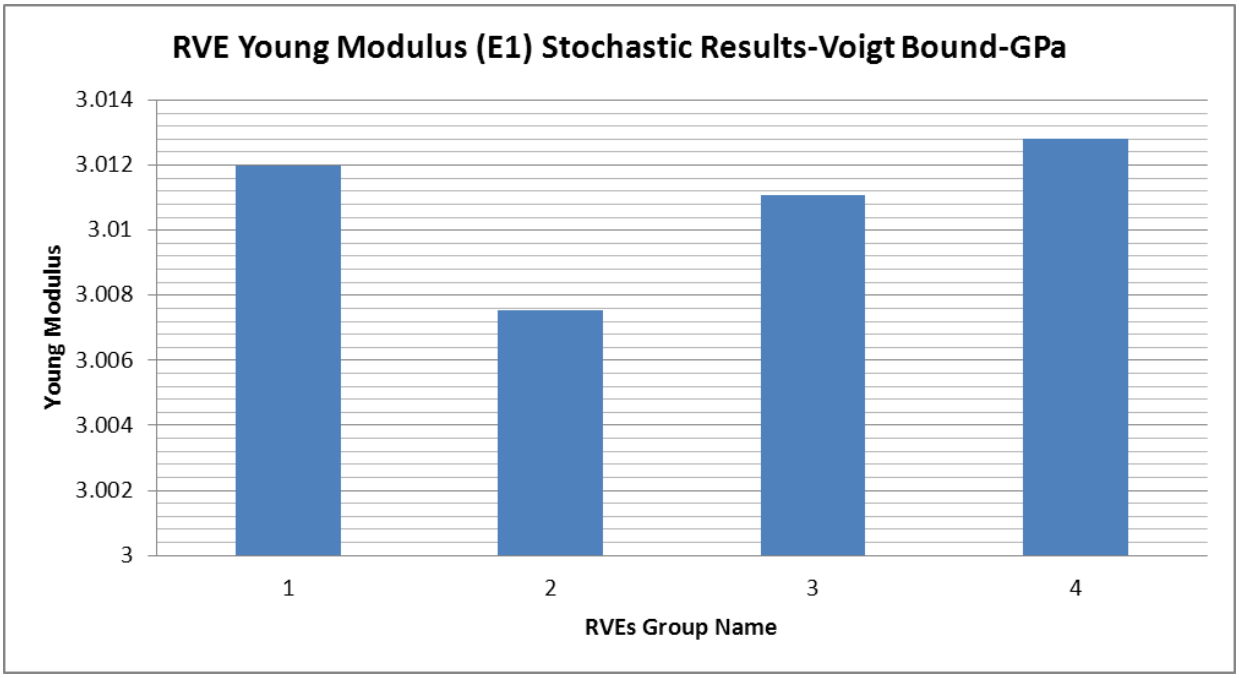

Diagram 46 - RVE Young Modulus (E1) - Stochastic Results - Voigt Bound

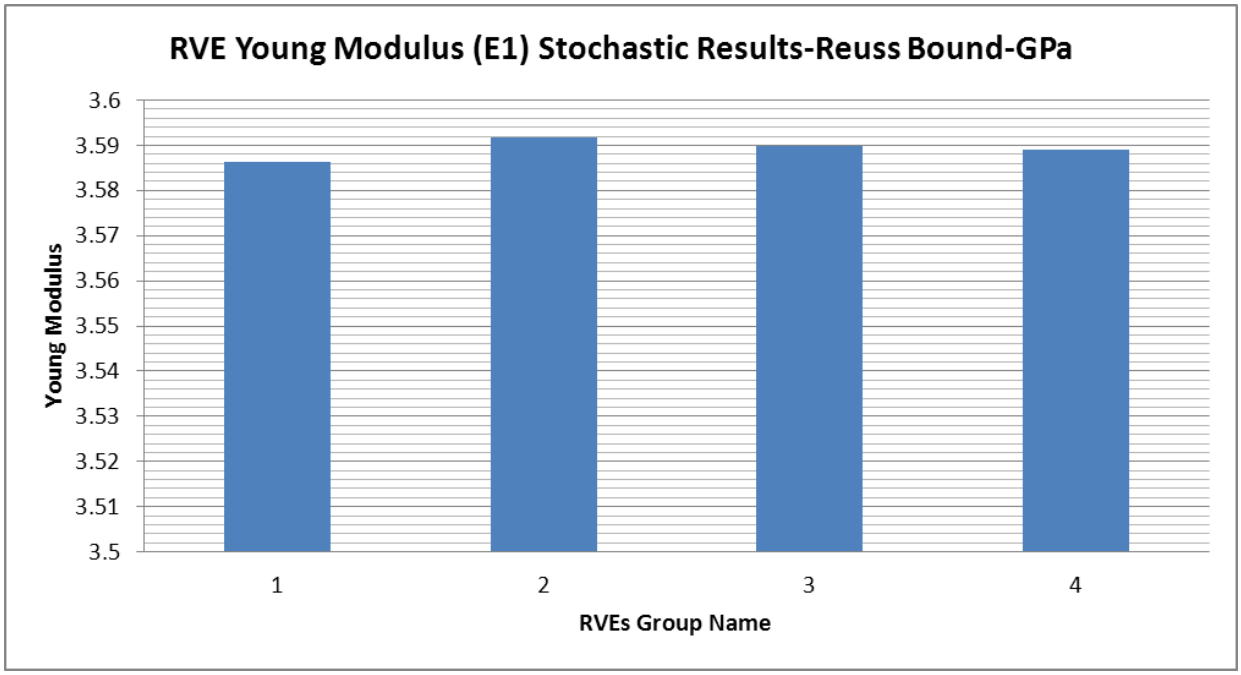

Diagram 47 - RVE Young Modulus (E1) - Stochastic Results - Reuss Bound

In the next step both vertical and horizontal coordinates are randomly assigned. This latter case is an RVE model which can represent the real case manufactured material micro-scale so precisely, from the point of view that is related to the inclusions dispersion in the composite matrix.

In this step, the former procedure is done for 4 groups of 100 models. Having a more number of models increases the level of certainty in the probabilistic model. Every group represents an RVE model with a different area fraction.

The area fractions 0.13, 0.22, 0.3 and 0.5 are chosen to represent wide range of the composite material diluteness. As it is evident in the Figure-48 the inclusions are present in the RVE with a low volume fraction with respect to the matrix with a large remaining area to accept more inclusions, while Figure-51 shows that there's no space to add any more inclusions due to the dense population of the inclusions in the RVE.

*For every group of 100 RVE models four photos of the stochastic arrangement is shown

Inclusion Area Fraction=0.13

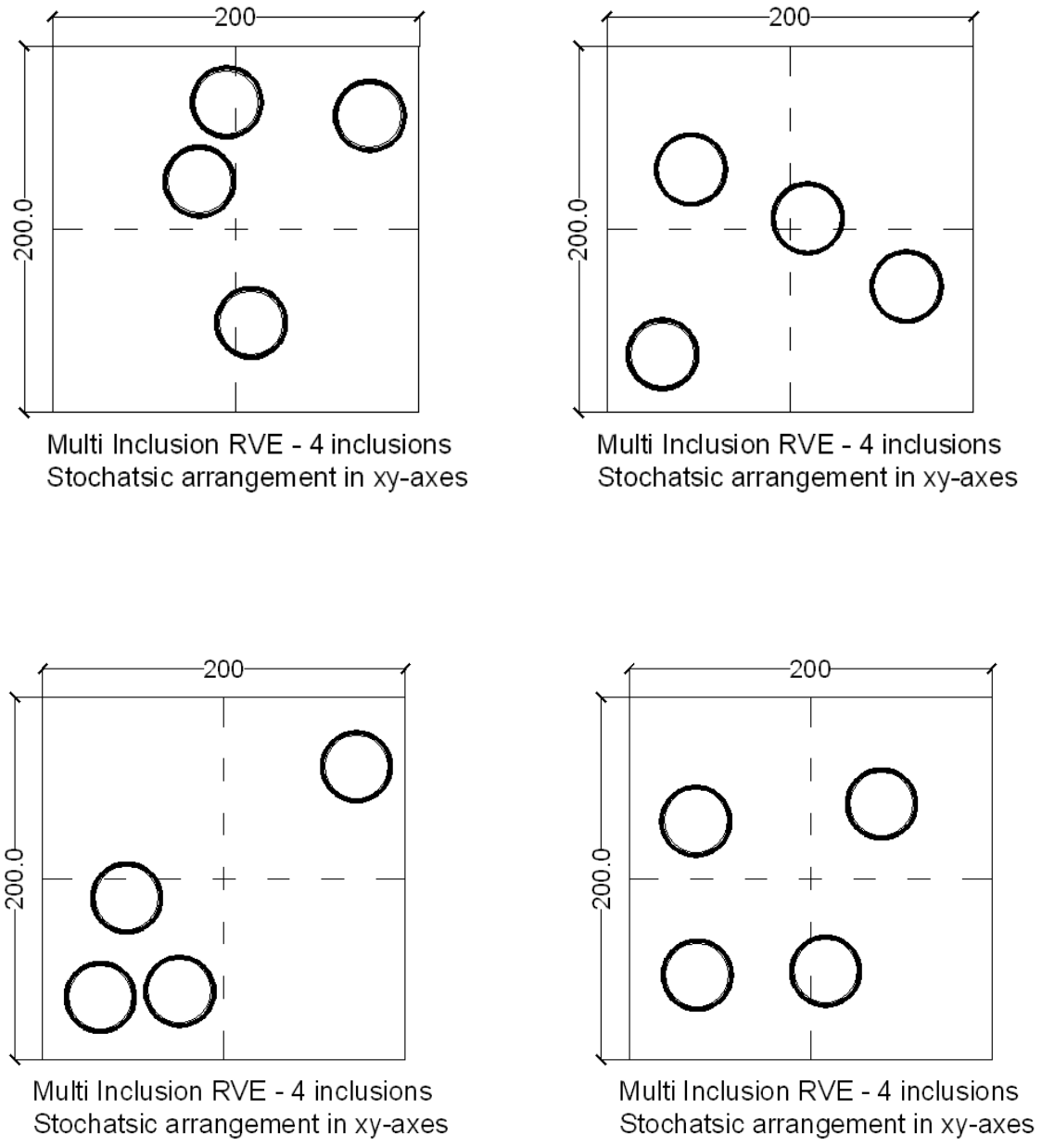

Figure 48 - RVE with stochastic arrangement of inclusions - Volume Fraction 13%

Inclusion Area Fraction=0.22

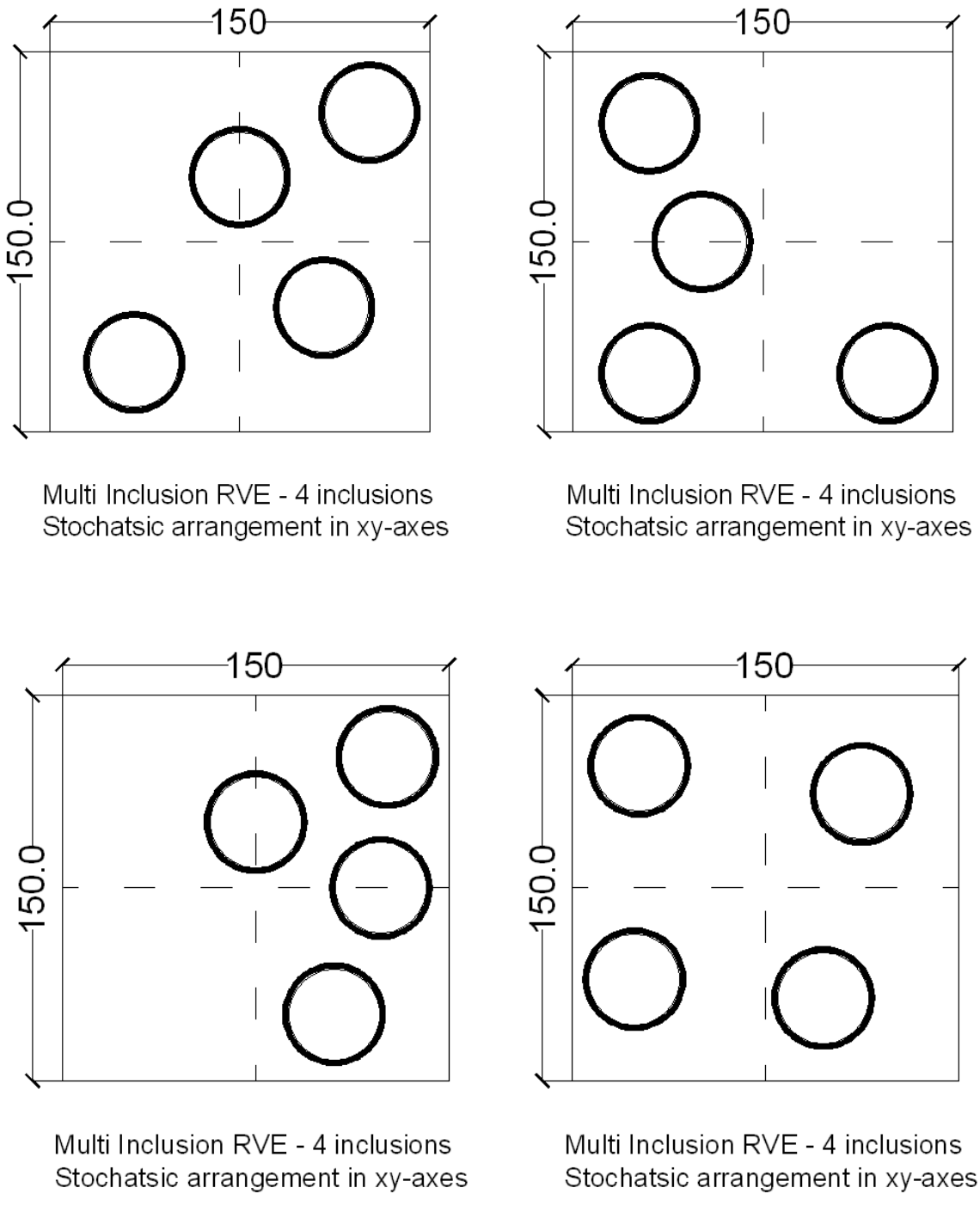

Figure 49 - RVE with stochastic arrangement of inclusions - Volume Fraction 22%

Inclusion Area Fraction=0.30

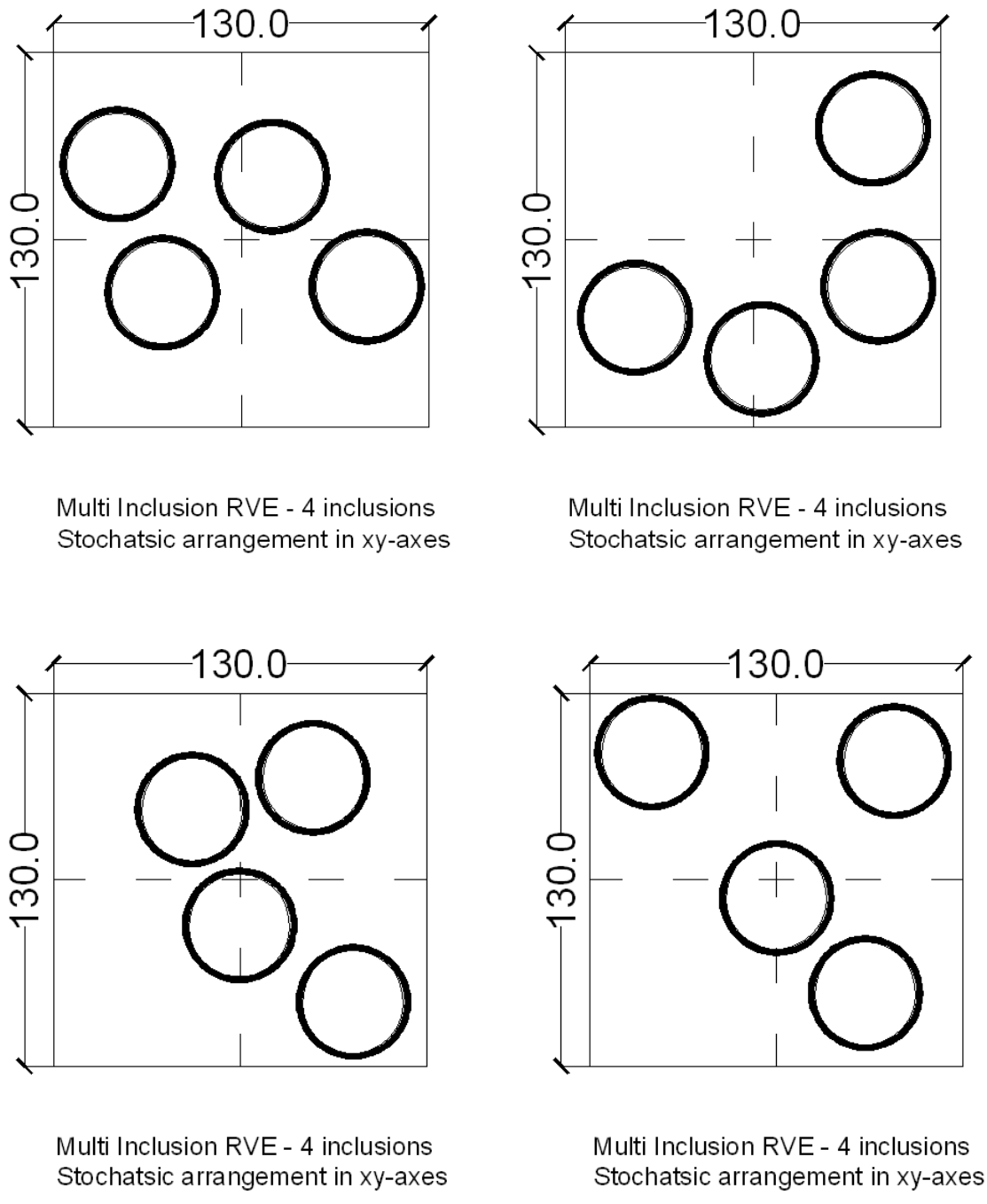

Figure 50 -RVE with stochastic arrangement of inclusions - Volume Fraction 30%

Inclusion Area Fraction=0.50

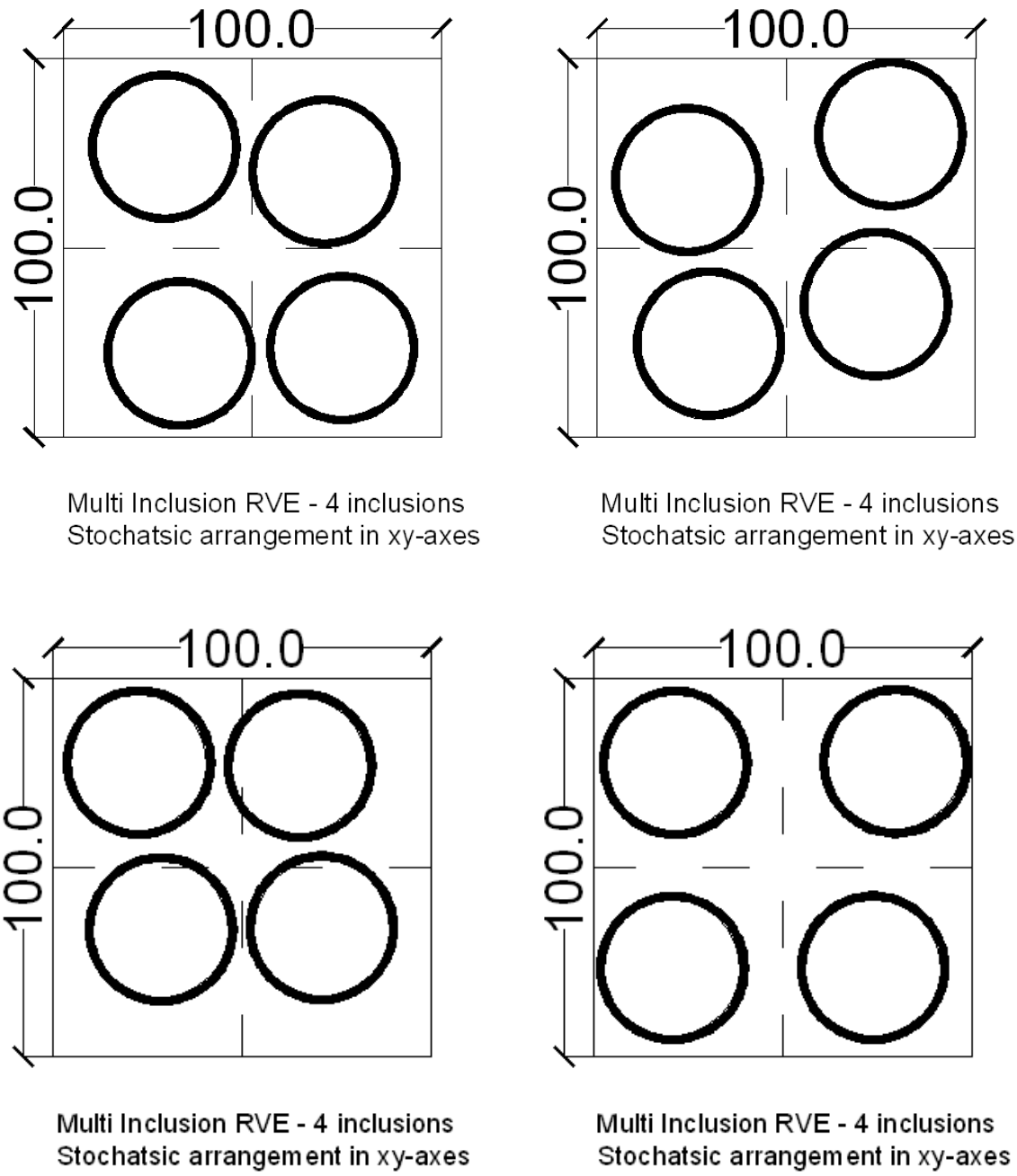

Figure 51 - RVE with stochastic arrangement of inclusions - Volume Fraction 50%

In fact there are 100 models for every "Area Fraction" of inclusions in the composite material. The models are categorized into 4 groups of 25. After deriving the results of the

overall mechanical parameters, the average and standard deviation values of each group of 25 models are calculated and compared to check the influence of the inclusions random. Then the average value of 100 models overall mechanical parameters is assumed as the representative value for that area fraction from a stochastic computational modeling procedure.

The probabilistic results of each volume fraction group of 100 models are shown below:

Area fraction = 0.5

Reuss	E1		E2		ni12		ni21	
N	Average	STdv	Average	STdv	Average	STdv	Average	STdv
1--25	5.414	0.036	5.417	0.034	0.403	0.010	0.402	0.010
26--50	5.436	0.030	5.420	0.041	0.399	0.008	0.404	0.010
51--75	5.425	0.032	5.419	0.036	0.401	0.008	0.403	0.009
75--100	5.426	0.045	5.440	0.032	0.403	0.011	0.399	0.009
Total	5.425	0.036	5.424	0.037	0.401	0.009	0.402	0.009
Voigt	**E1**		**E2**		**ni12**		**ni21**	
N	**Average**	**STdv**	**Average**	**STdv**	**Average**	**STdv**	**Average**	**STdv**
1--25	2.6906E+00	6.2896E-03	2.6903E+00	6.4225E-03	5.0314E-01	1.1452E-03	5.0318E-01	1.1718E-03
26--50	2.6867E+00	6.9657E-03	2.6868E+00	6.9923E-03	5.0384E-01	1.2851E-03	5.0384E-01	1.2898E-03
51--75	2.6881E+00	7.4923E-03	2.6881E+00	7.1950E-03	5.0359E-01	1.3763E-03	5.0358E-01	1.3177E-03
75--100	2.6866E+00	5.6166E-03	2.6867E+00	5.6729E-03	5.0386E-01	1.0256E-03	5.0384E-01	1.0367E-03
Total	2.6880E+00	6.7211E-03	2.6880E+00	6.6611E-03	5.0361E-01	1.2323E-03	5.0361E-01	1.2206E-03

Table 52 - Probabilistic results of RVE models with stochastic dispersion inclusions - Volume Fraction 0.5

Area fraction = 0.3

Reuss	E1		E2		ni12		ni21	
N	Average	STdv	Average	STdv	Average	STdv	Average	STdv
1--25	4.3270E+00	9.3371E-02	4.3325E+00	9.3846E-02	3.3747E-01	1.5925E-02	3.3605E-01	1.5370E-02
26--50	4.3212E+00	8.0289E-02	4.3101E+00	8.3189E-02	3.3689E-01	1.3510E-02	3.4107E-01	1.4608E-02
51--75	4.3123E+00	8.4799E-02	4.3195E+00	8.8168E-02	3.3974E-01	1.4764E-02	3.3776E-01	1.5448E-02
75--100	4.3011E+00	8.4590E-02	4.3081E+00	7.6982E-02	3.4212E-01	1.5257E-02	3.3946E-01	1.2847E-02
Total	4.3154E+00	8.5150E-02	4.3175E+00	8.5015E-02	3.3906E-01	1.4809E-02	3.3859E-01	1.4506E-02
Voigt	**E1**		**E2**		**ni12**		**ni21**	
N	**Average**	**STdv**	**Average**	**STdv**	**Average**	**STdv**	**Average**	**STdv**
1--25	2.7740E+00	4.4497E-02	2.7694E+00	4.8365E-02	4.5124E-01	8.8158E-03	4.5201E-01	9.4883E-03
26--50	2.7801E+00	4.1275E-02	2.7810E+00	3.9331E-02	4.4996E-01	8.1271E-03	4.4980E-01	7.7951E-03
51--75	2.7843E+00	4.1866E-02	2.7800E+00	4.3827E-02	4.4923E-01	8.2854E-03	4.4994E-01	8.6251E-03
75--100	2.7862E+00	4.3298E-02	2.7844E+00	4.1979E-02	4.4880E-01	8.5690E-03	4.4909E-01	8.3080E-03
Total	2.7811E+00	4.2364E-02	2.7787E+00	4.3204E-02	4.4981E-01	8.3763E-03	4.5021E-01	8.5158E-03

Table 53 - Probabilistic results of RVE models with stochastic dispersion inclusions - Volume Fraction 0.3

Area fraction = 0.22

Reuss	E1		E2		ni12		ni21	
N	Average	STdv	Average	STdv	Average	STdv	Average	STdv
1--25	3.9672E+00	4.1592E-02	3.9697E+00	4.3776E-02	3.3003E-01	8.3869E-03	3.2878E-01	8.6955E-03
26--50	3.9497E+00	3.5104E-02	3.9556E+00	3.4968E-02	3.3361E-01	7.0861E-03	3.3082E-01	7.3536E-03
51--75	3.9640E+00	4.4332E-02	3.9600E+00	3.8245E-02	3.2970E-01	9.2282E-03	3.3105E-01	7.3099E-03
75--100	3.9748E+00	3.2038E-02	3.9799E+00	3.3822E-02	3.2886E-01	6.8534E-03	3.2691E-01	7.2695E-03
Total	3.9639E+00	3.9077E-02	3.9663E+00	3.8490E-02	3.3055E-01	8.0371E-03	3.2939E-01	7.7498E-03
Voigt	**E1**		**E2**		**ni12**		**ni21**	
N	**Average**	**STdv**	**Average**	**STdv**	**Average**	**STdv**	**Average**	**STdv**
1--25	2.8652E+00	3.3295E-02	2.8670E+00	3.6073E-02	4.1902E-01	6.7745E-03	4.1877E-01	7.1921E-03
26--50	2.8733E+00	2.9678E-02	2.8759E+00	2.8174E-02	4.1734E-01	5.9189E-03	4.1695E-01	5.6785E-03
51--75	2.8747E+00	3.4656E-02	2.8750E+00	3.4927E-02	4.1714E-01	6.9732E-03	4.1710E-01	7.0045E-03
75--100	2.8579E+00	2.7680E-02	2.8561E+00	2.7534E-02	4.2061E-01	5.5591E-03	4.2088E-01	5.5459E-03
Total	2.8678E+00	3.1707E-02	2.8685E+00	3.2430E-02	4.1853E-01	6.3942E-03	4.1842E-01	6.4995E-03

Table 54 - Probabilistic results of RVE models with stochastic dispersion inclusions - Volume Fraction 0.22

Area fraction = 0.13

Reuss	E1		E2		ni12		ni21	
N	Average	STdv	Average	STdv	Average	STdv	Average	STdv
1--25	3.5832E+00	1.2283E-02	3.5807E+00	9.1042E-03	3.1817E-01	3.6213E-03	3.1943E-01	2.2867E-03
26--50	3.5819E+00	1.3829E-02	3.5830E+00	1.2014E-02	3.1902E-01	3.6167E-03	3.1842E-01	2.9559E-03
51--75	3.5825E+00	1.1291E-02	3.5780E+00	1.3907E-02	3.1810E-01	2.5261E-03	3.2028E-01	3.5907E-03
75--100	3.5775E+00	1.0946E-02	3.5782E+00	1.2075E-02	3.1965E-01	3.1043E-03	3.1955E-01	3.5637E-03
Total	3.5813E+00	1.2161E-02	3.5800E+00	1.1897E-02	3.1873E-01	3.2631E-03	3.1942E-01	3.1673E-03
Voigt	**E1**		**E2**		**ni12**		**ni21**	
N	**Average**	**STdv**	**Average**	**STdv**	**Average**	**STdv**	**Average**	**STdv**
1--25	3.0088E+00	1.2578E-02	3.0065E+00	1.4325E-02	3.7018E-01	2.6182E-03	3.7047E-01	2.8522E-03
26--50	3.0073E+00	1.7168E-02	3.0073E+00	1.8781E-02	3.7038E-01	3.5431E-03	3.7038E-01	3.7474E-03
51--75	3.0096E+00	2.0549E-02	3.0084E+00	1.7526E-02	3.6997E-01	4.1079E-03	3.7010E-01	3.7186E-03
75--100	3.0139E+00	1.3036E-02	3.0121E+00	1.3488E-02	3.6909E-01	2.6876E-03	3.6931E-01	2.7463E-03
Total	3.0099E+00	1.6109E-02	3.0086E+00	1.6077E-02	3.6991E-01	3.2853E-03	3.7007E-01	3.2813E-03

Table 55 - Probabilistic results of RVE models with stochastic dispersion inclusions - Volume Fraction 0.13

Checking the average values of four groups in the Tables 52, 53, 54 and 55 it is evident that the composite material (RVE) Young Modulus and Poisson's Ratio don't change considerably as a result of the inclusions arrangement change over the RVE. This leads to the *Statistical Homogeneity* of composite introduced overall properties (Young Modulus and Poisson's Ratio) with respect to the inclusions arrangement.

*If any possible RVE of a composite material has the same properties then the composite material is *Statistically Homogeneous*. [23]

The diagrams 56 and 57 compare the results which were obtained from single inclusion models and the stochastic models of the same area fraction.

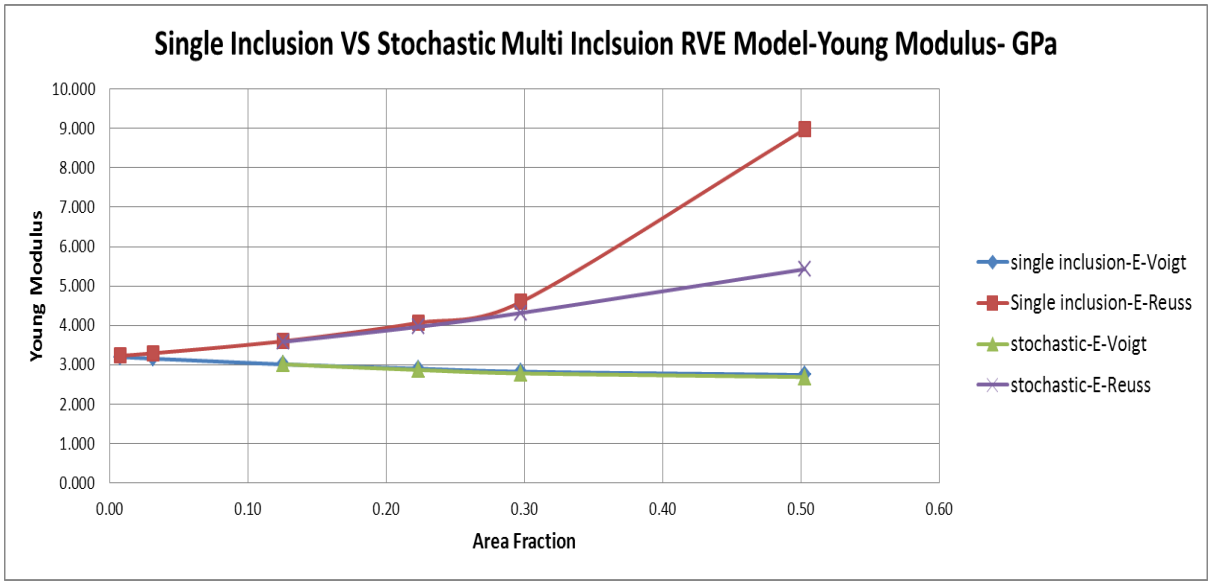

Diagram 56 – Young Modulus - Single Inclusion VS Stochastic Multi Inclusion RVE model

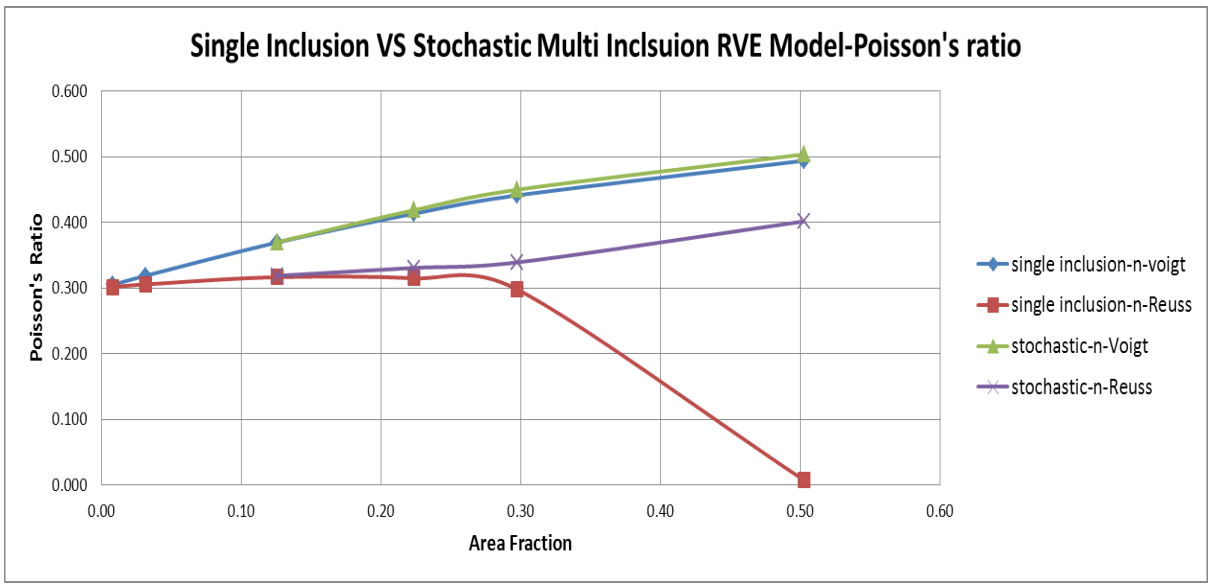

Diagram 57 – Poisson's ratio - Single Inclusion VS Stochastic Multi Inclusion RVE model

Diagrams 58 and 59 compare the results which were obtained from analytic estimation of overall properties and the stochastic models of the same area fraction.

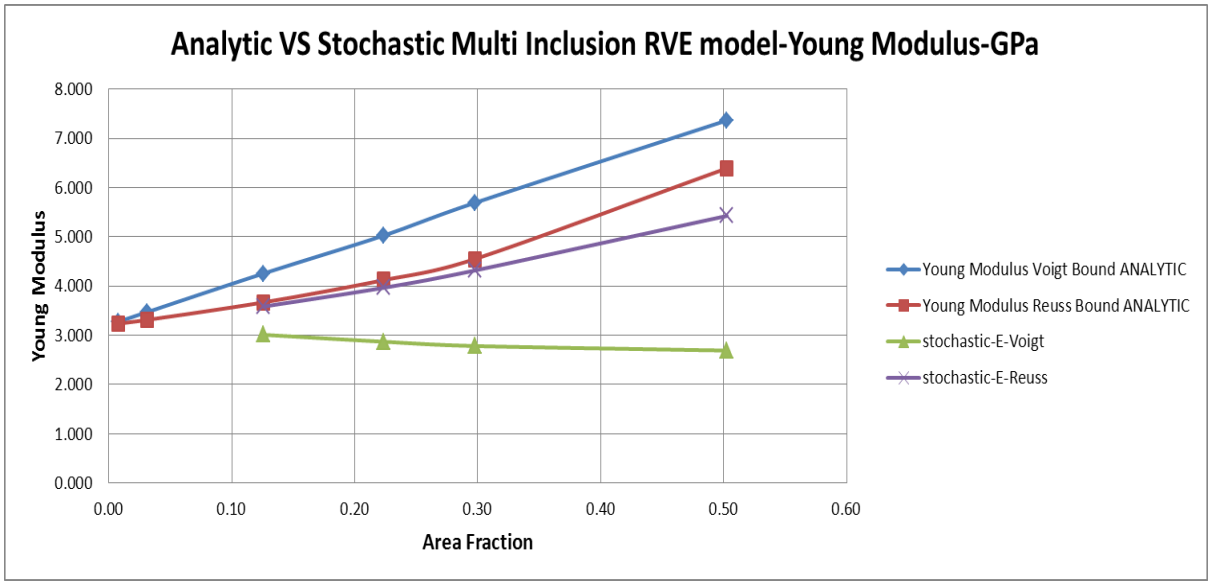

Diagram 58 - Young Modulus - Analytic VS Stochastic Multi Inclusion RVE model

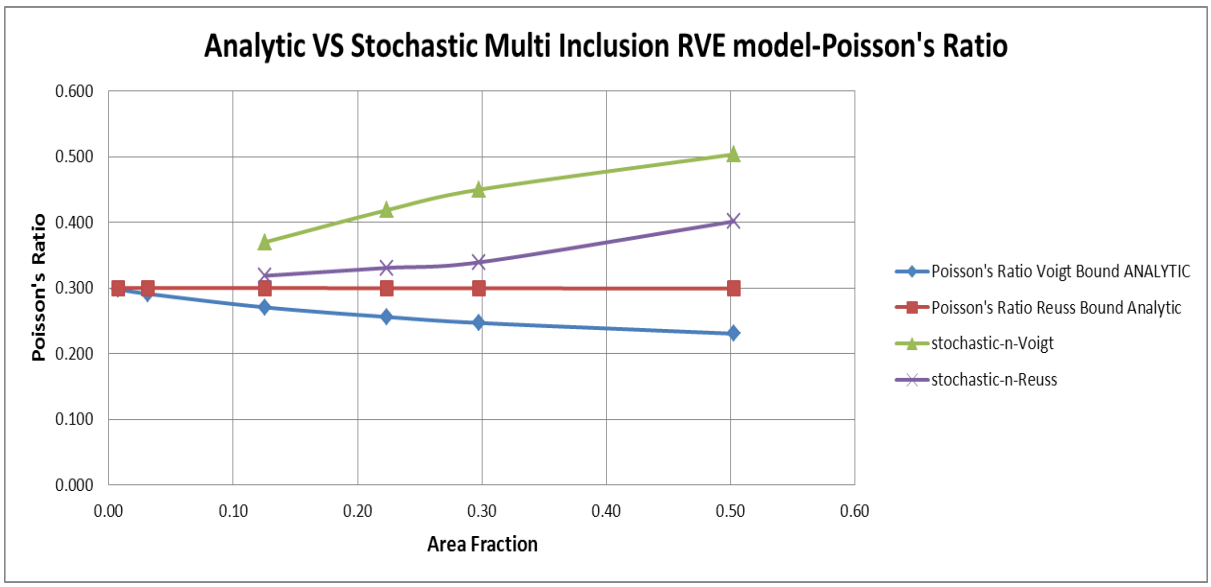

Diagram 59 - Poisson's Ratio - Analytic VS Stochastic Multi Inclusion RVE model

Diagrams 60 and 61 compare the results which were obtained from single inclusion models and the analytic bounds.

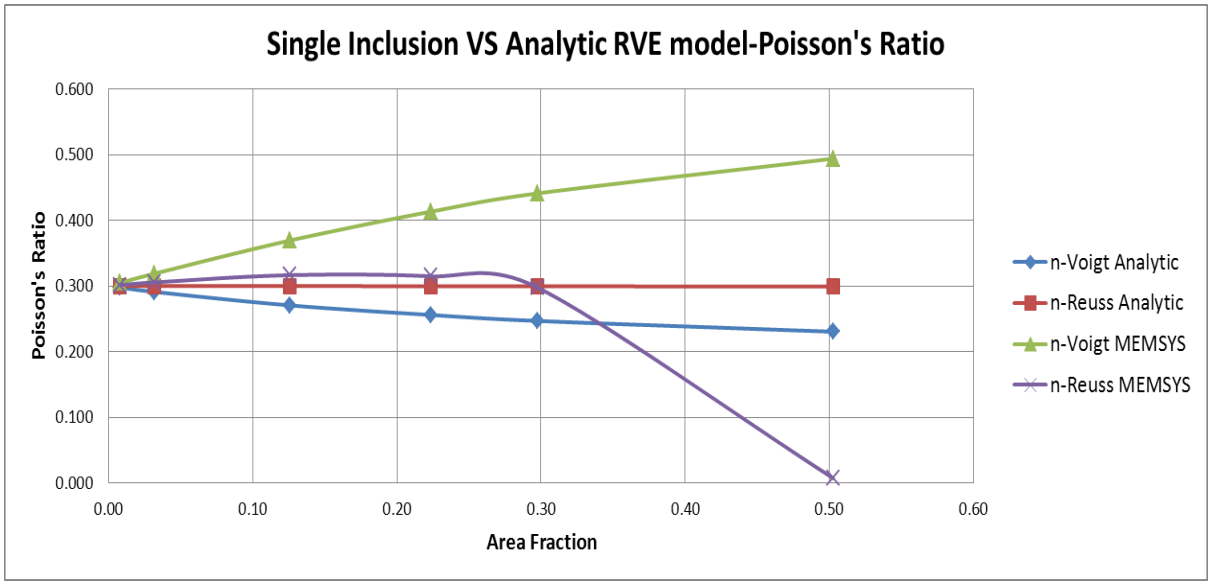

Diagram 60 – Poisson's Ratio - Analytic VS Single Inclusion RVE model

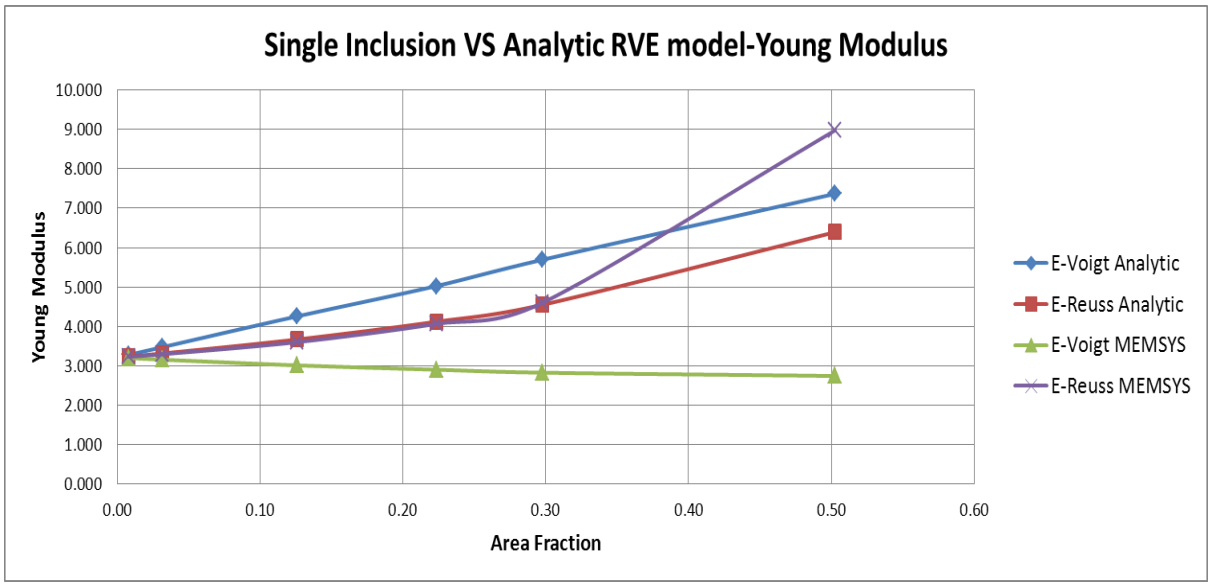

Figure 61 – Young Modulus - Analytic VS Single Inclusion RVE model

Diagram-62 [28] which shows Homogenized analytic and numerical values of Young Modulus of syntactic composite made of different inclusion types which are introduced in Figure-19 is used as a benchmark to compare the MEMSYS homogenization results. The comments and concluding remarks are given at the end of this section.

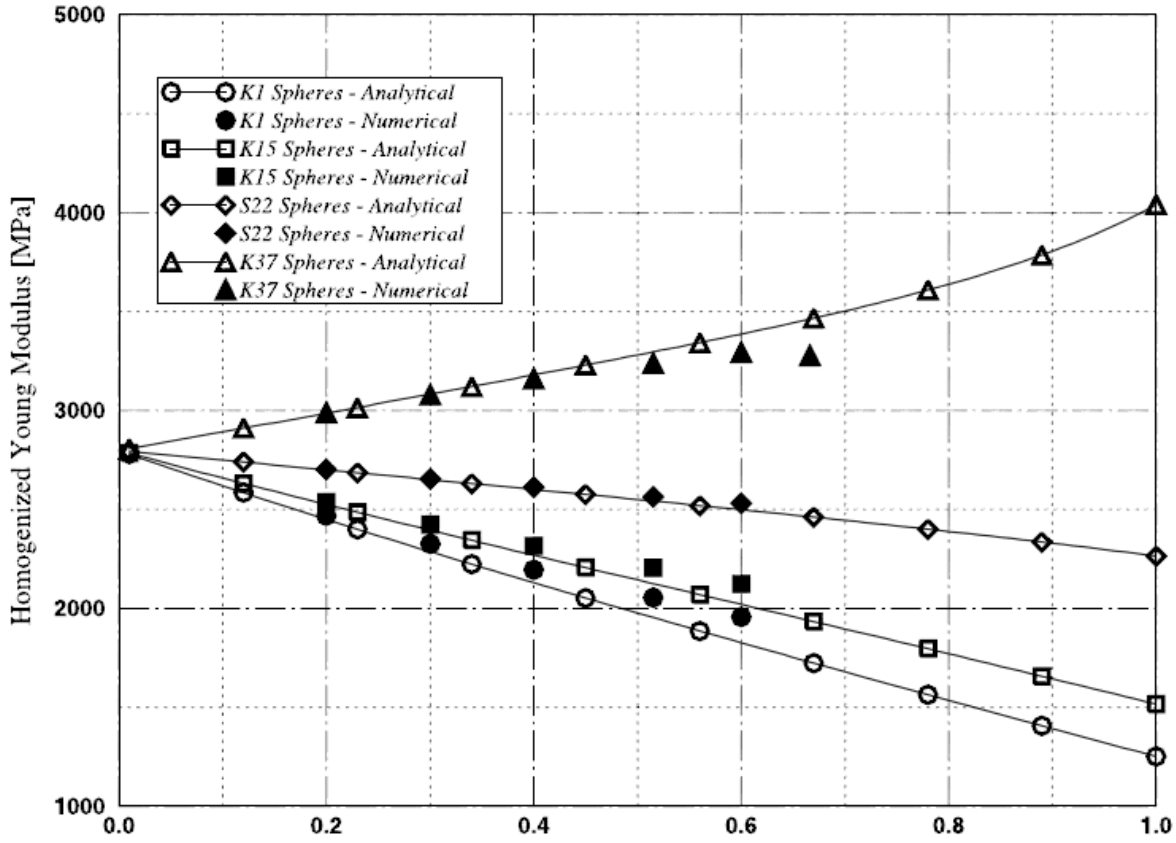

Diagram 62 – Homogenized Young Modulus of Syntactic Foams as a Function of Inclusion Volume Fraction and Inclusion Type [28]

Diagrams 63 and 64 compare the average results which were obtained from single inclusion models and the average results of the stochastic models of the same area fraction.

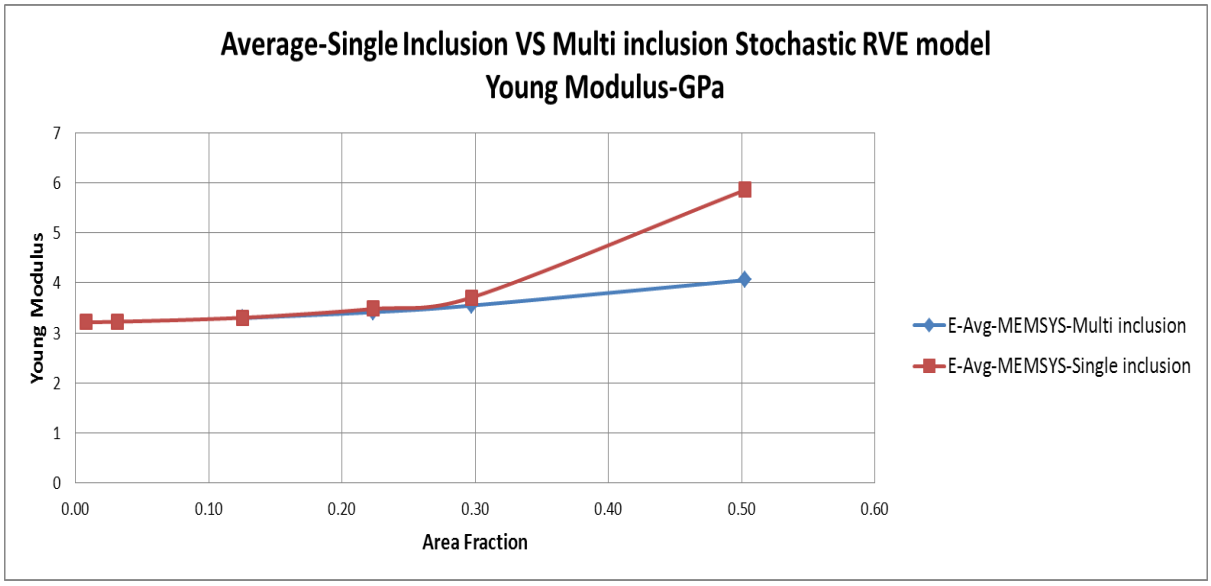

Diagram 63 – Average Values of Homogenization Bounds - Young Modulus – MEMSYS

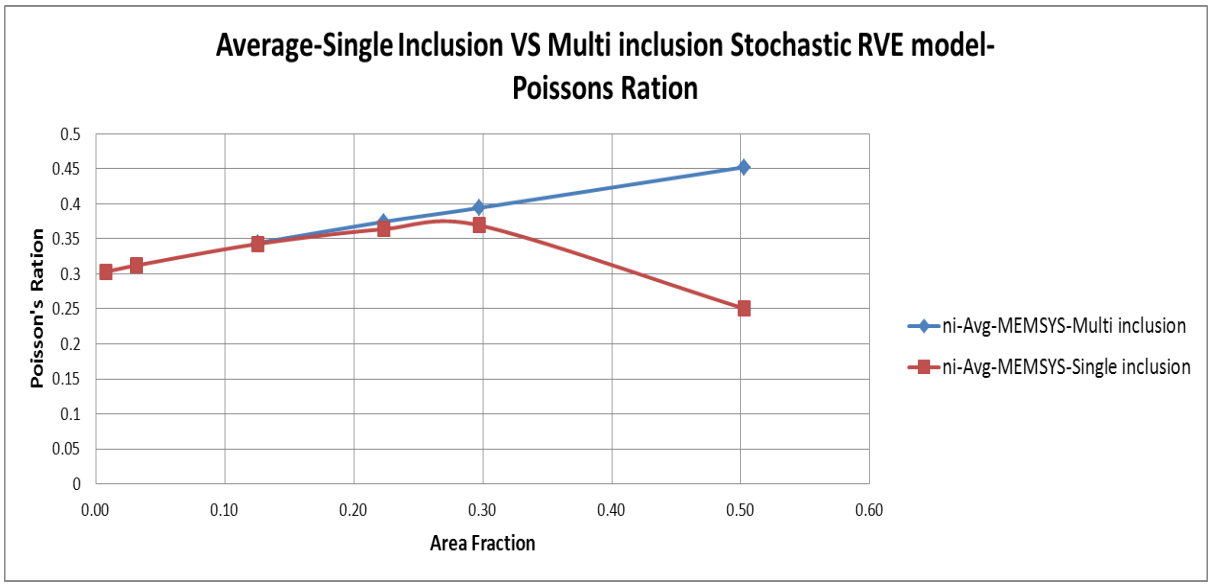

Diagram 64 - Average Values Homogenization Bounds - Poisson's Ratio Bounds – MEMSYS

Reviewing the Diagrams 56 and 57, the significant change with respect to the Single-Inclusion model results which were given in chapter 3.2.1 is the correction of the Reuss bound results by using multi-inclusion results. In multi-inclusion RVE models results, the visible deviation of results due to area fraction transgress over 30% is not visible anymore and the results follow the expected path. This is in fact a result of resolving the problem of largeness of the ratio between the phase material size over the RVE length (width). Using Multi-Inclusion RVE, the RVE length becomes larger with respect to the phase material specific size (i.e. inclusion membrane thickness) and the ratio falls within an acceptable range. This issue is well-explained in 3.2.1.5.

Diagram-64 shows the average of Young Modulus Voigt and Reuss bounds for multi-inclusion RVEs. The inclusion used in these models has a nominal density of 710 kg/cm^3 as stated in Table-20. Diagram-62 shows the numerical results of homogenization of syntactic foams made of standard inclusions – Table-19. Comparing the inclusion used in the MEMSYS models with the ones used in models with their Young Moduli stated in Diagram-62, the most similar inclusion to the one used in MEMSYS models with nominal density of 710 kg/cm^3 is K37.

Comparing the MEMSYS results in Diagram 64, with numerical results of the syntactic foam made of inclusion code K37 in Diagram 62, the increasing trend of the Young Modulus as a result of inclusion volume fraction increase, is evident in both models. The values of Young Modulus resulted from MEMSYS models, with inclusions having a nominal density of 710 kg/cm^3 are around 10% more than those of K37 numerical results. This could be explained based on the thicker membrane –Table-20- of MEMSYS models inclusions with respect to K37 which makes the composite stiffer. The effect of inclusions thickness is investigated thoroughly in section 3.2.3.

3.2.3. Inclusion membrane thickness ratio

Overall mechanical properties of Syntactic Foams also depend on the hollow particulate inclusion membrane thickness. In industrial forms the common values of the inclusion thickness ranges between 5 μm to 25 μm [8]. While in theory there could be inclusions even without any inner void part. Thus, the effect of inclusion membrane thickness on the overall properties of syntactic foam RVEs is investigated in the following [7].

3.2.3.1. Single Inclusion RVE Modeling with different Inclusion Thickness Ratio Inclusion

As it was explained, other than inclusion volume (area) fraction, the other key parameter in the overall parameters of a composite material is the wall (membrane) thickness of the inclusions [7]. This issue is investigated by creating single inclusion models for inclusions with different wall thickness. A series of inclusions with different wall thicknesses are adopted for two RVE sizes which result in two composite models with inclusion area fractions equal to 0.13 and 0.03. The inclusion area fraction equal to 0.13 is adopted as a common value and the area fraction equal to 0.03 is a rather comparable model to the infinitely dilute RVE model explained by Mariani et al. [7]. The concept of infinitely dilute RVE model in theory is a single particle in an infinite matrix medium [7]. The infinite matrix medium in this thesis is approximately substituted with a RVE size 200 μm and a common inclusion with a diameter equal to 40 μm, which corresponds to the composite material model with area fraction equal to 0.03.

Inclusion thickness ratio is the independent parameter which stands for:

$$\eta = \frac{R_{int}}{R_{ext}}$$

In the article by Porfiri et al. [7] the wall thickness ratio is considered the same while the diagrams are set as a function of the independent parameter (1-η).

Therefore, the evolution of η from 0 towards 1, means a transition from a non-hollow fully filled inclusion towards a void of 40 μm diameter. Referring to Table-19 and 20, it is noteworthy to highlight that the diameter of a common particulate inclusion is 40 μm.

Analytic results are calculated using the MATLAB code which is given in the Appendix - B, the diagrams of the stated results are rendered in order to be used as a benchmark for the computational results.

Inclusion Area Fraction=0.13

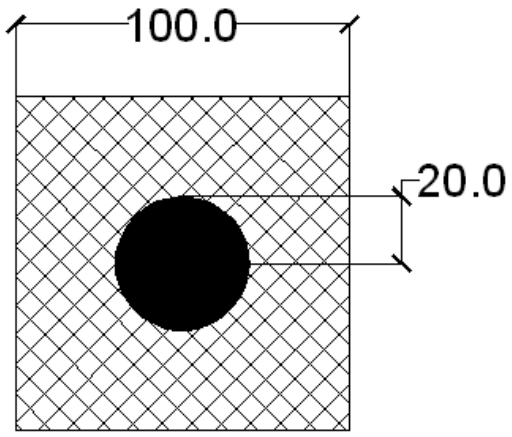

Inclusion thickness ratio: 0

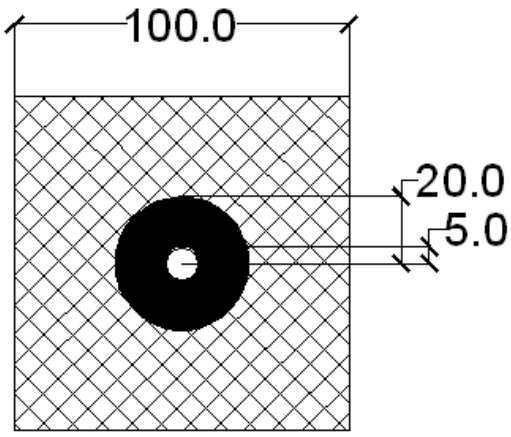

Inclusion thickness ratio: 0.25

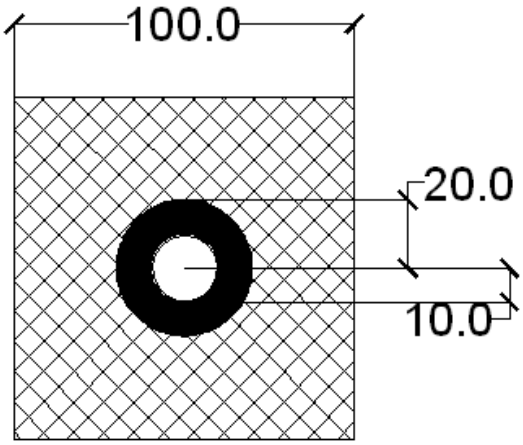

Inclusion thickness ratio: 0.5

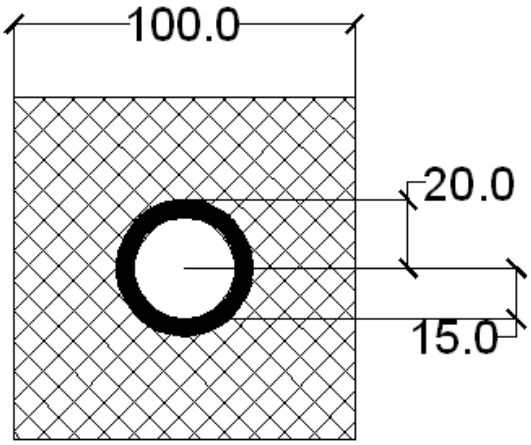

Inclusion thickness ratio: 0.75

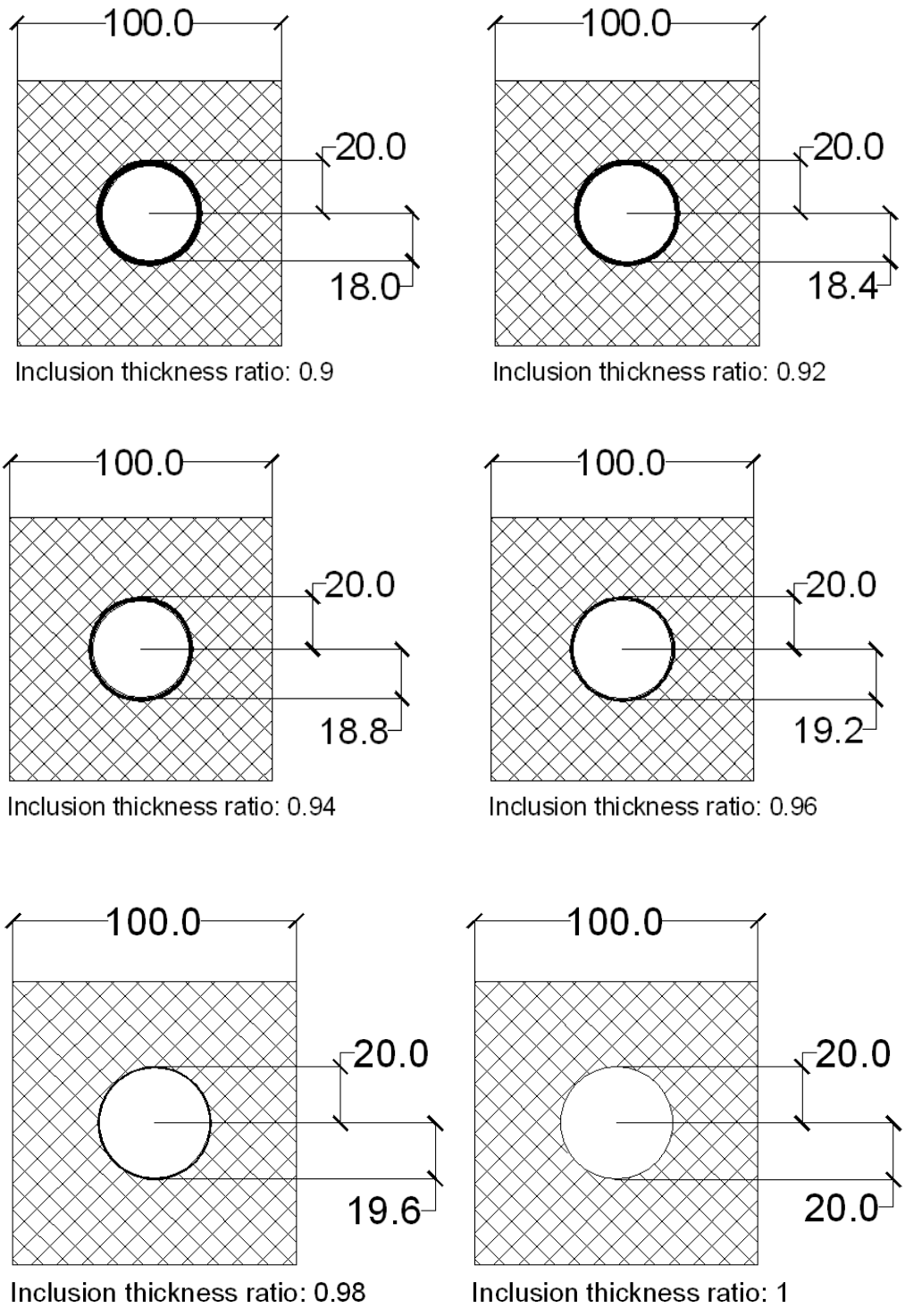

Figure 65 - RVEs with different inclusion wall thickness - Volume Fraction 13%

Inclusion Area Fraction=0.03

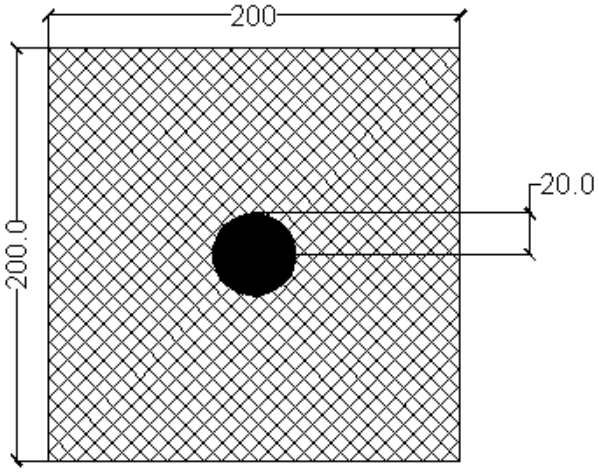

Inclusion thickness ratio: 0

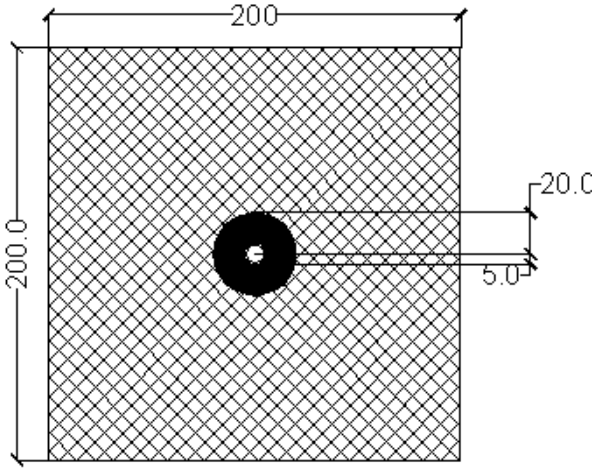

Inclusion thickness ratio: 0.25

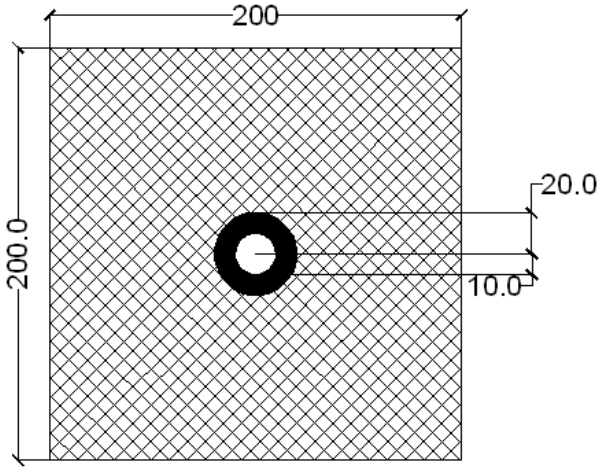

Inclusion thickness ratio: 0.5

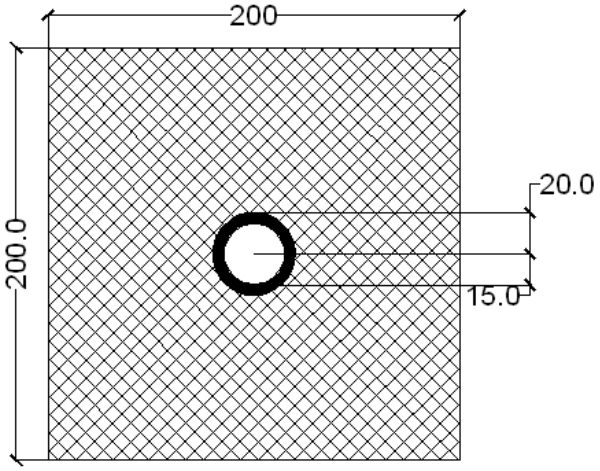

Inclusion thickness ratio: 0.75

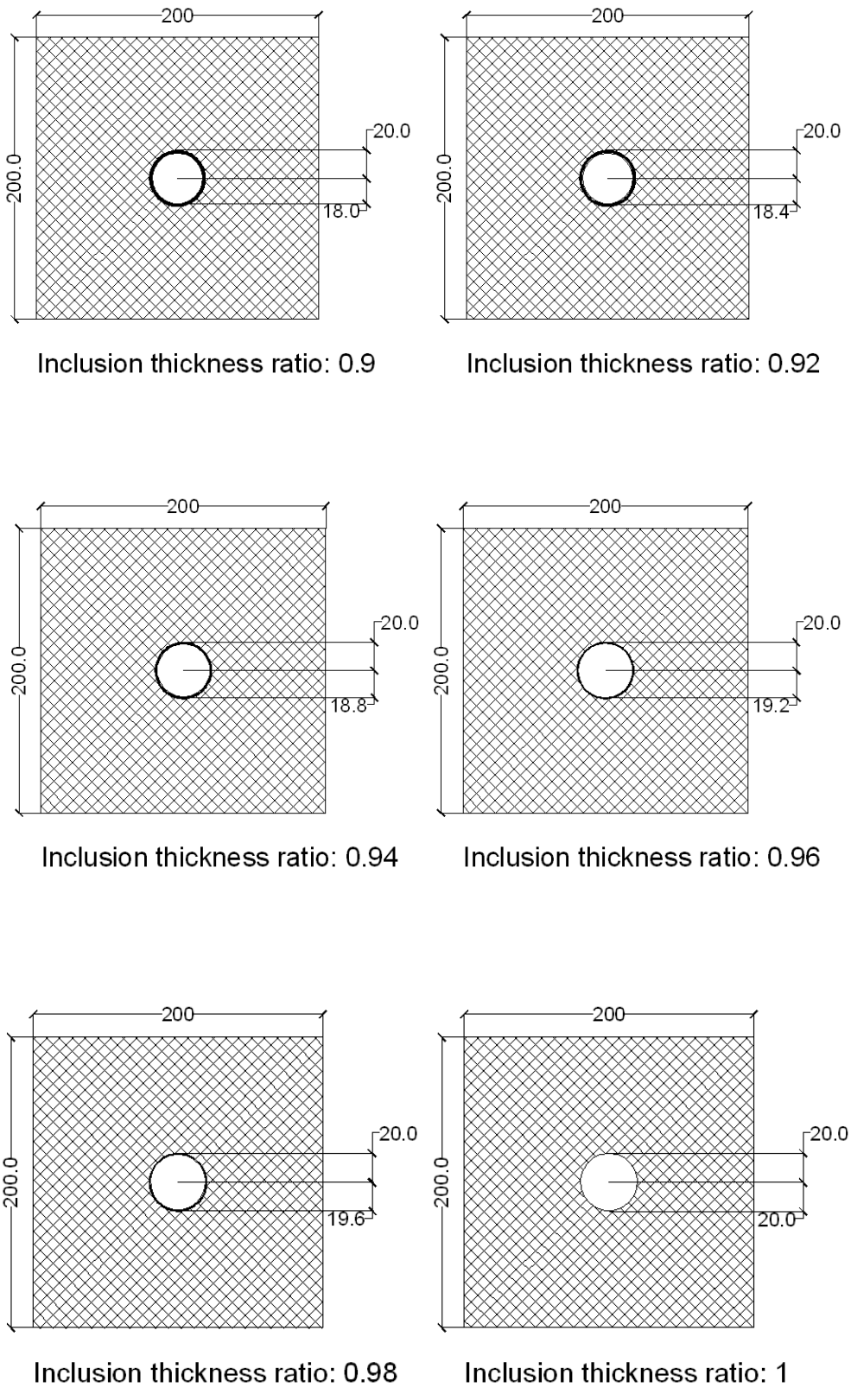

Figure 66 - RVE with different inclusion wall thickness - Volume Fraction 3%

The results are shown in the Diagrams 67 to 83.

RVE model-1:
RVE length = 100
Volume fraction = 0.13

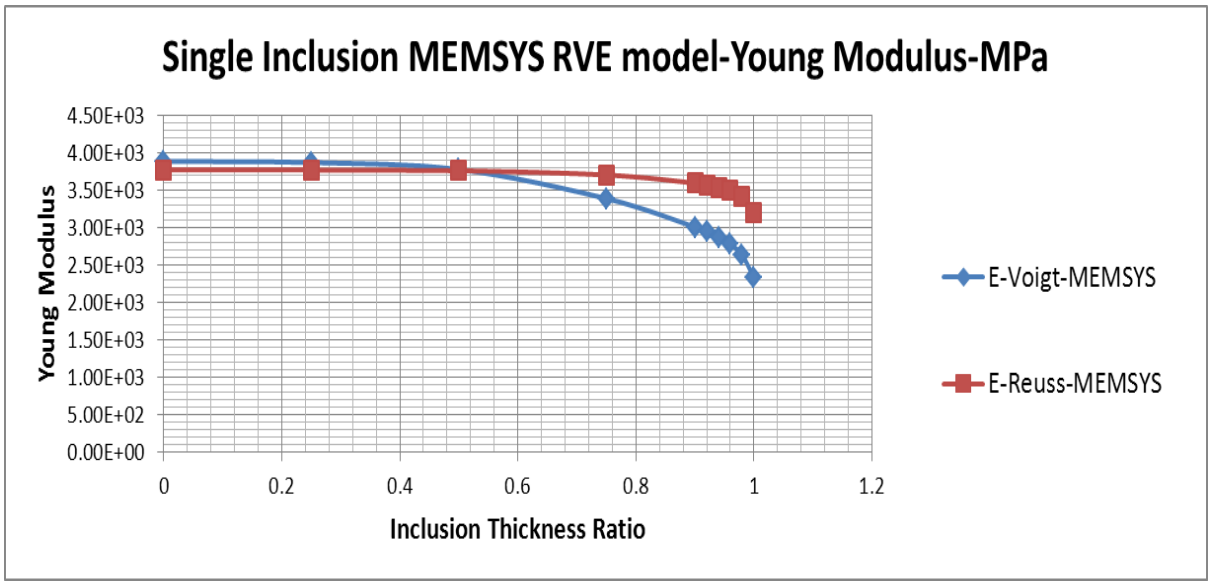

Figure 67 – RVE Young Modulus as a function Inclusion Membrane Thickness Ratio – Inclusion Area Fraction = 0.13 – MEMSYS results

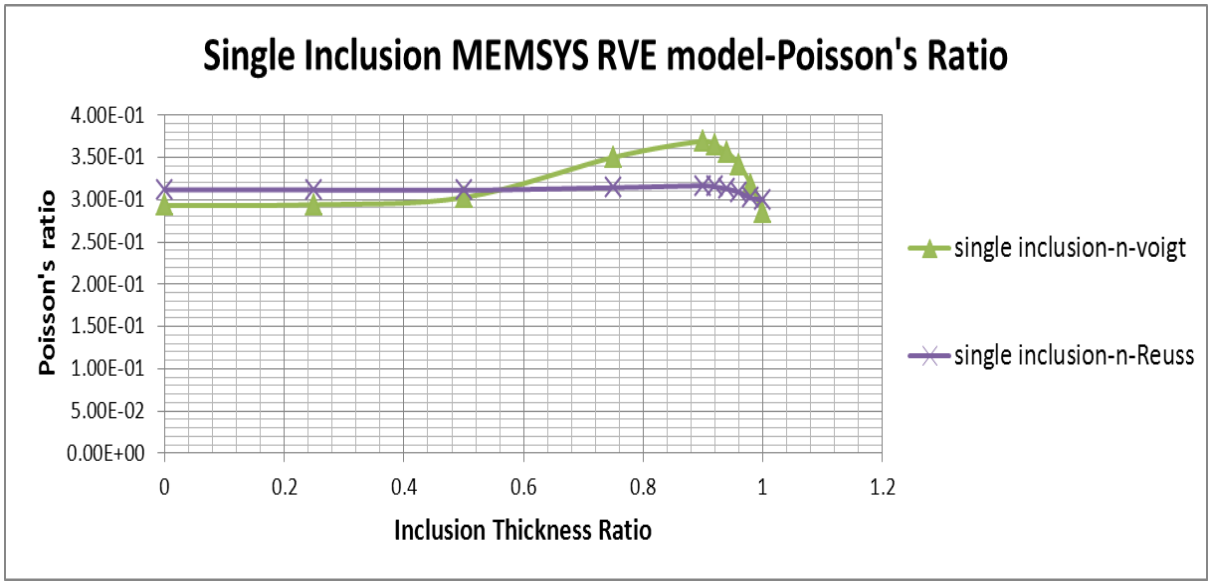

Figure 68 - RVE Poisson's Ratio as a function Inclusion Membrane Thickness Ratio – Inclusion Area Fraction = 0.13 – MEMSYS results

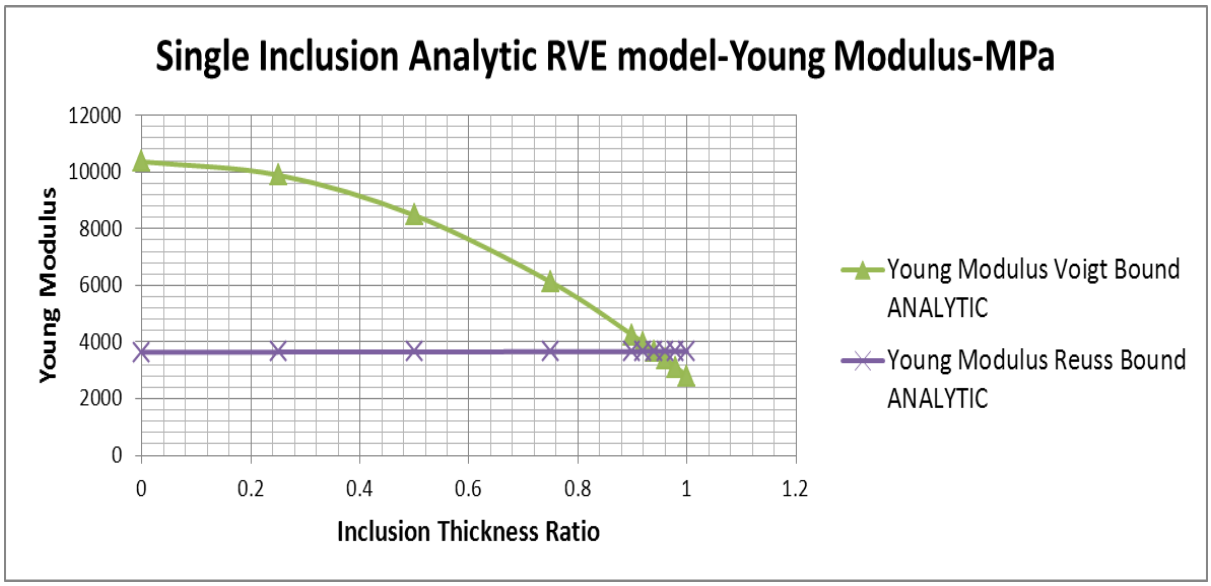

Figure 69 - RVE Young Modulus as a function Inclusion Membrane Thickness Ratio – Inclusion Area Fraction = 0.13 – Analytic results

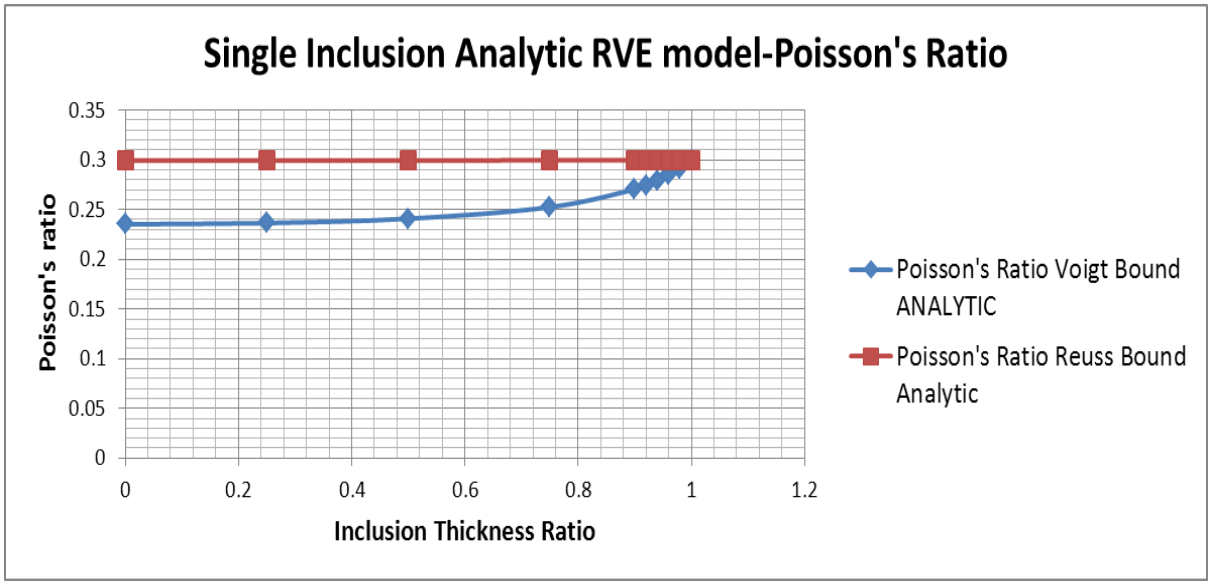

Figure 70 - RVE Poisson's Ratio as a function Inclusion Membrane Thickness Ratio – Inclusion Area Fraction = 0.13 – MEMSYS results

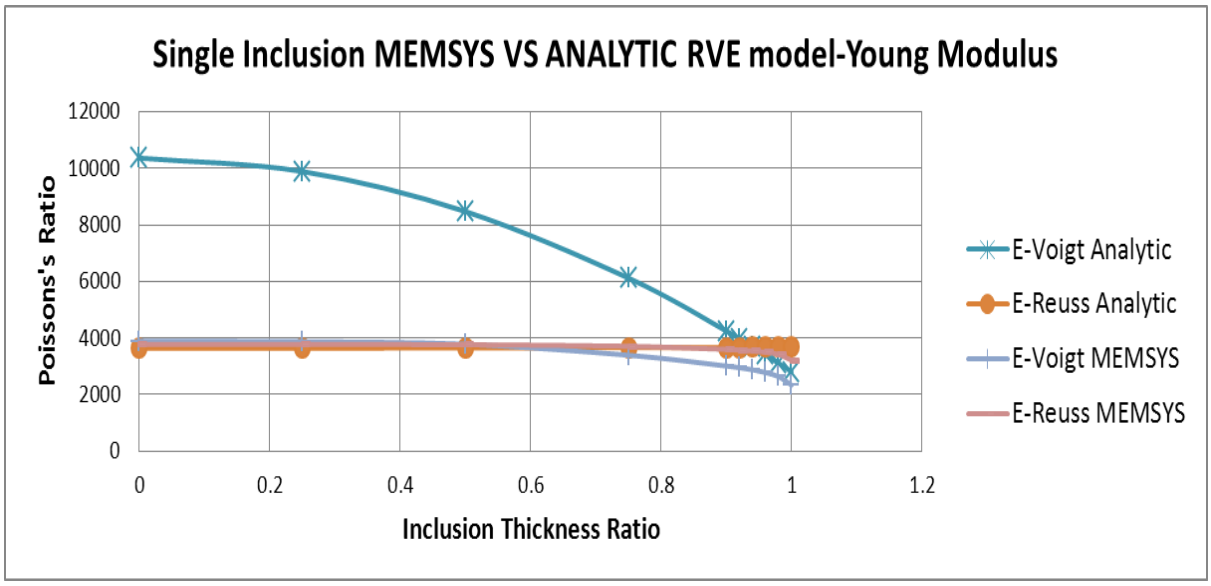

Figure 71 - RVE Young Modulus as a function Inclusion Membrane Thickness Ratio – Inclusion Area Fraction = 0.13 – MEMSYS VS Analytic

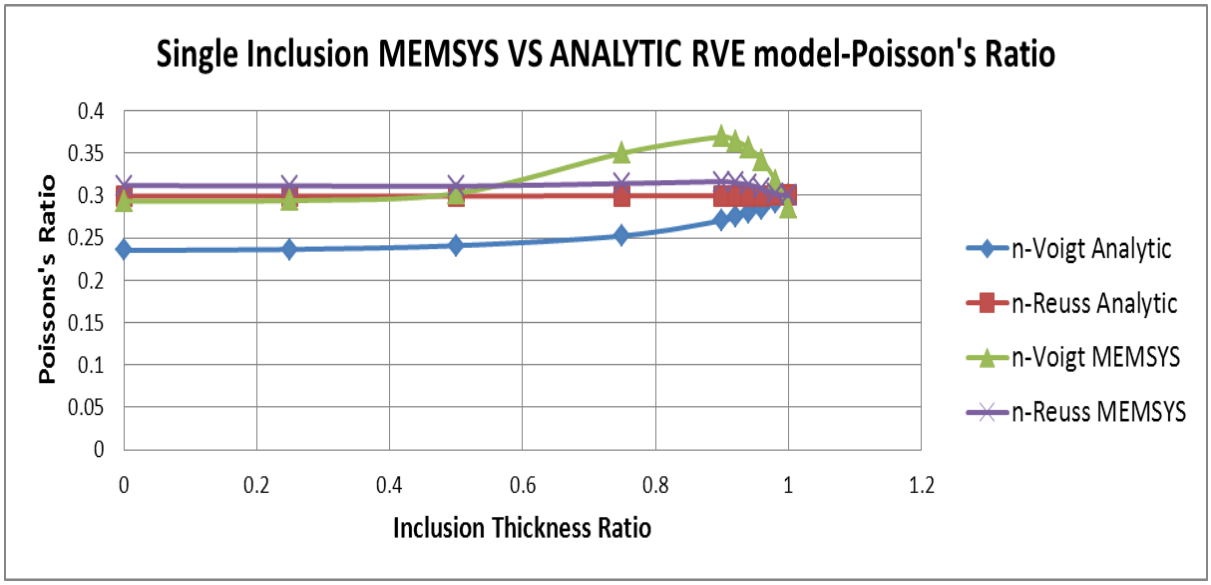

Figure 72 - RVE Poisson's ratio as a function Inclusion Membrane Thickness Ratio – Inclusion Area Fraction = 0.13 – MEMSYS VS Analytic

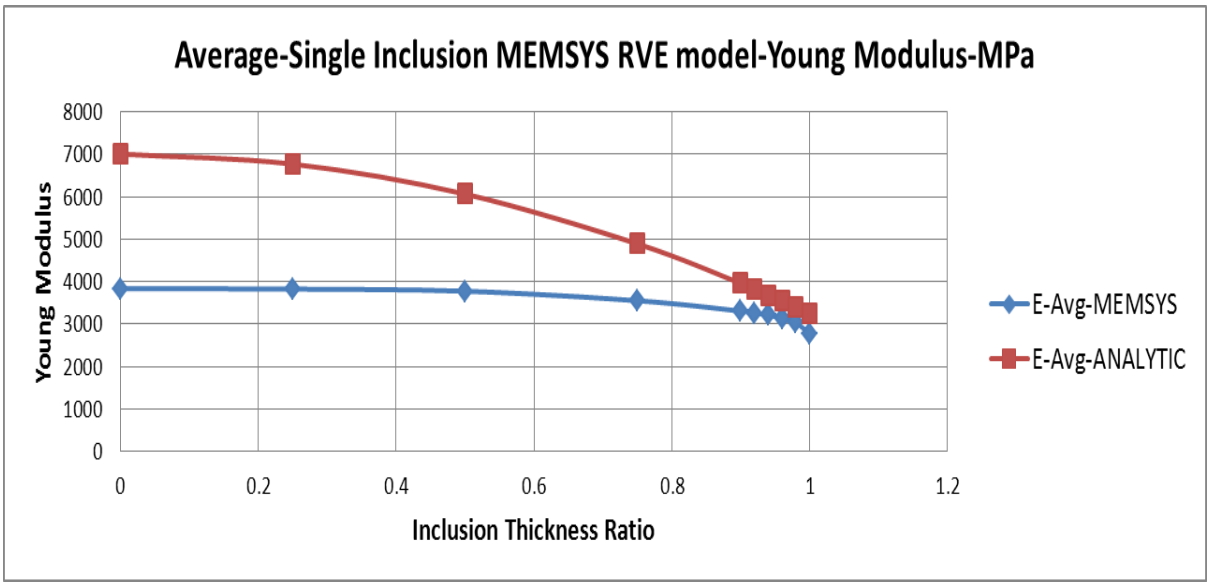

Figure 73 - RVE Average Young Modulus as a function Inclusion Membrane Thickness Ratio – Inclusion Area Fraction = 0.13 – MEMSYS VS Analytic

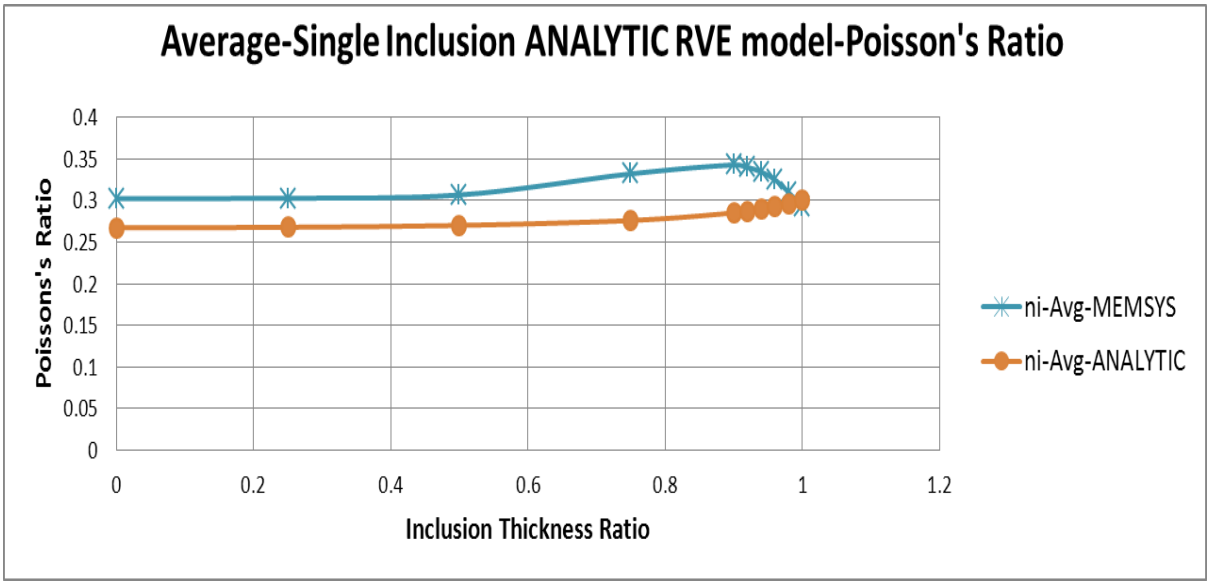

Figure 74 - RVE Average Young Modulus as a function Inclusion Membrane Thickness Ratio – Inclusion Area Fraction = 0.13 – MEMSYS VS Analytic

RVE model-2

RVE Length = 200

Volume Fraction = 0.03

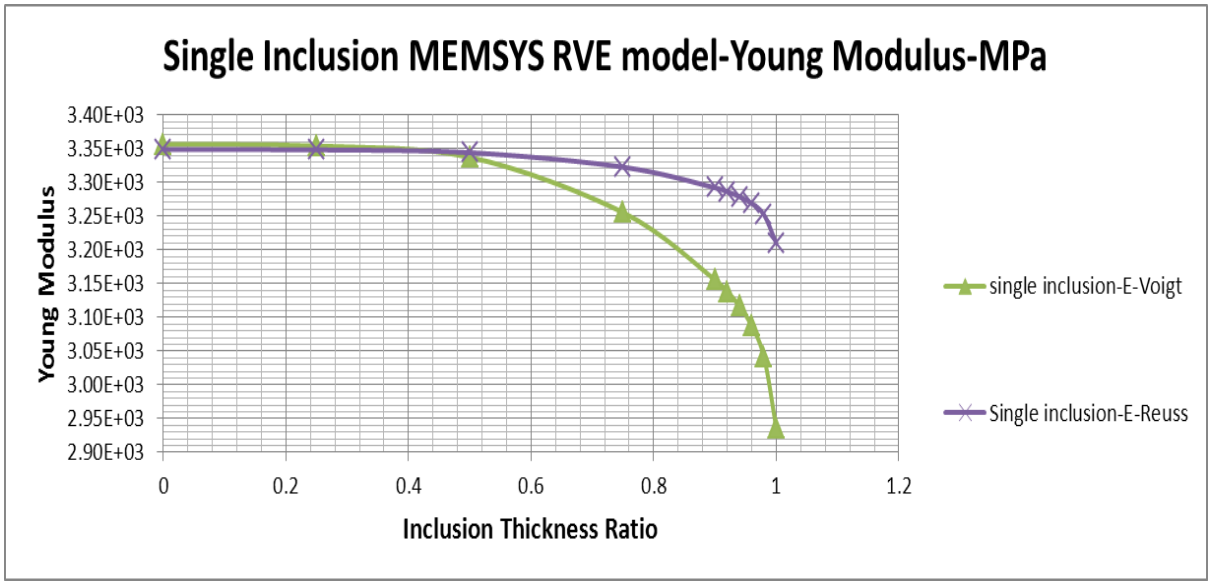

Figure 75 - RVE Young Modulus as a function Inclusion Membrane Thickness Ratio – Inclusion Area Fraction = 0.03 – MEMSYS results

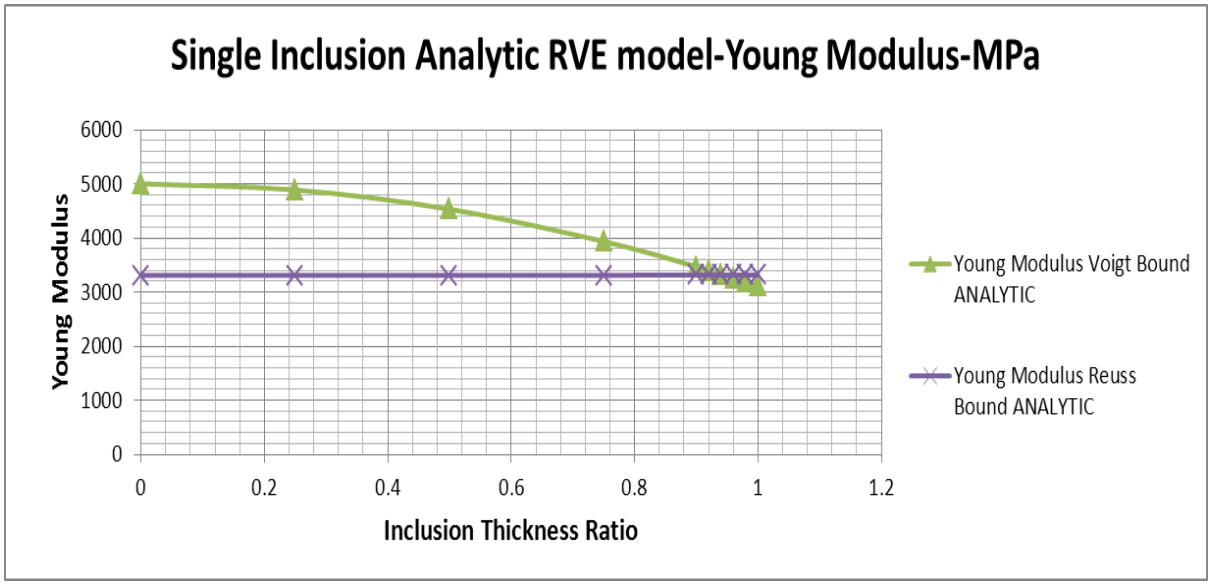

Figure 76 - RVE Young Modulus as a function Inclusion Membrane Thickness Ratio – Inclusion Area Fraction = 0.03 – Analytic results

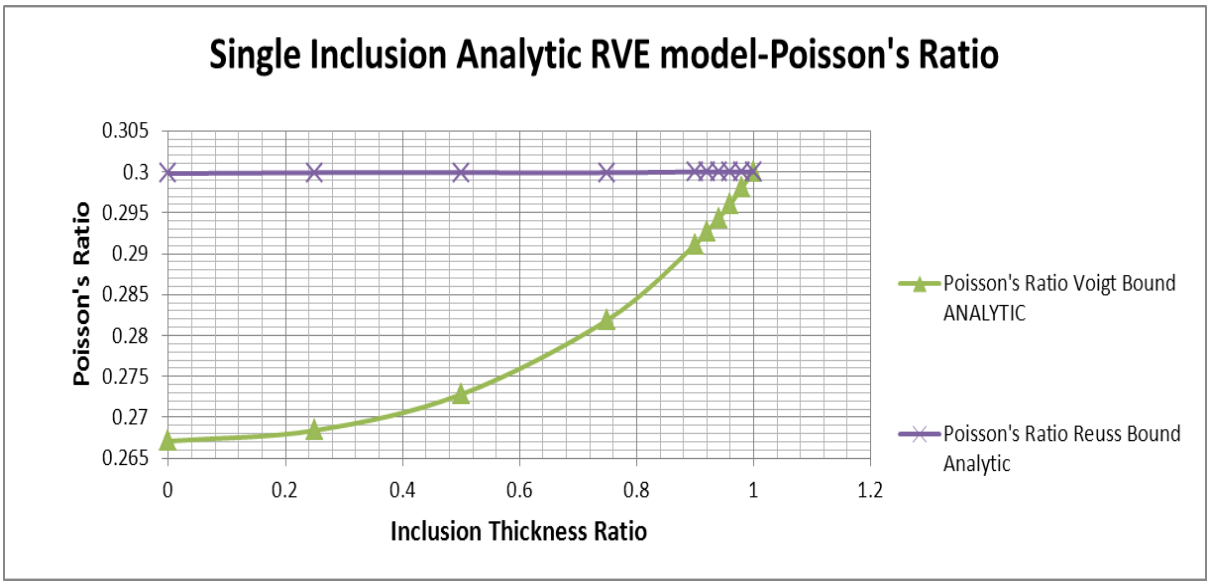

Figure 77 - RVE Poisson's Ratio as a function Inclusion Membrane Thickness Ratio – Inclusion Area Fraction = 0.03 – Analytic results

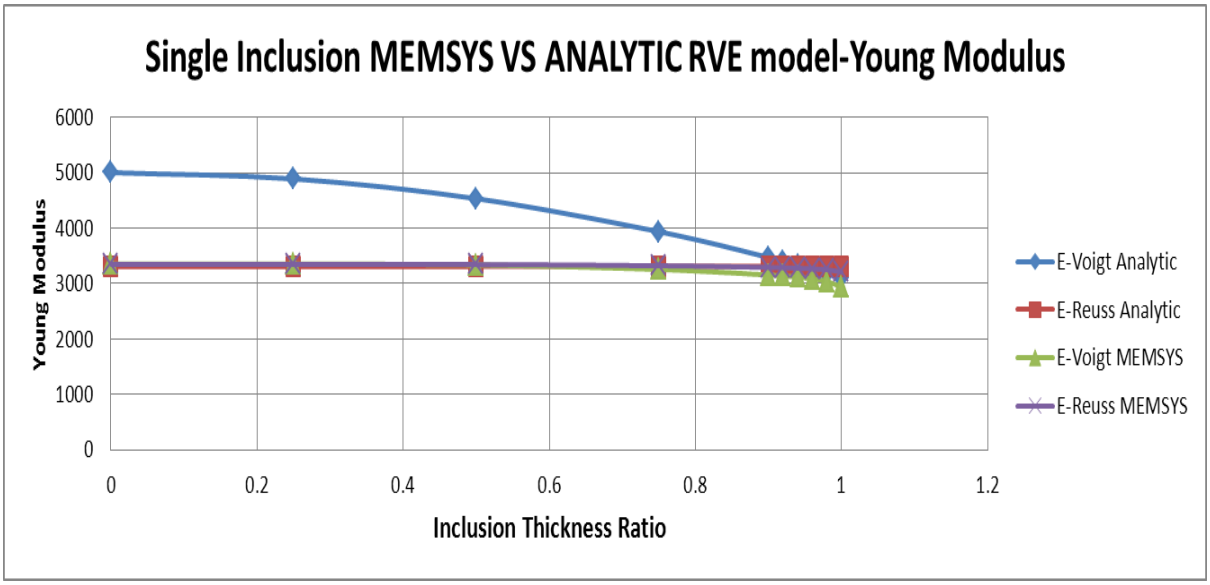

Figure 78 - RVE Young Modulus as a function Inclusion Membrane Thickness Ratio – Inclusion Area Fraction = 0.03 – MEMSYS VS Analytic

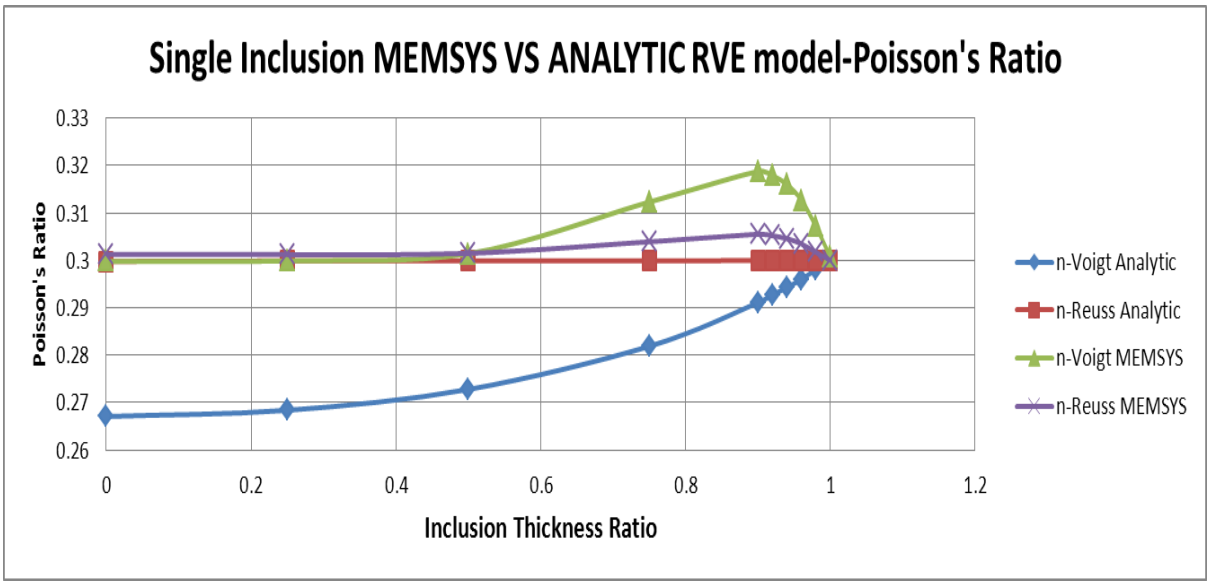

Figure 79 - RVE Poisson's ratio as a function Inclusion Membrane Thickness Ratio – Inclusion Area Fraction = 0.03 – MEMSYS VS Analytic

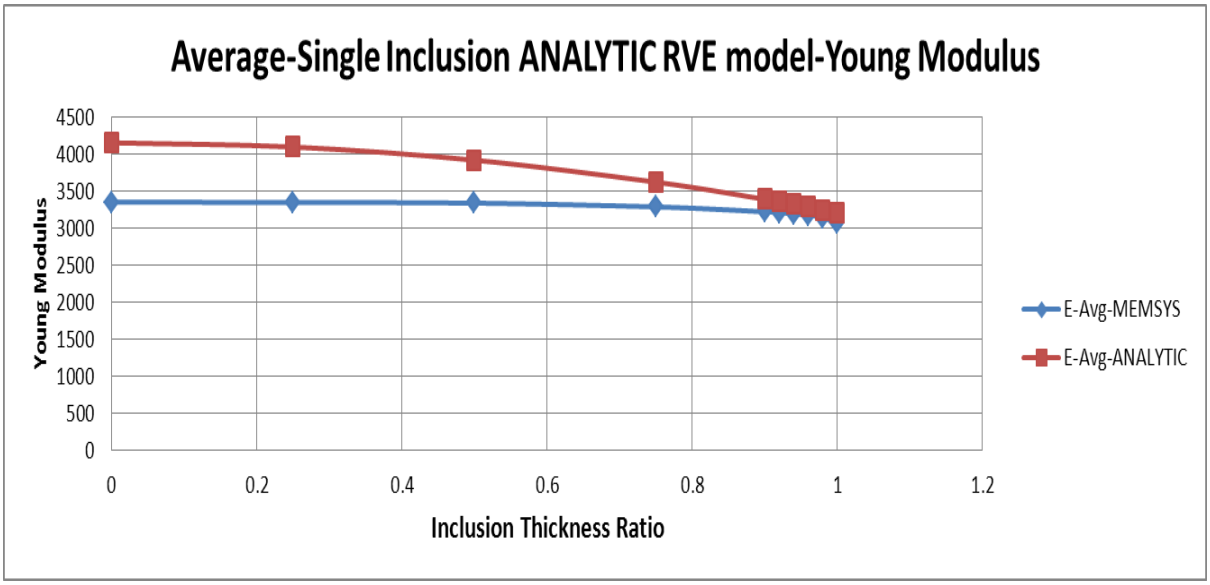

Figure 80 - RVE Average Young Modulus as a function Inclusion Membrane Thickness Ratio – Inclusion Area Fraction = 0.03 – MEMSYS VS Analytic

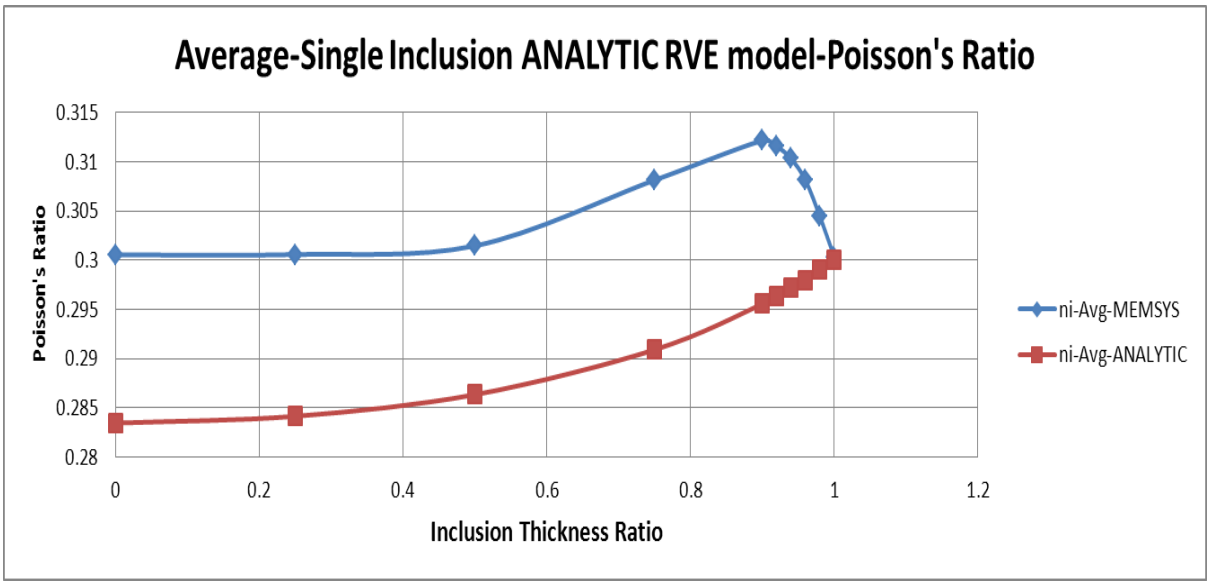

Figure 81- RVE Average Poisson's Ratio as a function Inclusion Membrane Thickness Ratio – Inclusion Area Fraction = 0.03 – MEMSYS VS Analytic

Comparing RVE models L-100 and L-200 with inclusions with various wall thicknesses:

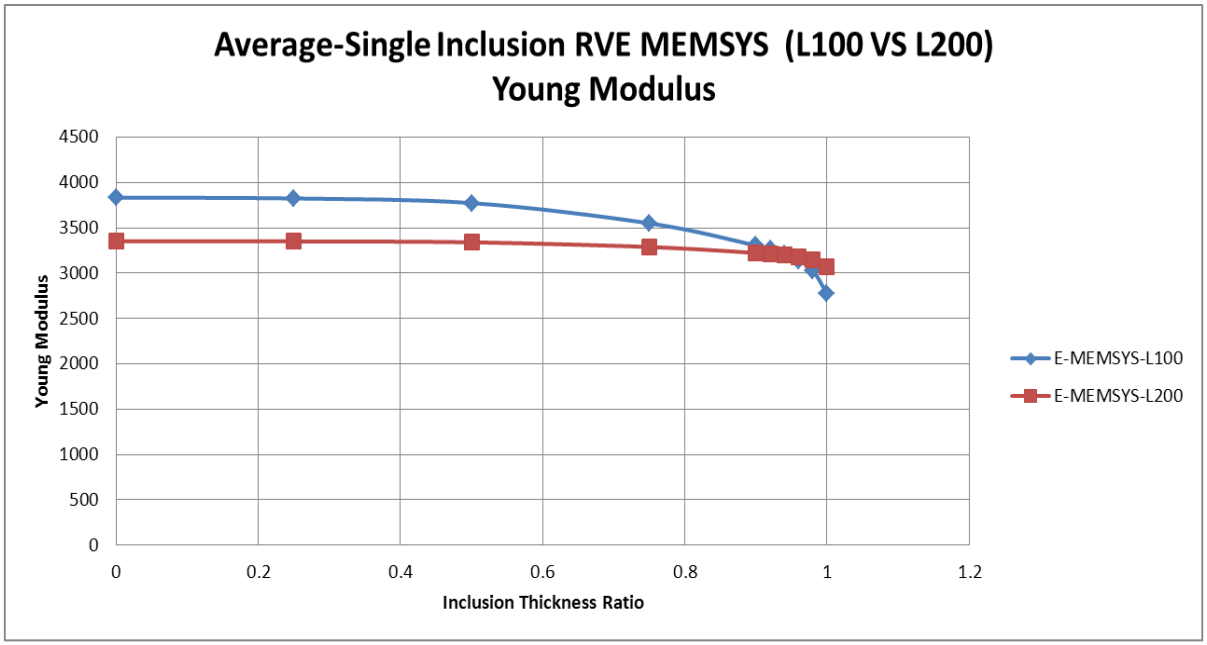

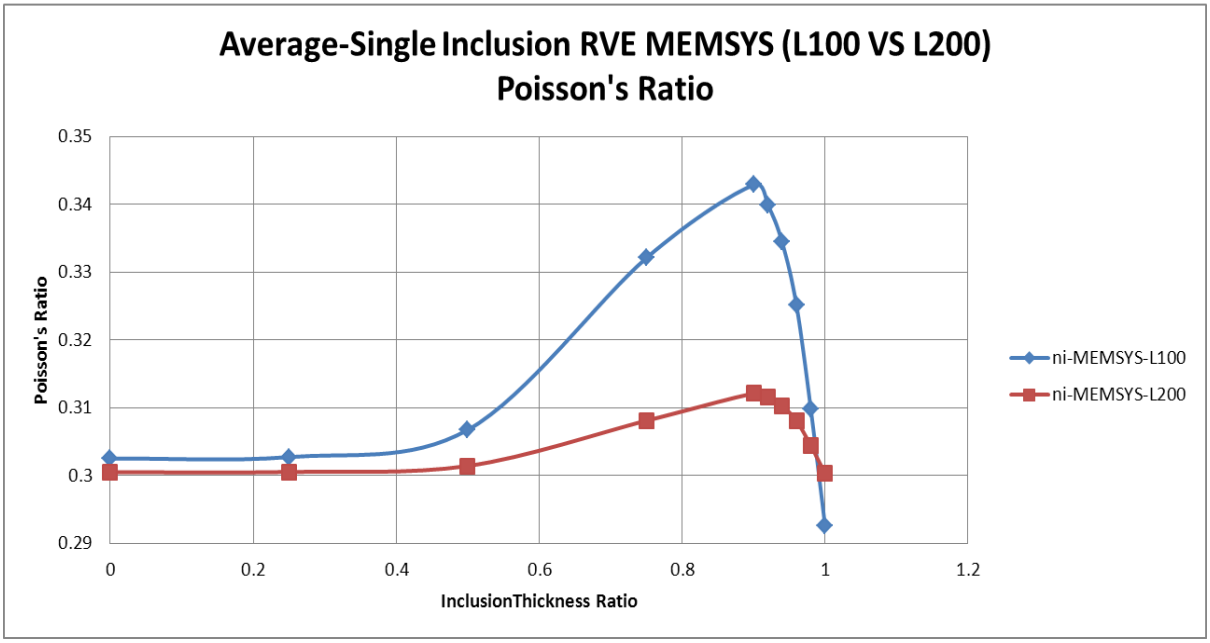

Diagram 82 – Comparing Young Modulus and Poisson's Ratios of RVE models with inclusion area fractions equal to 0.03 and 0.13 as a function of Inclusion Thickness Ratio - MEMSYS

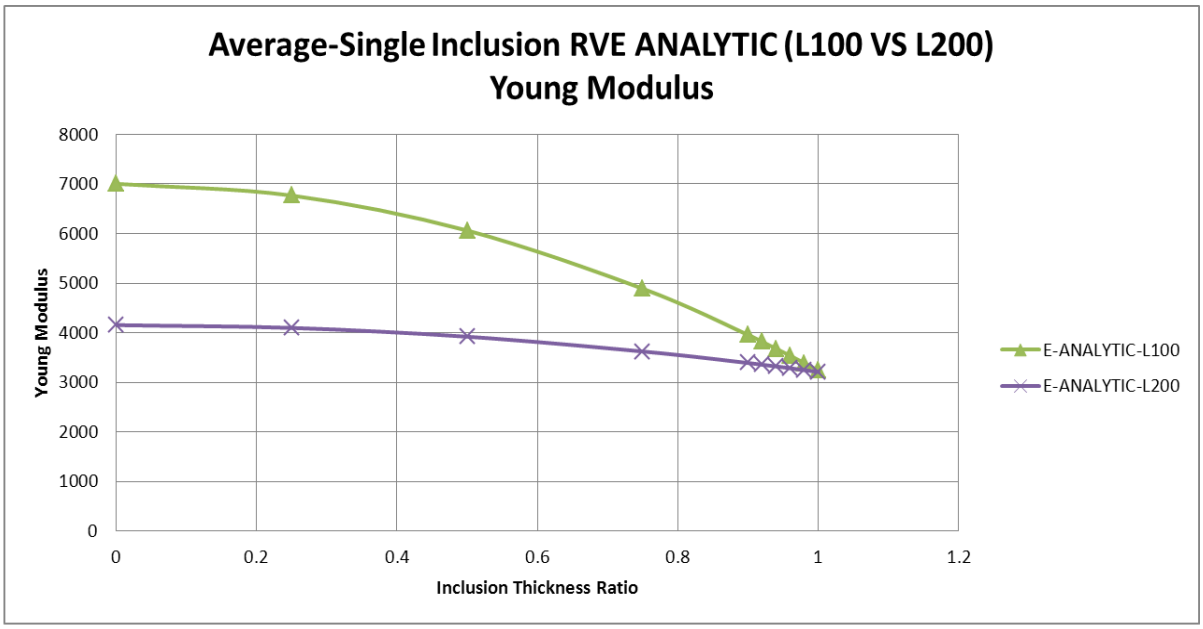

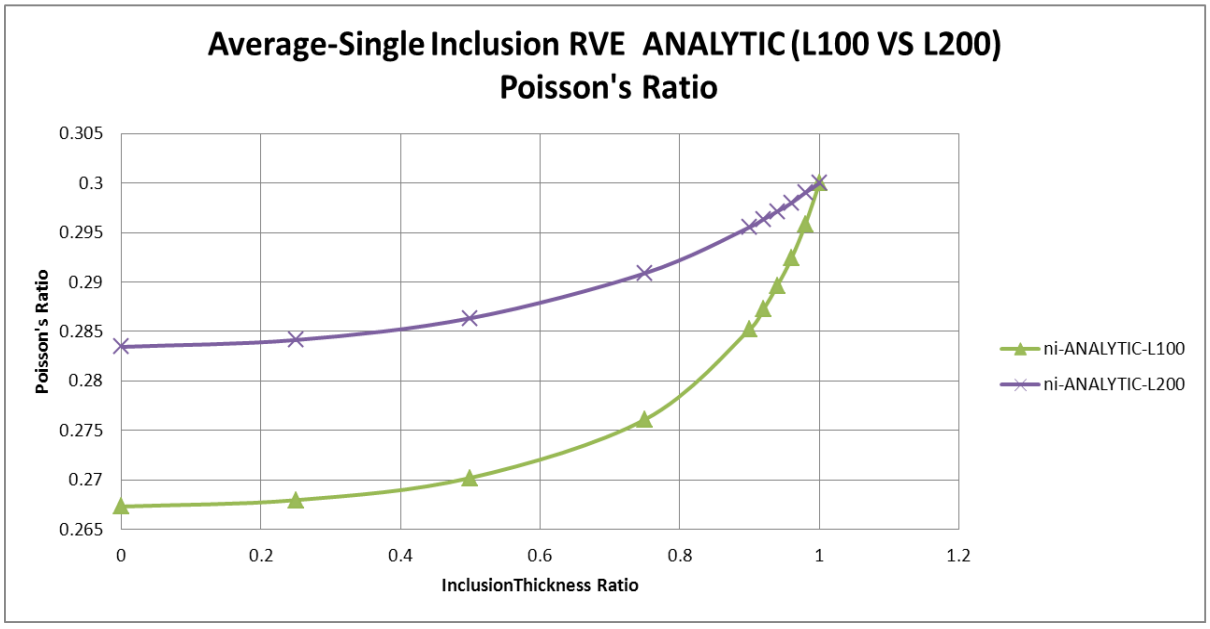

Diagram 83- Comparing Young Modulus and Poisson's Ratios of RVE models with inclusion area fractions equal to 0.03 and 0.13 as a function of Inclusion Thickness Ratio - Analytic

The value of Young Modulus in both bounds reduces due to increase of the Inclusion Thickness Ratio for RVEs of volume fractions equal to 0.13 and 0.3. This is well-shown in Porfiri et al [7]. It is noteworthy to highlight that the results in the Diagrams 84 and 85 are shown as a function of 1-η, which leads to an inverse trend comparing to the results

shown in Diagrams 67 to 83. The concluding remarks about the MEMSYS and Analytic results and their resemblance with results from Diagrams 84 and 85 [7] are given in the next paragraph.

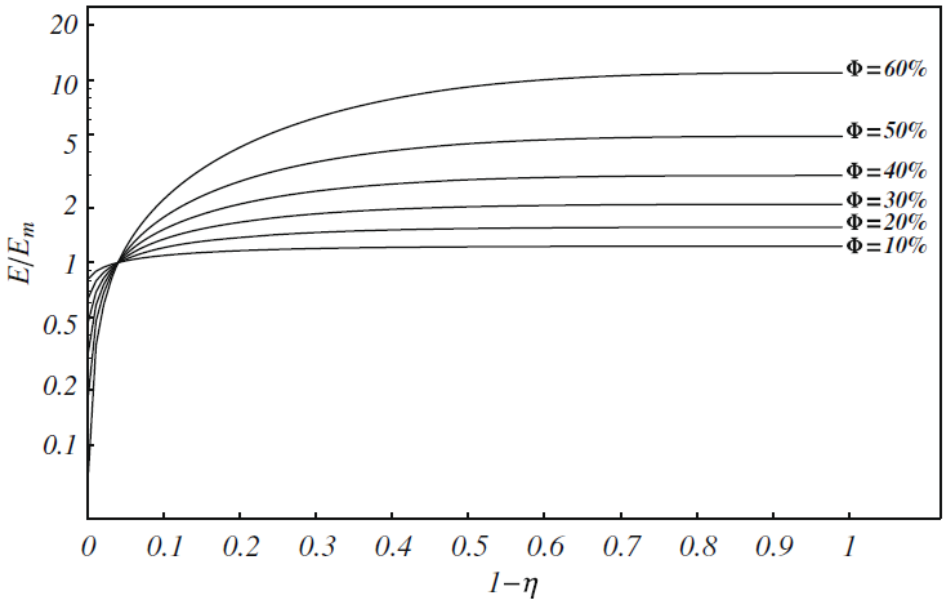

Diagrams 84 - Change in the Young Modulus with respect to the microballoon wall thickness [7].

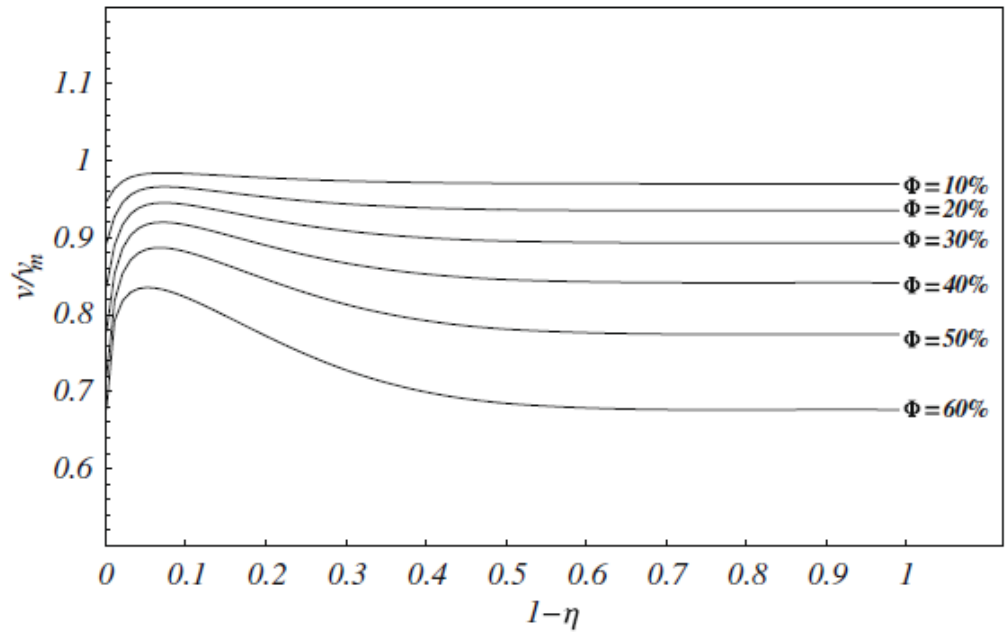

Diagram 85 - Change in the Poisson's Ratio with respect to the microballoon wall thickness [7].

It's reminded that in the diagrams 84 and 85 the vertical axes shows the ratio between the composite material Young Modulus over that of the matrix material, E/E_m. The volume fraction of the composite material is shown by Φ. Note that the E/E_m axis is plotted on the log-scale in this figure. Note also that $\eta = 0$ refers to solid inclusions while $\eta = 1$ signifies the presence of only voids. This figure shows two important trends. First, it should be noted that as the value of η decreases the change in E/E_m diminishes. This trend indicates that the rate of increase of the Young's modulus decreases as η decreases. The values of E/E_m are strongly dependent on the volume fraction. At lower values of volume fractions the effect of η diminishes faster. Second, there is a region in the neighborhood of $(1 - \eta) = 0.04$ where all the curves for different volume fractions values intersect. This narrow region represents $E/E_m=1$ and it signifies that only the particles that have $\eta < 0.96$ constitute syntactic foams having higher Young's Modulus than E_m.[7]

The results derived by Profiri et al. [7] in Diagram-84, which show the change of Young Modulus as a function of 1-η, prove to have similar trends with MYMSYS results in Diagram-67 and Analytic results given in Diagrams-69.

Diagram-82 which shows the MEMSYS results of RVE Young Modulus and Poisson's ratio, confirms that for values of η smaller than 0.96, the overall Young Modulus of the RVE is higher than that of Vinyl Ester which is equal to 3.21 GPa.

The important point which could be deducted from Diagram-83 is the fact that in case of having inclusions with zero thickness or in other words voids, the area fraction doesn't play a significant role. This is quite trivial in low volume fractions of void inside an RVE due to its zero stiffness modulus of void areas.

3.2.4. Inclusion size distribution pattern

Various types of inclusions were introduced in Figures 52 and 53, the external diameter assigned to each type is merely the average of the all inclusions sizes present in the industrial package of that inclusion type. In fact every inclusion type should be assigned to a size distribution pattern which could have any probabilistic shape. In the following a simple method is considered to model the theoretic inclusion probabilistic distribution and investigate their overall properties. This model is merely based on the average and standard deviation values of the inclusions diameters which exist in a RVE model. Thus, every RVE model which represents one inclusion size distribution pattern is introduced with its inclusions diameter average and standard deviations as shown in Figures 87 to 91.

3.2.4.1 Multi-Inclusion RVE Modeling with different Inclusion Size Distribution Patterns

As described in the previous section (3.2.4), all inclusion particles of a bulk mass in a real manufacturing material of glass spheres don't have the same size. In fact a continuous probability distribution function could be assigned to the size range of a bulk mass of glass spheres. In this thesis, the explained continuous probability distribution is simply substituted with a physical RVE model with four inclusions of different diameters, while the inclusion area fraction of all models are approximately the same as shown in Table-86. There are five different inclusion size distribution patterns with their corresponding RVE and for every RVE model a computational MEMSYS model is created.

In each model it's assumed that the material bulk mass is constituted from a few sizes of glass spheres. The models details are given in Table-86 and shown in the Figures 87 to 91.

These inclusion material (glass sphere) size distributions are selected in a way which leads to creation of RVE models with approximately equal inclusion area fraction. One specific code is assigned to each inclusion size distribution pattern and its corresponding RVE.

RVE		Inclusion		Single Inclusion Particle Sizes (Radius)							Overall RVE Inclusion Diameter	
Code	Dimension Length	Thickness Ratio	Quantity	5.0	10.0	15.0	20.0	25.0	30.0	35.0	Average	Variance
1.0	200.0	0.9	4.0	0.0	0.0	0.0	**4.0**	0.0	0.0	0.0	40.0	0.0
2.0	200.0	0.9	4.0	0.0	0.0	**1.0**	**2.0**	**1.0**	0.0	0.0	40.0	50.0
3.0	200.0	0.9	4.0	0.0	0.0	**2.0**	0.0	**2.0**	0.0	0.0	40.0	100.0
4.0	200.0	0.9	4.0	0.0	**1.0**	0.0	**2.0**	0.0	**1.0**	0.0	40.0	200.0
5.0	200.0	0.9	4.0	0.0	**1.0**	**1.0**	0.0	**1.0**	**1.0**	0.0	40.0	250.0

Code	Inclusion Area Fraction
1.0	0.126
2.0	0.130
3.0	0.134
4.0	0.141
5.0	0.145

Table - 86 – RVE models with different inclusion size distribution patterns

The following charts and figures show the inclusion size distribution model for every code:

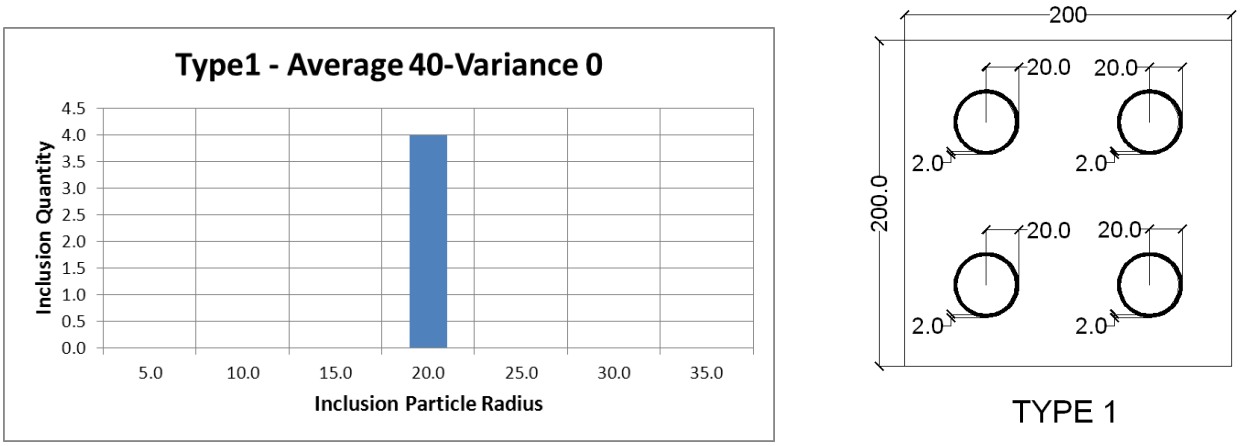

Figure 87 – Inclusion Pattern Type-1

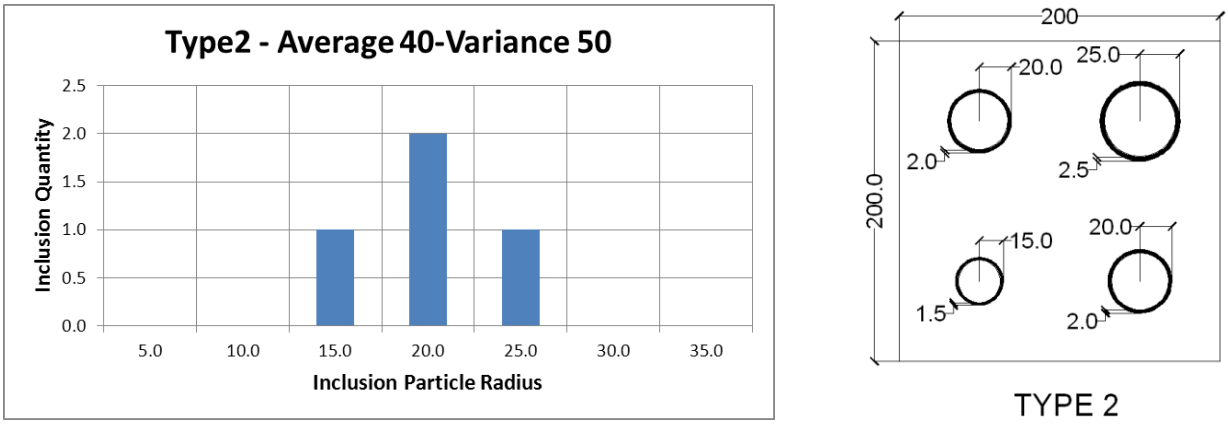

Figure 88– Inclusion Pattern Type-2

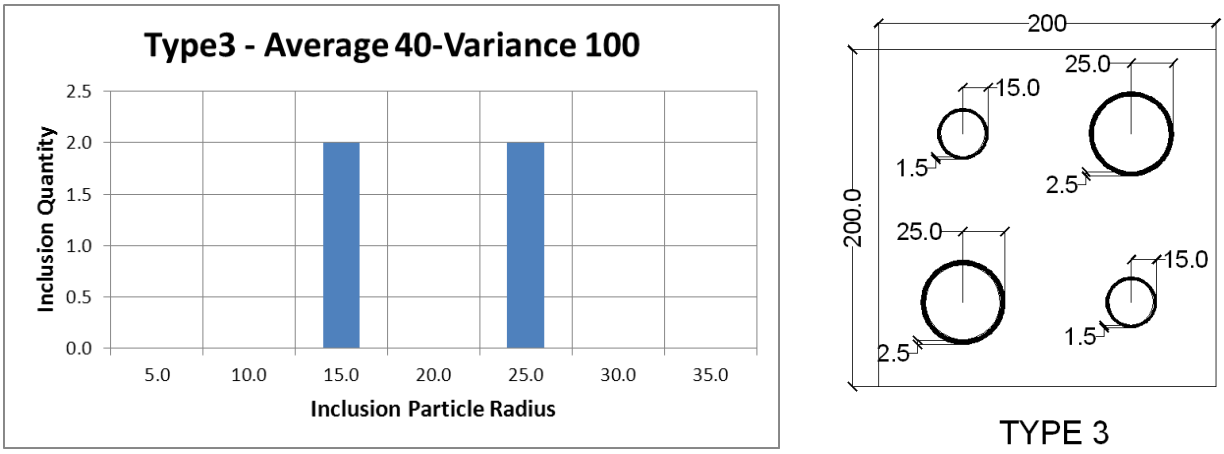

Figure 89– Inclusion Pattern Type-3

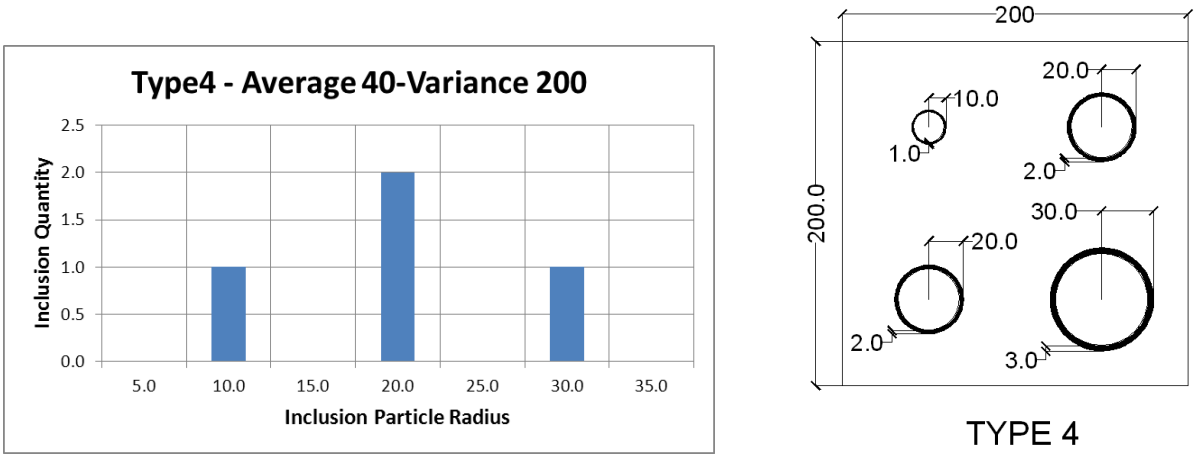

Figure 90– Inclusion Pattern Type-4

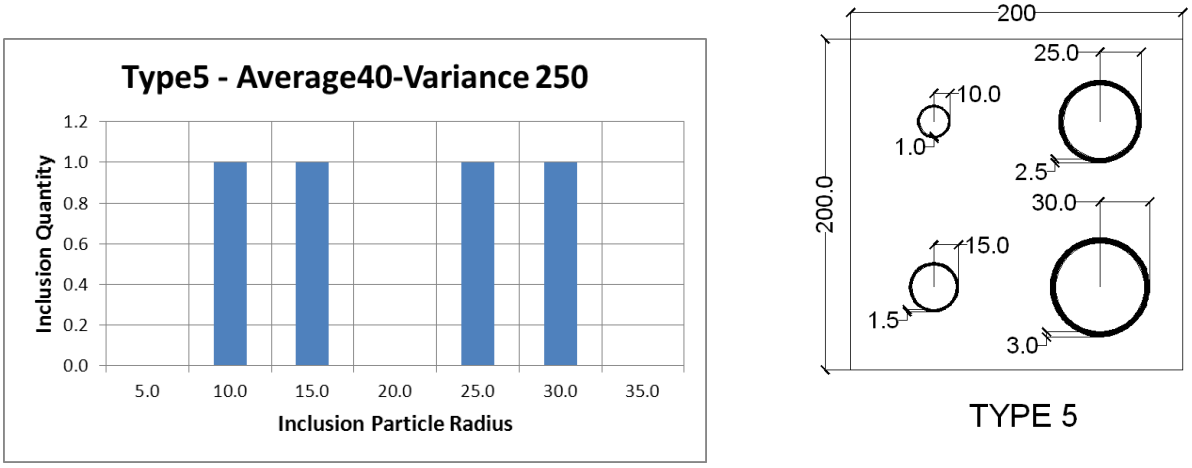

Figure 91– Inclusion Pattern Type-5

Here the overall mechanical properties of the RVE models are rendered as a function of the inclusion distribution variance, it must be considered that the average diameter of the inclusion in every distribution model is the same, therefore every code represents one size distribution variance:

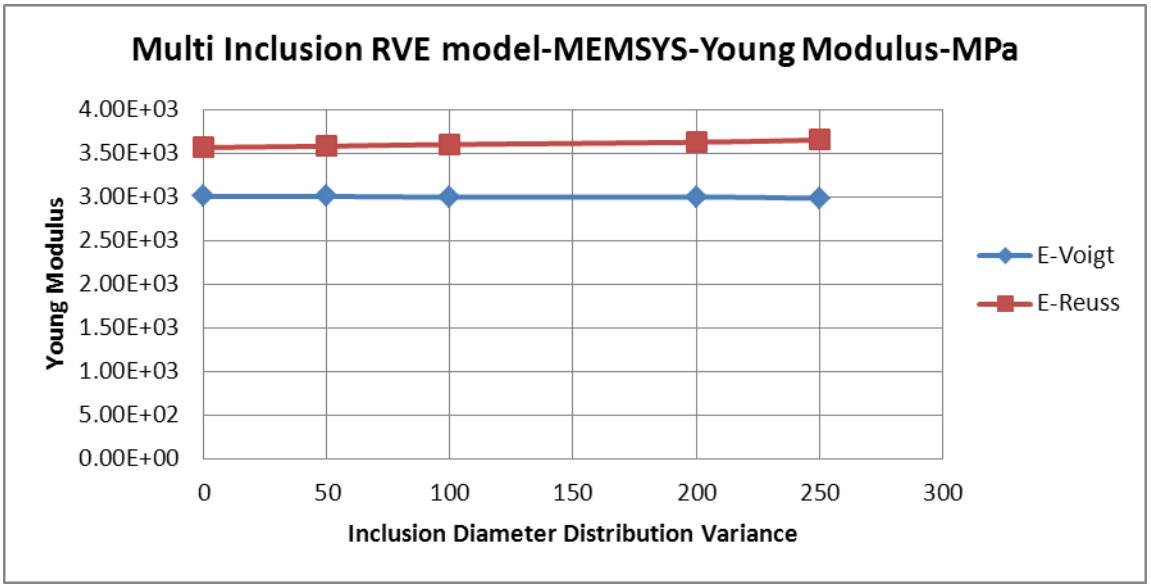

Figure 92-Young Modulus of RVE models with different inclusion size distribution patterns

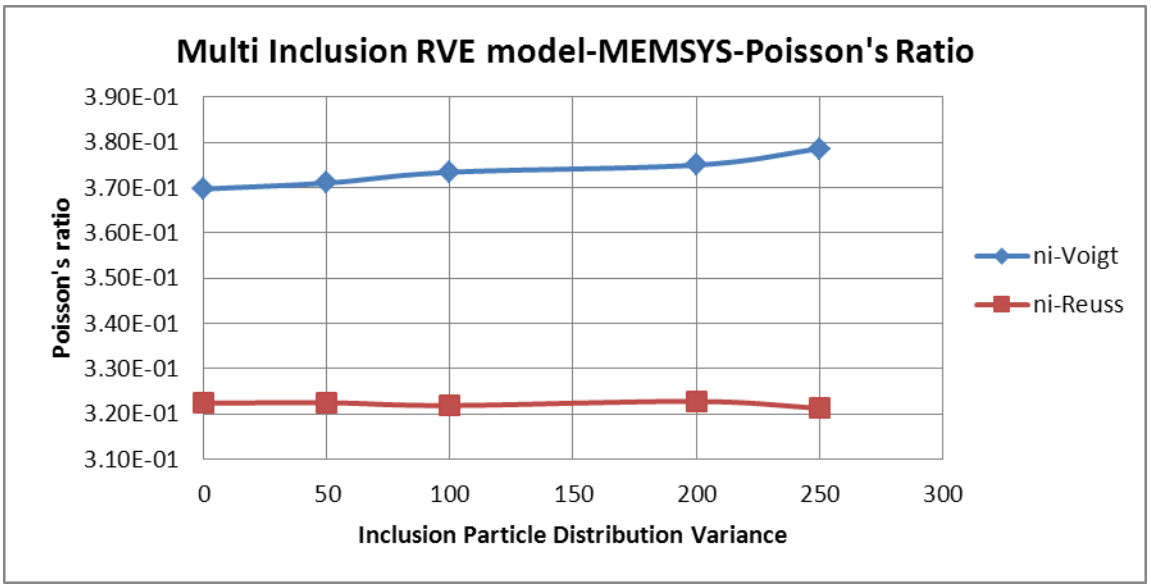

Figure 93- Poisson's Ratio of RVE models with different inclusion size distribution patterns

The results show insignificant and untraceable changes in the values of the overall properties as a function of Inclusion Size Distribution Variance. This means that in the investigated scope, the important parameter is the overall volume fraction of phase (inclusion) material. However, the current scope is restricted to the cases where inclusions do not have any physical interactions with each other. As it was shown in

section 3.2.4.1 and Figure-51, for inclusion area fractions greater than 0.5, the probability of interaction between the surface of inclusions is high and this leads different mechanical overall properties which is out of the scope of this thesis. Furthermore, for composite materials with area fractions greater than 0.5, inclusions with distribution patterns which contain a wider range of particle sizes, smaller inclusions can act as filler to avoid the formation of the entrapped air or voids in the composite material. This type of inclusion distribution pattern could be compared to well-graded soils which contain fine and coarse grains together and this makes the bulk mass of soil to have a low void content. This phenomenon is not investigated in this thesis and could be a good subject for further researches.

4. Conclusions

4.1. Outline of Main Results

In this research the influence of four important parameters on the overall behavior of Syntactic Foams were investigated through computational homogenization method using MEMSYS code by creating about 900 Finite Element Models. The four parameters were inclusion area (volume) fraction, asymmetric distribution of inclusions, inclusion membrane thickness and inclusion distribution pattern. The extent of influence of every parameter was checked and compared with the experimental and analytic results from other reliable scientific resources. The MEMSYS code results were validated at two steps successfully in order to have certainty about the functionality and desired precision of the computational tool.

The Inclusion Volume (Area) Fraction variation has proven to have a significant effect on the overall properties of Syntactic Foam, although the trend of influence shows to have a large domain of scattering in MEMSYS results and results rendered from other resources. However for every Inclusion Volume Fraction a reliable range between Voigt and Reuss bounds is given. The models were improved step by step, by implementing better computational input data such as RVE geometries with small ratios of composite microscopic phase material element size ‘l’ to RVE Length ‘L’. Stochastic arrangement of inclusions which is a quite innovative computational task in this field, showed perfect adaptability with the expected results and improved the assurance of the results from previous steps.

Asymmetric RVEs were investigated with two modeling concepts. The first modeling concept was creating RVEs with constant RVE length and the second one, creating RVEs with constant inclusion area fraction. Both models were representing a case in which the inclusions coordinate with respect to one other may be managed to form a desired arrangement other than the ideally equal one. The asymmetric arrangement of inclusions has shown to be of minor importance with respect to the other parameters. Although this result is limited to the investigated scope of the modeled RVEs and is not exclusive.

The Inclusion Thickness Ratio variation has again a determining effect on the overall properties of the syntactic foam. In this case the results show a rather acceptable compliance with the comparing results from other resources. Confirming the previous state-of-art, MEMSYS model results showed the range of inclusions membrane thickness in which the composite material behaves stiffer than pure matrix (Vinyl Ester).

The Inclusion Size Distribution parameter which was targeted to input the diversity of the inclusions sizes -in an inclusion product category- into the modeling procedure, has shown to be of minor importance in case of approximately equal Inclusion Area Fractions of compared RVEs.

To sum up, it shall be highlighted that, Inclusion Volume Fraction and Thickness Ratio parameters have proven to be able to tailor and improve the matrix material (Vinyl Ester) properties from a structural point of view considerably, while asymmetric arrangement and size diversity of inclusions have shown not to be able to impose any significant changes to the overall properties.

4.2. Future Developments

The current research could be of much value for sake of introducing computational methods which could be used in complicated homogenization problems.

Starting from the fact that the currently conveyed homogenization procedure is by having the assumption of a linear elastic constitutive model, MEMSYS code has the ability to take into account the plasticity and fracture mechanics of the material. The latter one could be of much importance for sake of Syntactic Foams to model the crushing of inclusions and the debonding phenomenon between inclusion and matrix.

The other issue is making a 3D model which is merely a matter of producing the geometry. MEMSYS has been updated to intake 3D coordinates as geometry input files and assign proper finite elements to that.

Having the ability to assign the stochastic nature of the composite materials, by applying the two highlighted assumptions (Constitutive Models Containing Fracture Mechanics and 3D geometry) the Finite Element RVE Model is precisely close to the realistic composite material microscopic morphology with the same properties in the details. This leads to more accurate and reliable results with respect to the ones in this thesis.

5. Extension

The current research extends into the second part which follows through a rather practical use of Composite Materials Homogenized results. The homogenized overall properties of the syntactic foam composite material are used as input for modeling circular slabs made of very material subjected to blast. This is in order to check the dissipative potential of

the Syntactic foams. The same procedure has been conveyed for Fiber Reinforced Materials (**FRC**). This is a very practical instance of Composite Material analysis- design problem.

Part-2: Syntactic Foam Materials Subjected to Extreme Loads (Blast)

Abstract

In this work the dissipative capacity of syntactic foams evaluated in confrontation to extreme loads (blast). This capacity is defined through evaluation of the safe regions on the Pressure-Impulse diagrams which are derived through calculating the critical loads resulting in Ultimate Limit States of circular slabs of specific geometry. The composite material is used as a replacement to FRC material, to evaluate the efficiency of this engineering innovation. Former present literature which is the analytical modeling and a series of experiments of circular slabs subjected to blasts, give input data and comparable results at hand. The current research is based on computational modeling of the problem using a range of material model definitions in order to optimize the modeling properties which best resemble the experimental and analytical results.

Introduction & Research outlines

The second part of the thesis is an extension to the former part about the homogenization of the syntactic foams composite materials. The aim of this part is to derive the Pressure-Impulse diagram of a circular slab made of Syntactic Foams. Like every general problem in the field of composite materials the first step prior to analysis and design is deriving the overall properties of the material which could be applied at macroscopic scale. Considering the first part of the thesis, a complete investigation of overall properties of the Syntactic Foams as a result of some determining manufacturing parameters are given; having the highlighted data, the behavior of the circular slab structure made of Syntactic Foam and subjected to blast is investigated in order to check its Ultimate Limit State (ULS) and dissipative potential in extreme loads such as blast.

A common kind of Syntactic foams with code name known as VE460-30. The principal of the code name used is described in the former, to be explained briefly, 460 stands for the hollow sphere glass density which is an indication to its membrane thickness and the number 30 is the percentage of Inclusion Volume Fraction in the syntactic composite.

The current research procedure is following the concepts of scientific task conducted by Colombo – Martinelli [29]. In the remarked research, Fiber Reinforced Concrete (FRC) and traditionally Reinforced Concrete (RC) are two investigated materials, constituting the slab materials. The modeling is conducted using an analytic procedure containing the yield line theory and on the other hand a series of experimental results approve the authenticity of the results.

In the case of slab constituted of VE460-30, the modeling tool used is the ABAQUS software. In order to validate the tool functionality in blast modeling, primarily a wide range of models were developed, with exact geometry and boundary conditions of the FRC models conveyed by Colombo-Martinelli [29]. The FRC material is modeled with two various material models – Concrete Damaged Plasticity [31] and Drucker Prager [30]. Finally the required Ultimate Limit State (ULS) [29] for sake of deriving P-I

diagrams is resulted with a very feasible accuracy with respect to the results derived by Colombo-Martinelli [29].

Then the material constitutive characteristics of VE460-30 syntactic foam has been implemented to the model again using the same two material models - Concrete Damaged Plasticity [31] and Drucker Prager [30] – which resulted in a schematic form for the P-I diagrams of the VE460-30 material. This is in fact a limitation (asymptote) stating the extinguishing the safe and unsafe response of the material for a given couple of (pressure, impulse) based on the assumed ULS [29].

2. Blast Load

2.1 Introduction

From a modeling point of view Blast Load is a pressure which its intensity is a function of time and a target coordinate with respect to the blast (detonation) origin [32]. There are several mathematical models which describe the blast load intensity with respect to time, at one set coordinate:

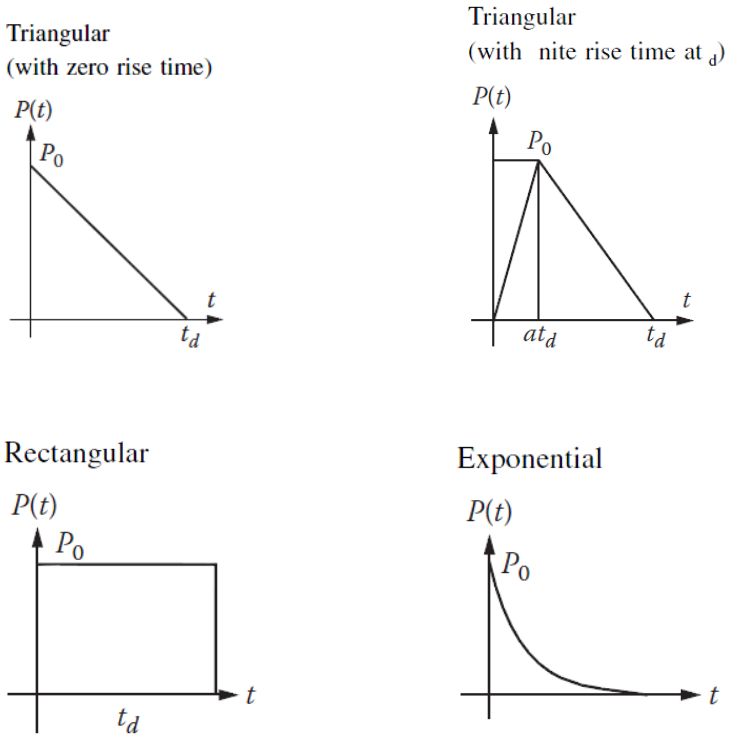

Figure 94- Different Schemes of Blast Load Models

Considering the fact that the Blast load intensity is of interest at its interacting zone with the structure and making the simplifying assumption that created distributed pressure is constant at various points of the slab, a Triangular Blast Load model with zero rise time is assumed for the distributed pressure over the slab.

2.2 Pressure – Impulse Diagrams

A pressure–impulse diagram is a design tool that allows one to evaluate the damage level of structural components induced by blast loads (Baker, Cox, Westine, Kulesz, & Strehlow, 1983). Once the maximum value of a certain response parameter (displacement, ductility, etc.) has been defined, the diagram provides the combination of pressure and impulse that will produce the same limit state level in the structural member under consideration. With reference to Figure-95, pressure and impulse combinations that fall above or to the right of the curve will produce a response greater than the limit state represented by the curve itself, vice versa combinations below or on the left of the curve will cause a response lower than the same limit state. [29]

In each P–I curve three domains can be identified: an impulsive, a dynamic, and a quasi-static loading regime (Figure-95). Adopting this classification, the maximum response may depend only on the applied impulse (impulsive region), the pressure only (quasi-static region), or on both the impulse and pressure (dynamic region) (Krauthammer, 2008). With reference to Figure-95, horizontal and vertical asymptotes define limiting values for each parameter. The impulsive asymptote represents the minimum impulse required to reach a certain limit state level, which is approached asymptotically by the P–I curve at high pressures, while the quasi-static asymptote defines the minimum peak pressure required to reach the specified limit state.

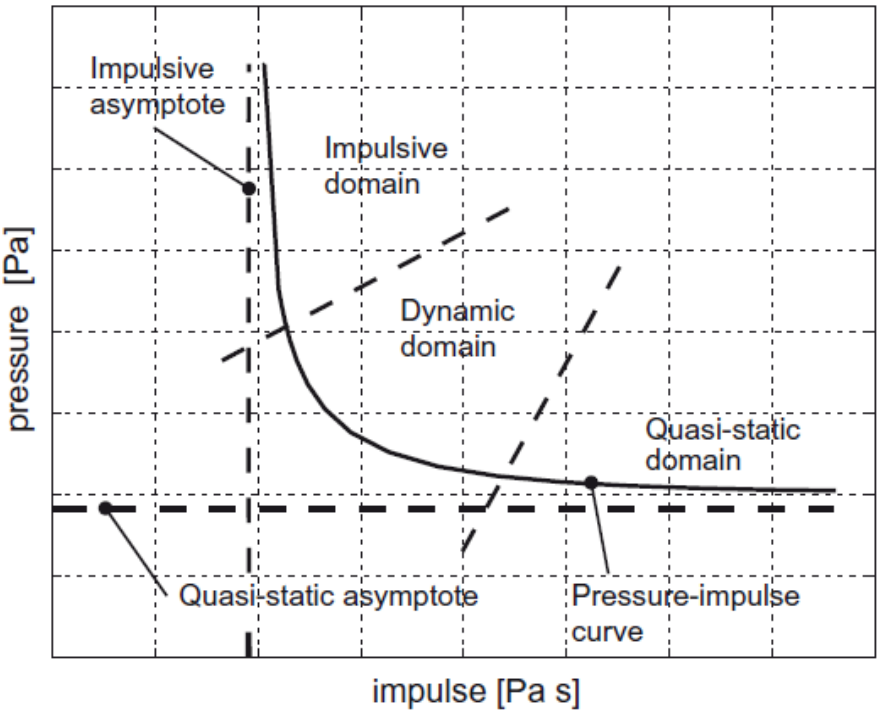

Limits for Loading Regimes

Loading Regime	(Approximate) Limits	
Impulsive	$\omega t_d < 0.4$	$t_d/T < 6.37 \times 10^{-2}$
Quasi-static	$\omega t_d > 40$	$t_d/T > 6.37$
Dynamic	$0.4 < \omega t_d < 40$	$6.37 \times 10^{-2} < t_d/T < 6.37$

Figure 95 – Schematic Pressure Impulse Diagram and Zones Response Behavior

3. Problem Stating: Slab Structures Subjected to Blast

3.1 Introduction

Geometry:

The geometry of the model is a circular slab with following dimensions:

Radius=290mm

Thickness=100mm

*The ratio (diameter/thickness) locates in a transitive state as for the validity of plate theorem and yield line pattern, thus a clarification was made using a computational static analysis, which leads to vivid signs of yield lines generated on the slab in its plastic phase of behavior.

Boundary Condition:

The boundary condition to stabilize the slab is a Pinned fixation on the slab

perimeter. Ux=Uy=Uz=0

*In the computational models this merely applied to the periphery of the lower circle. Implementation of the pinned boundary condition to the upper and lower circles of the circular slab is equal to have a moment resisting boundary condition.

Load:

As explained in the blast section (2.1) Pressure facing the slab surface is a linear function of time with zero rise time duration.

*Having the P-I diagrams, the pressure and impulse for one specific Blast are known, considering a triangular attenuation of the blast shock [28], the total time of the blast is calculated and divided to 10 increments to produce the pressure – time diagram. This diagram is later used as input for Abaqus models:

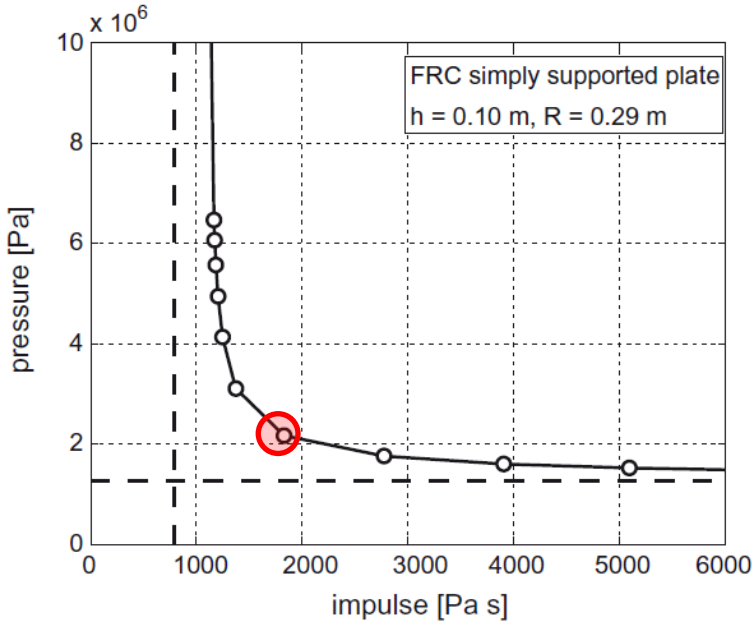

	P-I-1		
Dynamic zone			
P(MPa)	I(MPa.s)	t-final	increment
2.20E+00	0.0018	1.64E-03	1.64E-04
time	Pressure Magnitude	Pressure	
0	1.00E+00	2.20E+00	
1.64E-04	9.00E-01	1.98E+00	
3.27E-04	8.00E-01	1.76E+00	
4.91E-04	7.00E-01	1.54E+00	
6.55E-04	6.00E-01	1.32E+00	
8.18E-04	5.00E-01	1.10E+00	
9.82E-04	4.00E-01	8.80E-01	
1.15E-03	3.00E-01	6.60E-01	
1.31E-03	2.00E-01	4.40E-01	
1.47E-03	1.00E-01	2.20E-01	
1.64E-03	0.00E+00	0.00E+00	

Figure 96 – Pressure Impulse Diagram: P-I data inversion into pressure-time load diagram

The table above shows how Pressure-Time diagram that is derived from the red point on the P-I diagram.

3.2. Experimental tool

A series of experiments are conducted using the Shock Wave Tube Facility, this facility is used by Di prisco et al. [33] with its experiments results published by Colombo and Martinelli [29].

3.3. Analytic Solution

Considering the trend suggested by Colombo and Martinelli [29]; the overall analytic solution behavior is divided into elastic and plastic parts and the structure is assumed as a Single Degree of Freedom (SDOF) system, considering the displacement of the center point of the slab as the measuring node. The solution of the slab subjected to blast is based on the yield line theorem, in order to calculate the blast load which creates the ULS. Having the material properties of the slab; the ultimate possible displacement of the slab center point could be calculated as a function of the material Ultimate Crack Mouth Opening Diameter (COD_u) [29]. Reaching to this displacement for the slab center point means reaching to ULS. ULS is defined through the maximum displacement of the slab mid-point.

For FRC material:

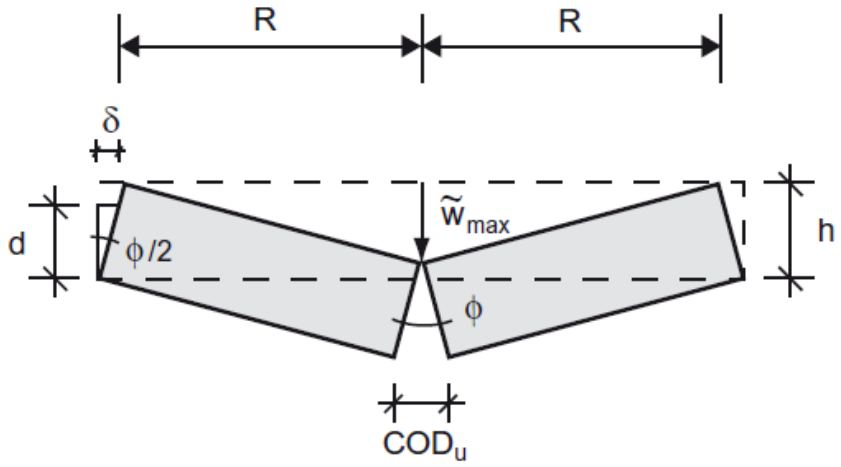

Figure 97 - Ultimate Limit State of the Slab

COD_u is an assumption for the ultimate crack opening diameter.

Figure-97 shows the ultimate limit state of the slab.

h: Slab Thickness

It's clear from the geometry that:

$$COD = h \times \varphi$$

And from the geometry again:

$$Wmax = R \times \varphi/2$$

Therefore, by substituting:

$$Wmax = R/2 \times COD/(h)$$

We know COD_u as an assumption:

$$COD_u = \min(3\,\text{mm}, \varepsilon_{Ftu}\, l_{cs}).$$

The structural characteristic length l_{cs} is equal to the slab thickness

$$l_{cs} = h$$

and the ultimate tensile strain of the FRC is equal to:

$$\varepsilon_{Ftu} = 2\%.$$

$COD_u = 0.02 \times 100 = 2$

$Wmax = R/2 \times COD/(h)$

W_{max} for R= 290 mm ------> **2.9 mm**

4. FRC material slab subjected to blast

4.1. Introduction

In the current research our tool for modeling the slabs subjected to blast is the Abaqus software. The final aim is to model the slab made of syntactic foam VE460-30. In order to validate the computational modeling procedure with Abaqus, primarily the slab model made of FRC which is solved by Colombo and Martinelli [29] in an analytic procedure is modeled with the Abaqus and the two set of results are compared to check the precision of the latter method.

4.2. Analytic Results

Colombo and Martinelli [28] have derived the P-I diagrams for slabs made of RC and FRC materials. In the current research the chosen model for sake of comparing is a slab with the properties stated in the section (3.1). The slab material is chosen to be FRC.

The final P-I diagram is as follows:

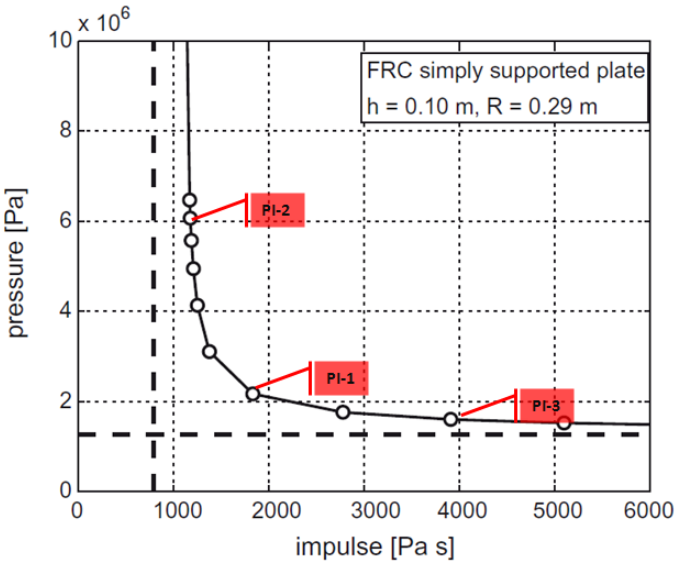

Figure 98 – Simply Supported FRC slab P-I diagram (Slab thickness=100mm) [28]

4.3. Computational Model

4.3.1. Introduction

In order to produce the computational model with Abaqus the following steps are taken, these steps are known as modules [34]:

1. Part

   The part module is in fact the creation of the geometry which is introduced in the section (3.1). To do so, a 2D circular shell part with deformable characteristics is created. The diameter of the shell elements is chosen to be 290mm.

   Abaqus doesn't have a standard unit choice by default for input values; the user shall choose all the numbers to match a unique set of unit standard. In the current research the explained set is chosen for units:

   All the parameters are to be in (N, mm) units which gives the unit (10^6 gr) for mass. Or one may assume (10^6 gr, mm) as principle dimensions which gives "N" as the force unit.

   [1N = 1Kg ×1m/s^2 ----> Mass Unit: N/(mm/s^2) = 10^3Kg = 1 ton]

   [Density unit (N, mm): Mass unit / (Volume unit) ^{3} = (10^3 kg) / (10^{-9}m) = 10^{12} Kg/m^3]

   For instance the density of concrete will be inserted as calculated below:

   2400 Kg/m^3 = 2400 × 10^{-12} (ton/mm^3)

2. Property

The FRC material properties are as follows [29]:

Material properties of the concrete (ρ = density, E_c = Young modulus, f_{ck} = cylindrical characteristic compressive strength, v = Poisson ratio, c = cover of reinforcement).

ρ [kg/m^3]	E_c [GPa]	f_{ck} [MPa]	v [–]	c [m]
2500	42.6	75	0.2	0.02

Material properties of fibre-reinforced concrete (f_{ck} = cylindrical characteristic compressive strength, $f_{eq,1}$ = Serviceability Limit State residual strength, $f_{eq,2}$ = Ultimate Limit State residual strength, ε_{Ftu} = uultimate tensile strain).

f_{ck} [MPa]	$f_{eq,1}$ [MPa]	$f_{eq,2}$ [MPa]	ε_{Ftu} [-]
75	5.34	3.91	0.02

Table 99 - FRC Material Properties

Density = 2500 Kg/m3 = 2500 × 10^{-12} gr/mm3

Young Modulus = 42.6 GPa = 42600 MPa

Poisson's ratio = 0.2

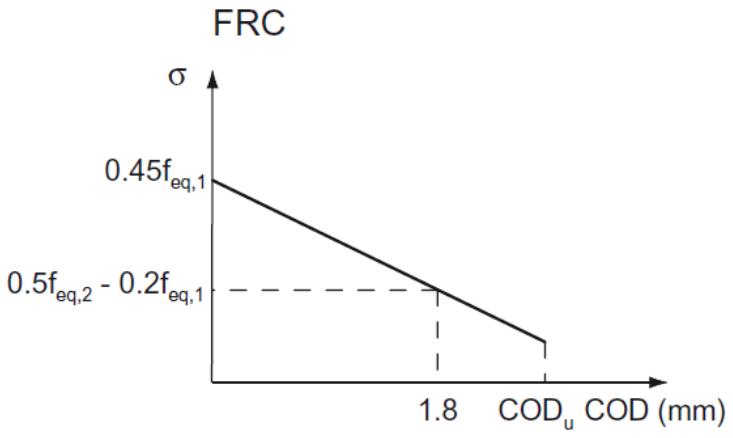

Diagram 100 – FRC Stress-Crack Mouth opening

Having the constitutive model of the FRC based Serviceability and Ultimate Limit State Residual Stress [29]; the following charts and constitutive models are derived for the current material:

Strain	Stress (Softening)	Stress (Perfectly Plastic)
0.000	2.403	1.645
0.018	1.039	1.645
0.020	0.887	1.645

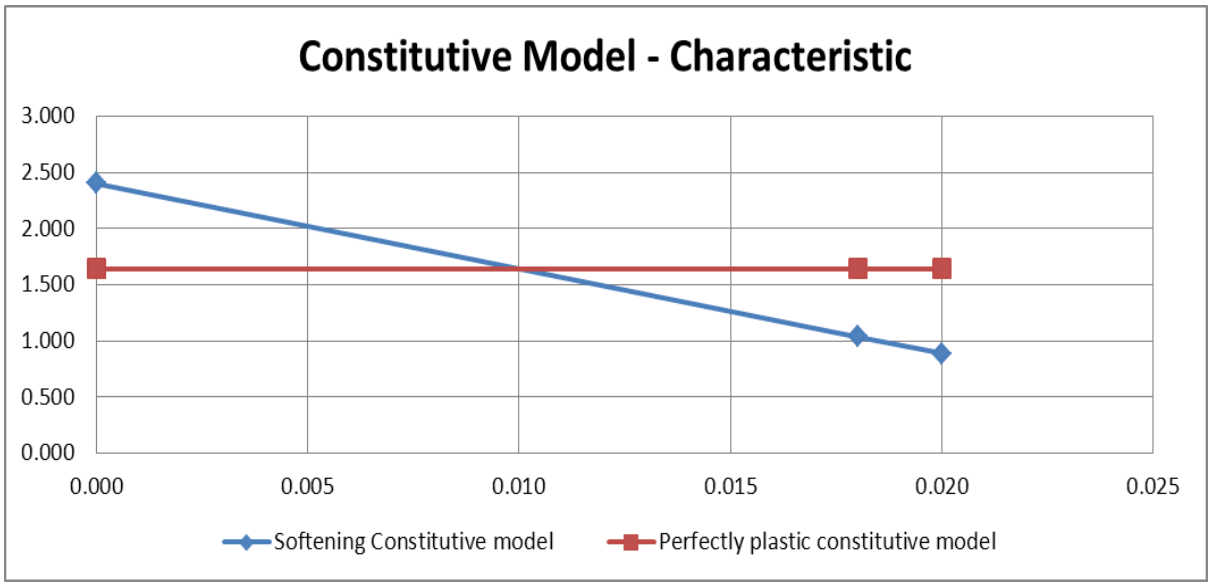

Figure 101 –Constitutive Model of FRC

We shall consider that the problem is a ULS one, with partial coefficients of Euro Code applied on the parameters. Considering a reducing partial coefficient for materials [35], the design values and corresponding design constitutive model is as follows:

Design Values		
Strain	Stress (Softening)	Stress (Perfectly Plastic)
0.000	1.60	1.10
0.020	0.59	1.10

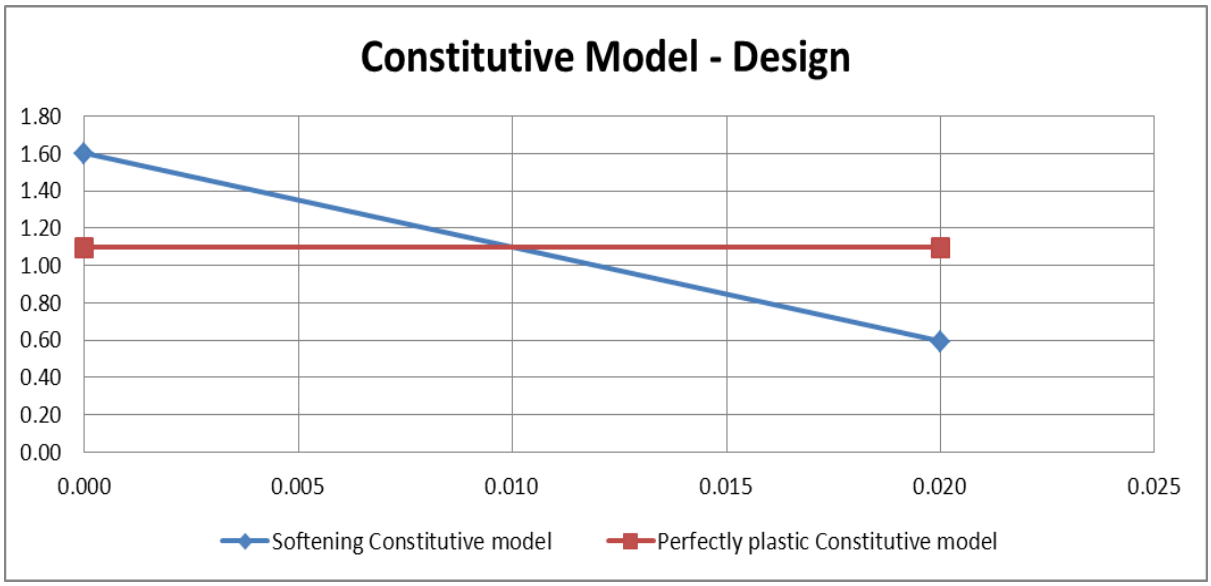

Figure 102 - Constitutive Model of FRC (Partial Safety Factors Applied)

And for the compressive constitutive model, an ultimate characteristic compressive strength of 75 MPa with ultimate strain being equal to 0.003 is assumed. The design value would be equal to 50 MPa.

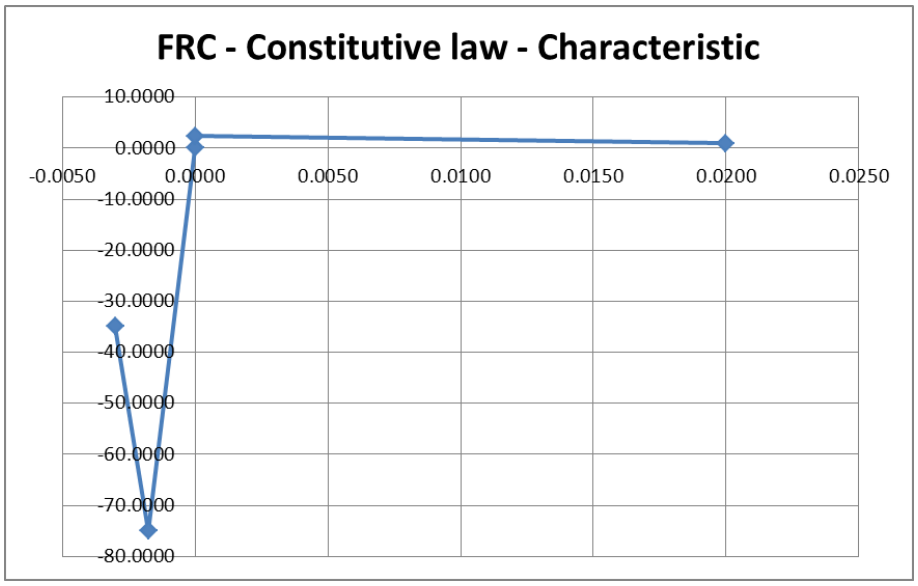

Figure 103 – Characteristic Constitutive Model of FRC

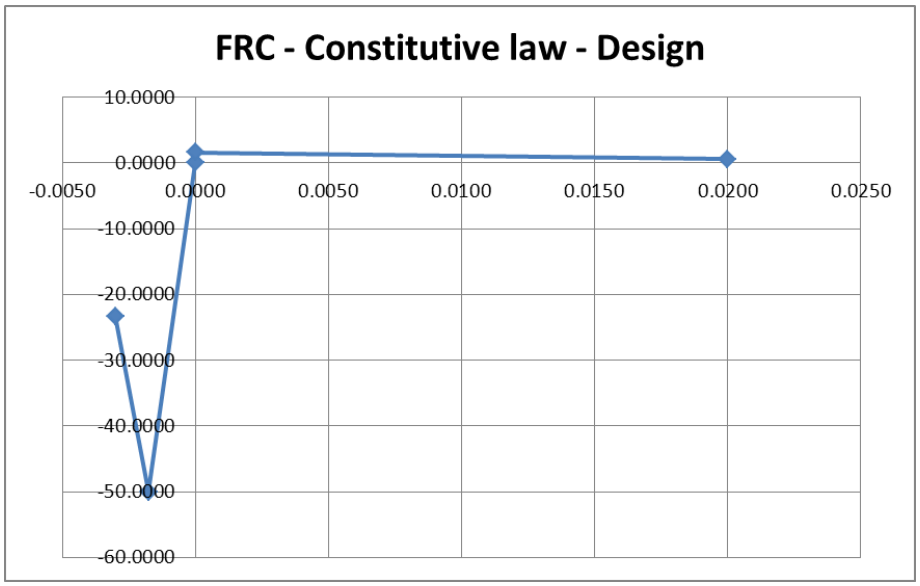

Figure 104- Design Constitutive Model of FRC

These assumptions result the following material models co-efficients, furthermore the material uniaxial parametric behavior values are inserted as ABAQUS input data:

- CDP: Concrete Damaged Plasticity [31]

Abaqus introduces a default set of parameters for modeling traditional concrete; these are acceptable as they mostly deal compressive behavior of the concrete which doesn't change considerably due to its reinforcement by fibers.

Then the uniaxial constitutive model of FRC is implemented as input data to compensate for the tensile strength.

Dilation Angle = 20

K=0.75

fb/fc = 1.16

Eccentricity = 0.1

Viscosity parameter = 0

- DP: Drucker-Prager [30]

Based on the ABAQUS scientific indications the model parameters are derived:

$$B = Arctan((2 \times \frac{f_c}{f_c + f_t} - 1) \times 3)$$

$$d = f_c \times (1 - 0.33 \times tan(B))$$

Characteristic Values

fc	75.0000	**d**	2.4857	
ft	0.8870	**B**	1.2419	71.1546

Design Values

fc	50.0000	**d**	1.6572	
ft	0.5913	**B**	1.2419	71.1546

3. Step

In this module the analysis type is chosen. For blast modeling, a dynamic explicit one is chosen [36].

It's noteworthy that the analysis steps are divided into two time durations (steps):

- Step short: Time increments are shorter than blast pressure time increments, in order to make sure the blast load is noted by the software, the overall time duration is greater than the blast duration time.
- Step long: Time increments are optimized by the software; the general post-blast behavior of the slab is investigated.

4. Load

A pinned boundary condition is created around the circular slab perimeter. And the blast load is inserted as a pressure which varies with respect to time. The points which are shown as P-I-1, P-I-2 and P-I-3 in the Figure-98 are selected from three different regimes of the diagrams in order to validate the computational

model in every loading phase. These points data are translated into Pressure-Time diagrams and inserted into Abaqus as tabular data for Pressure Load [37].

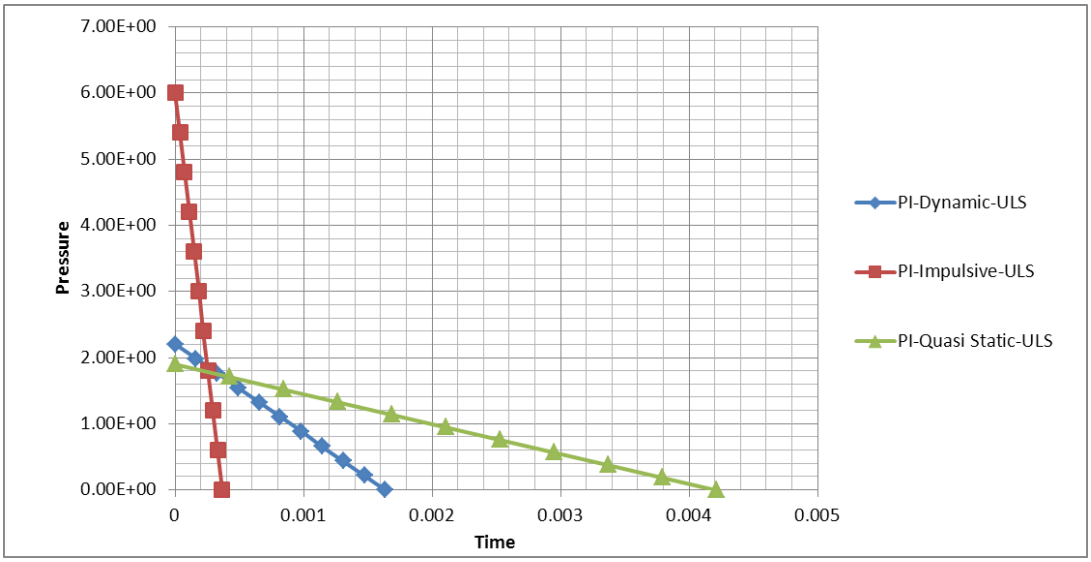

Figure 105 – Pressure-Time relations of blast loads

P-I-1	Dynamic			
P(MPa)	I(MPa.s)	t-final	increment	P-design (Mpa)
2.20E+00	0.0018	1.64E-03	1.64E-04	3.30E+00
P-I-2	Impulsive			
P(MPa)	I(MPa.s)	t-final	increment	P-design (Mpa)
6.00E+00	0.0011	3.67E-04	3.67E-05	9.00E+00
P-I-3	Quasi-Static			
P(MPa)	I(MPa.s)	t-final	increment	P-design (Mpa)
1.90E+00	0.004	4.21E-03	4.21E-04	2.85E+00

Figure 106 - FRC slab P-I diagram selected points data

We should also consider that the current problem is a ULS one, with Euro Code factors being applied [35], therefore the pressure values from the tabular data in Colombo-Martinelli Article is multiplied by 1.5, which stands for a partial factor of safety for accidental loads.

5. Mesh

The mesh elements are set to be Quad-dominated with a free meshing technique, the mesh element code is S4R which stands for A4-node doubly curved thin or thick shell. [38]

4.3.2. Results

Material Model: Concrete Damaged Plasticity

Load: PI-1

Total (t=0-0.06 s)

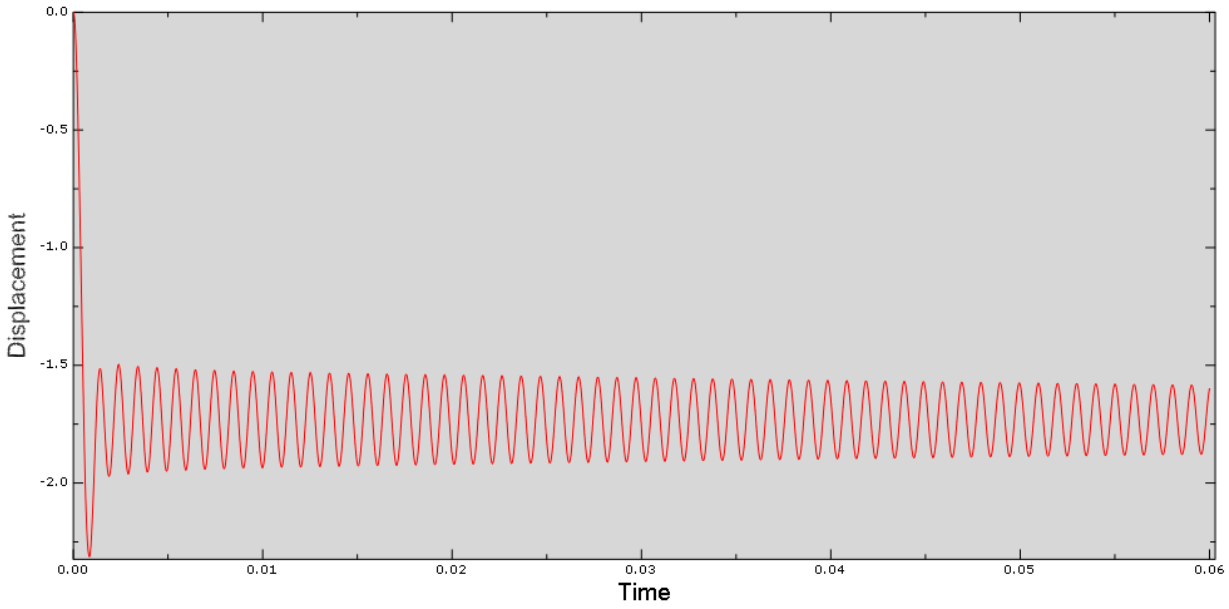

t: 0-0.01

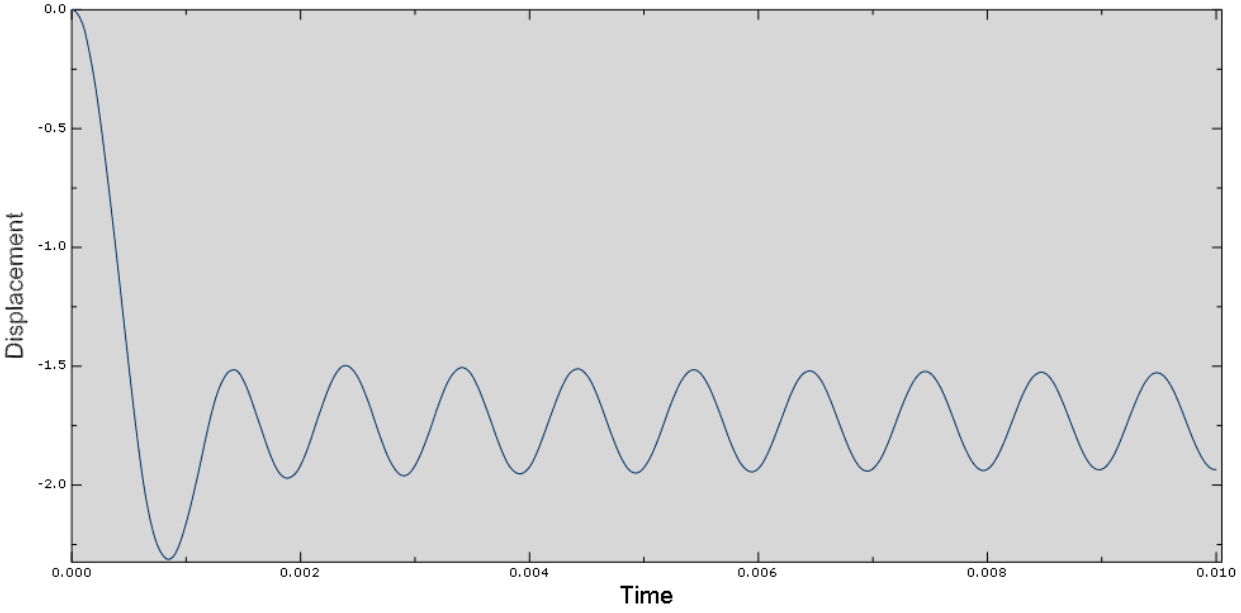

Load: PI-2

t= 0-0.06 s

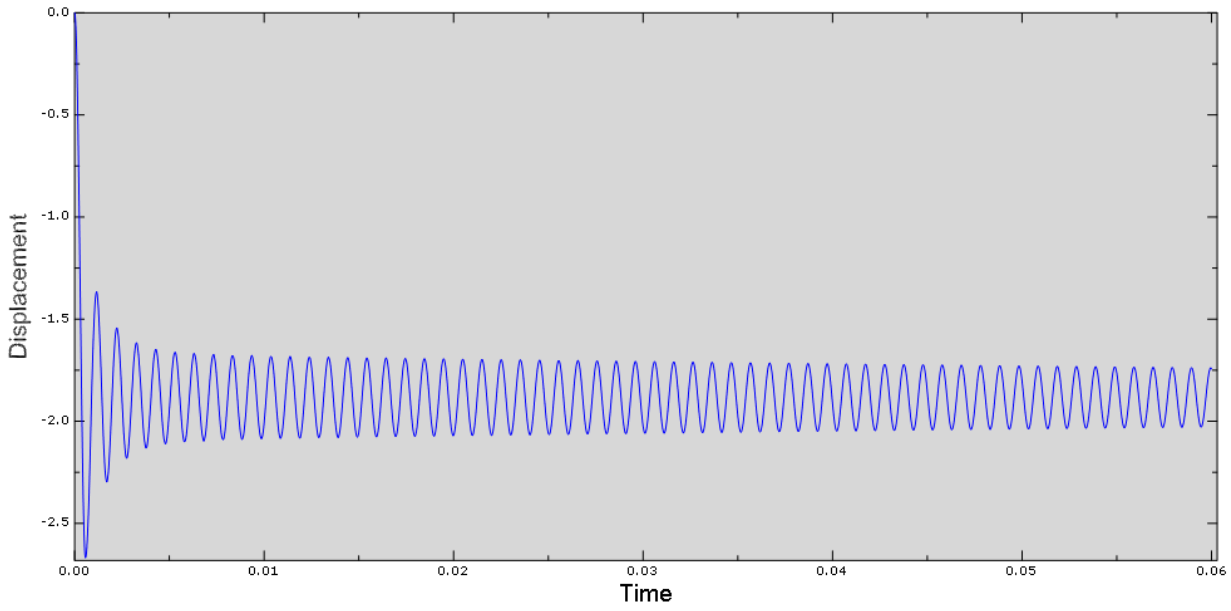

t=0-0.01 s

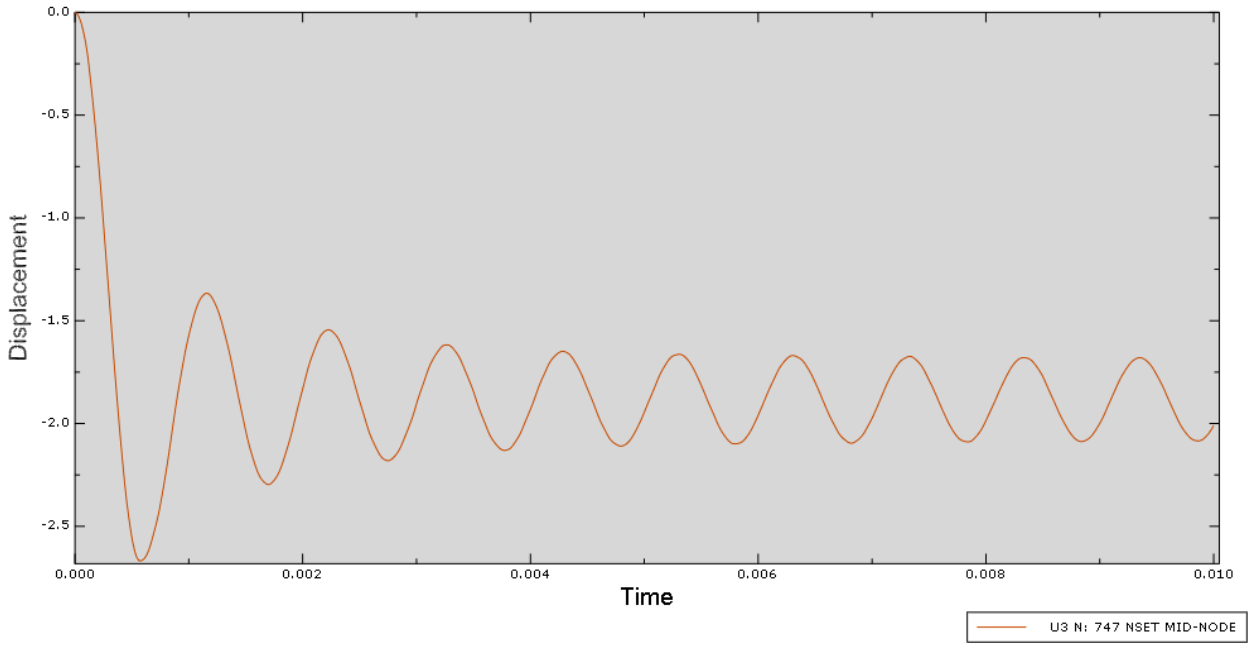

Load: PI-3

t=0-0.06

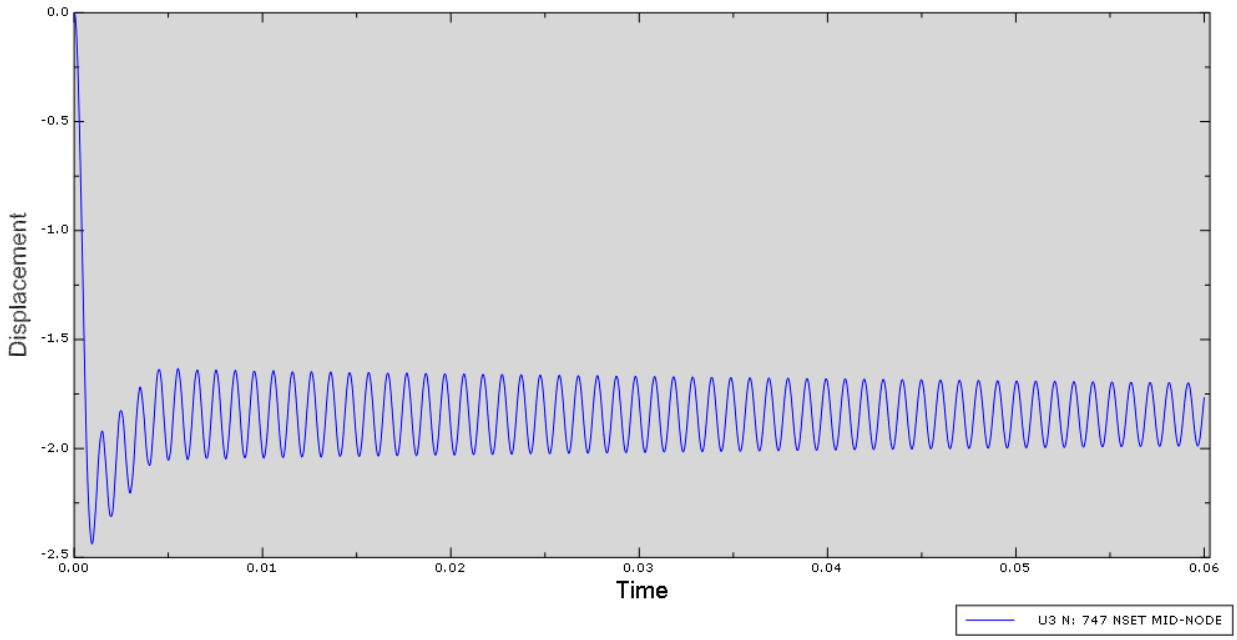

t= 0-0.01

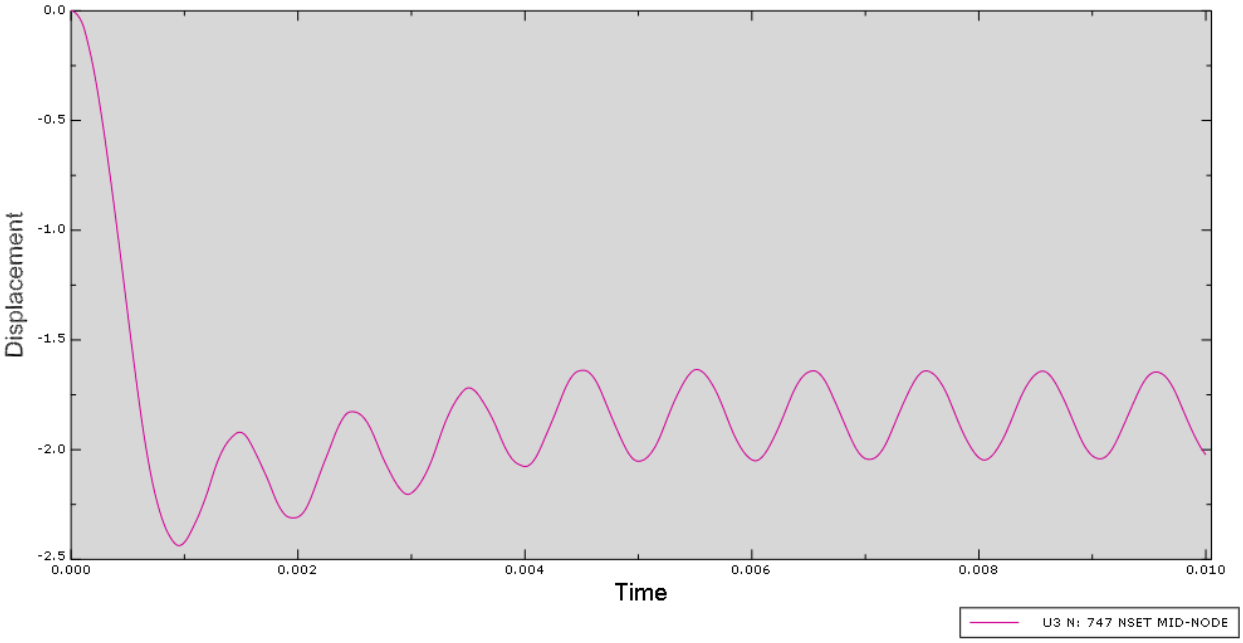

As it’s seen there’s a perfect match between the responses from three different pressure-time loads ,which respectively correspond to Dynamic, Impulsive and Quasi-Static zones of the pressure-impulse diagram, meaning that the maximum displacements of the slab mid-point are rather equal to each other, in three loading conditions, (2.4 mm – 2.6mm). Moreover, this value is very close to the predicted maximum displacement (ULS) which should have been achieved over the asymptote, by Colombo-Martinelli (2.9mm). [29]

This means that for producing the pressure – impulse asymptote, from the current modeling technic - based on ULS, Wmax = 2.9mm – the pressure or impulse must be slightly increased (individually or both at the same time).

Using a trial and error procedure, creating models with loaded by different pressure-time trends, results approximately equal to Wmax=2.9mm is reached.

PI-22

Impulsive Zone:

t=0-0.06

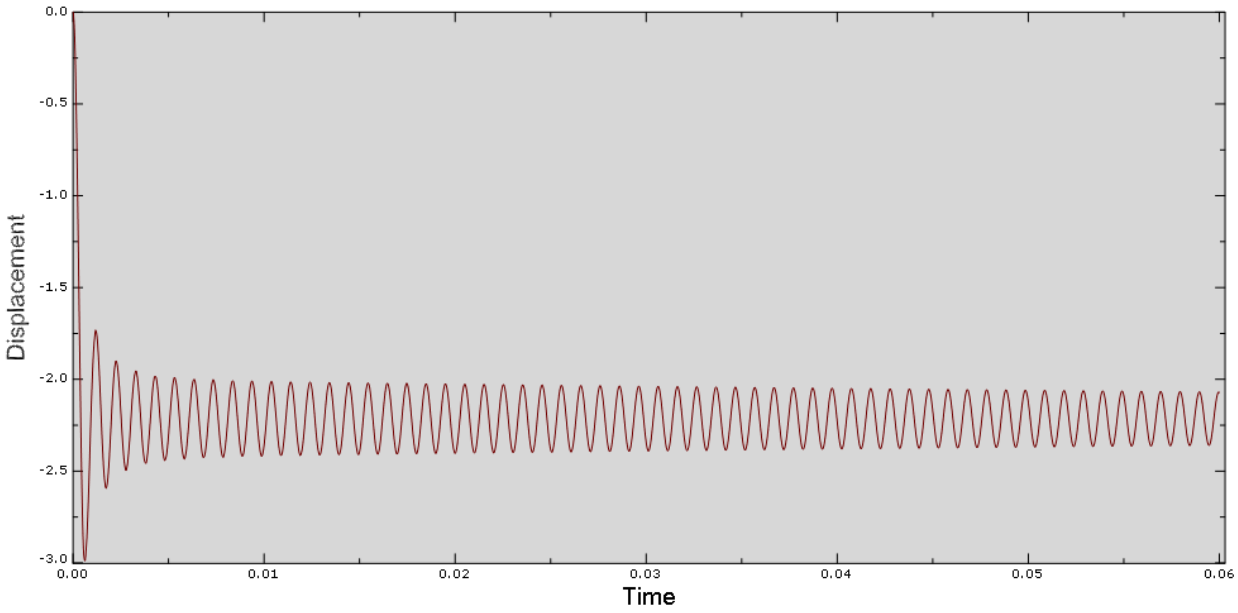

t=0-0.01 s

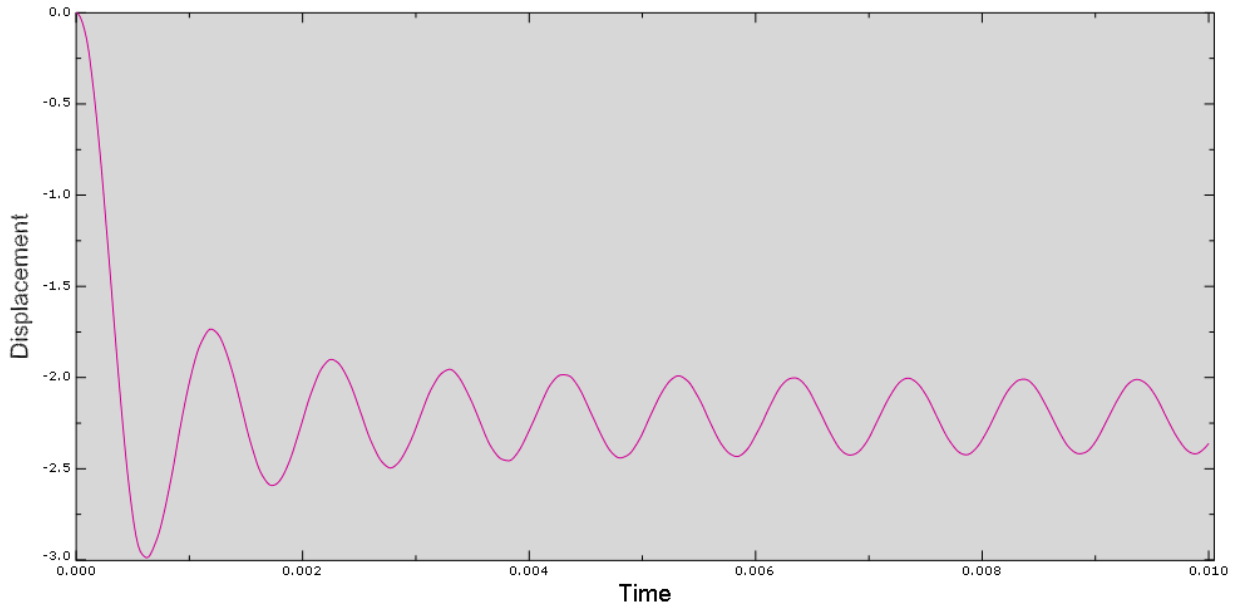

PI-12

Dynamic Zone

t=0-0.06

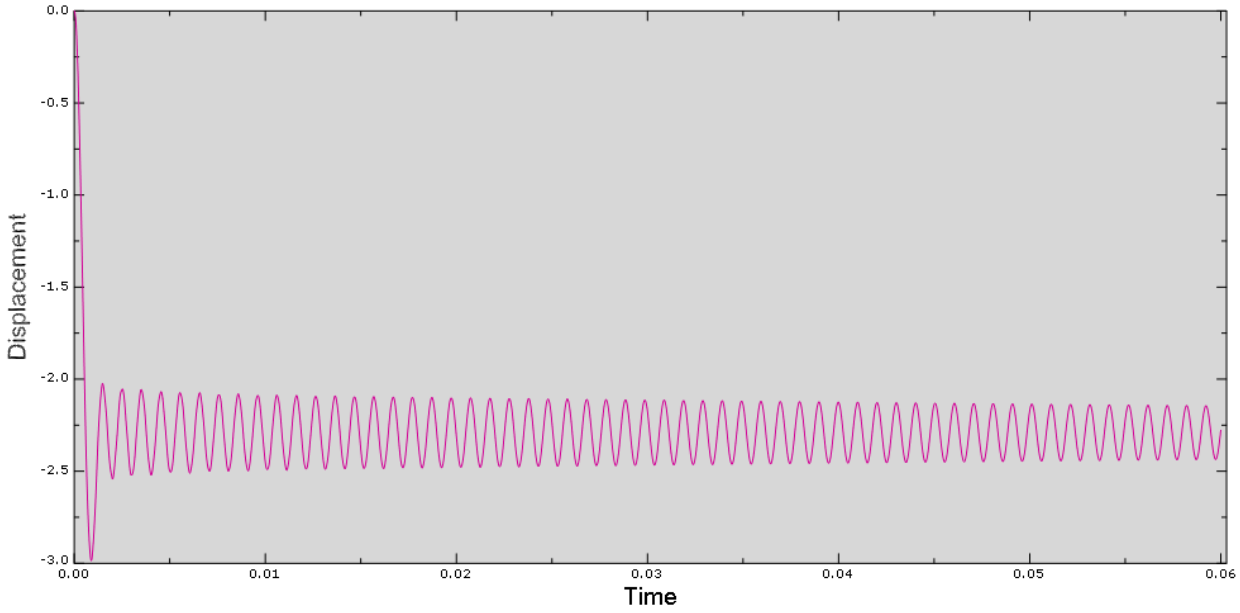

t=0-0.01 s

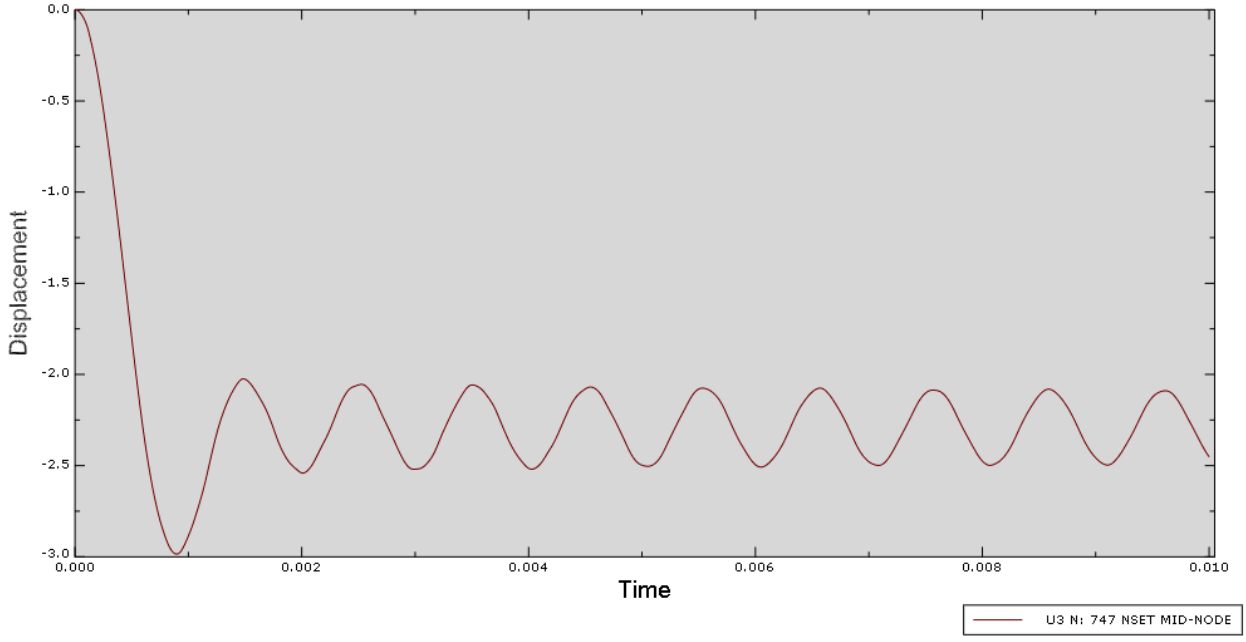

PI-32

Quasi-Static Zone

t=0-0.06

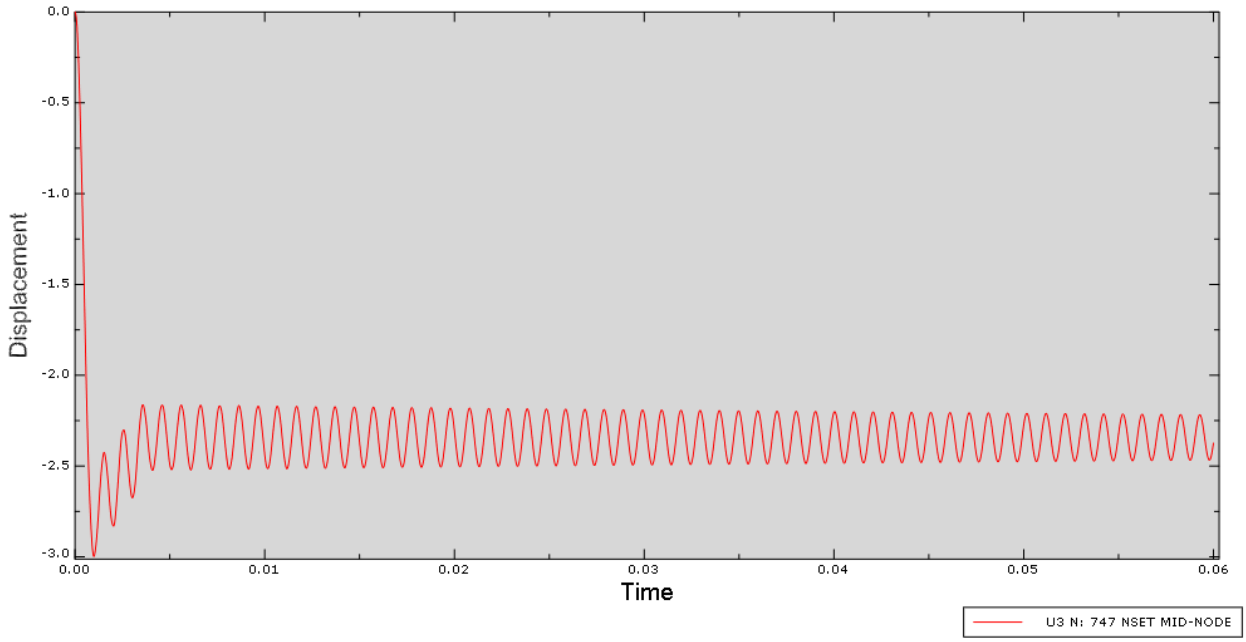

t=0-0.1s

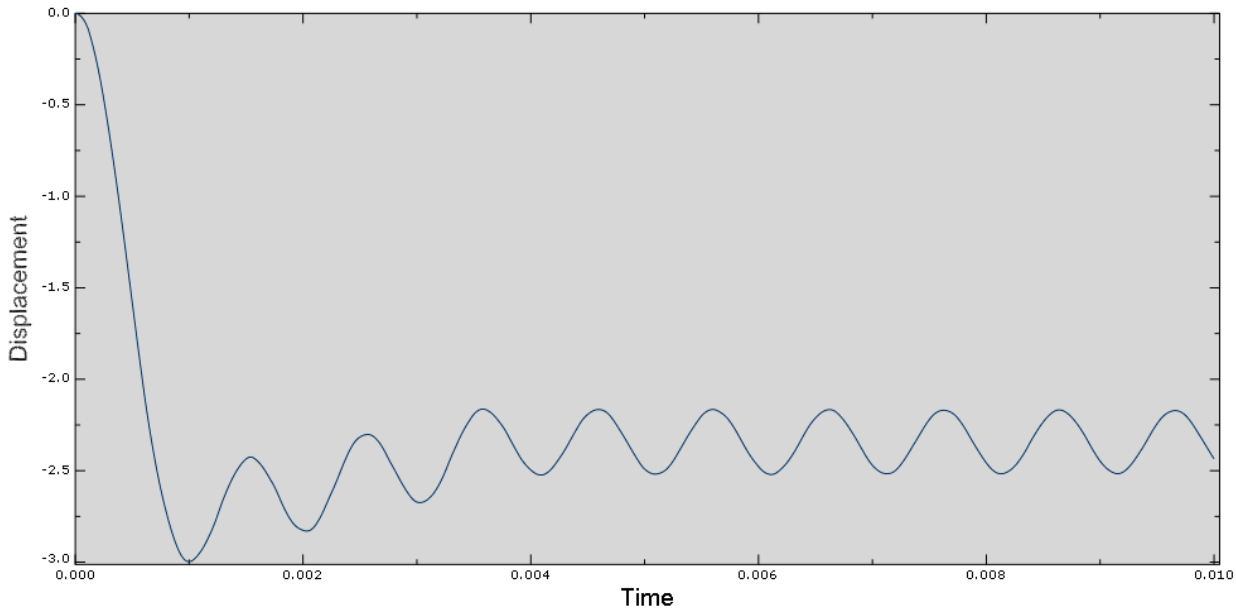

Finally continuing the trial and error procedure for other couples of Pressure and Impulse the PI-diagram is created using 5 points:

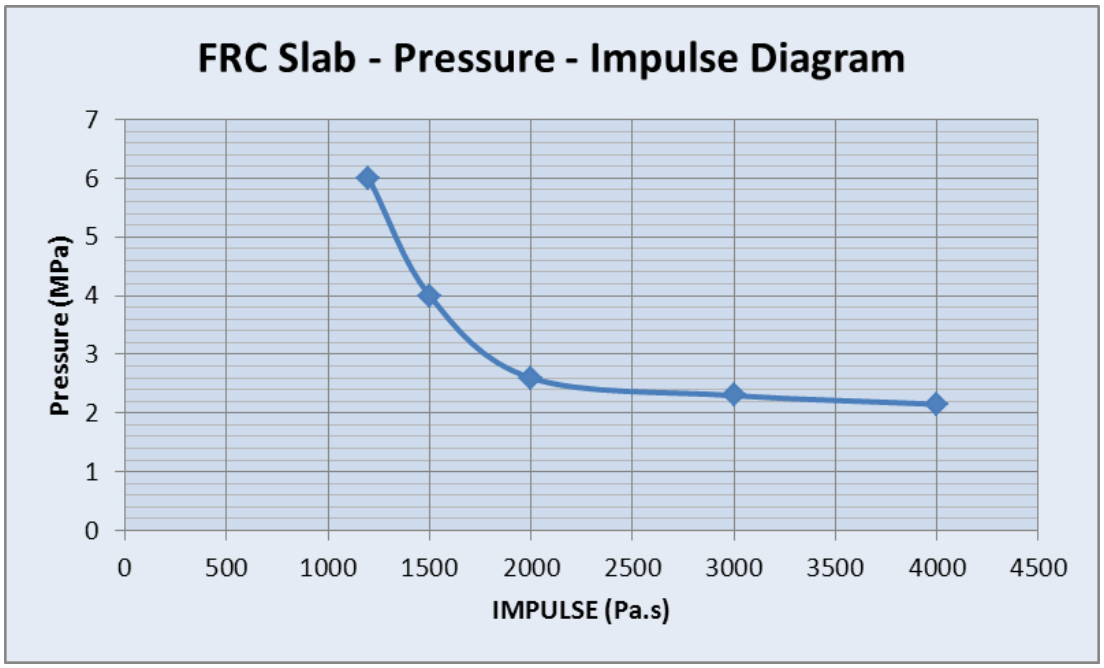

5. Syntactic Foam material slab subjected to blast

5.1. Introduction

Taking all the same assumptions of the model in section (4.3.1) expect the material model and the assumed ULS.

VE460-30 Material Properties [7]:

E = 3800 MPa

Density = 740 Kg/m^3

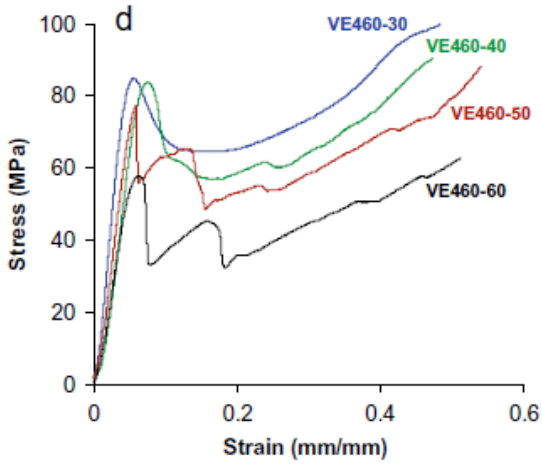

Figure 107 - Compressive Constitutive law [7]

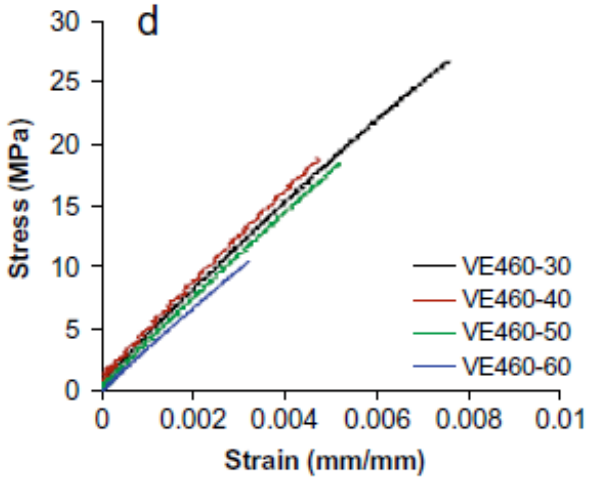

Figure 108 - Tensile Constitutive law [7]

Syntactic Foam	
Strain	**Stress**
-0.5000	-100.0000
-0.0243	-85.0000
0.0000	0.0000
0.0075	27.0000

Assumed Constitutive behavior:

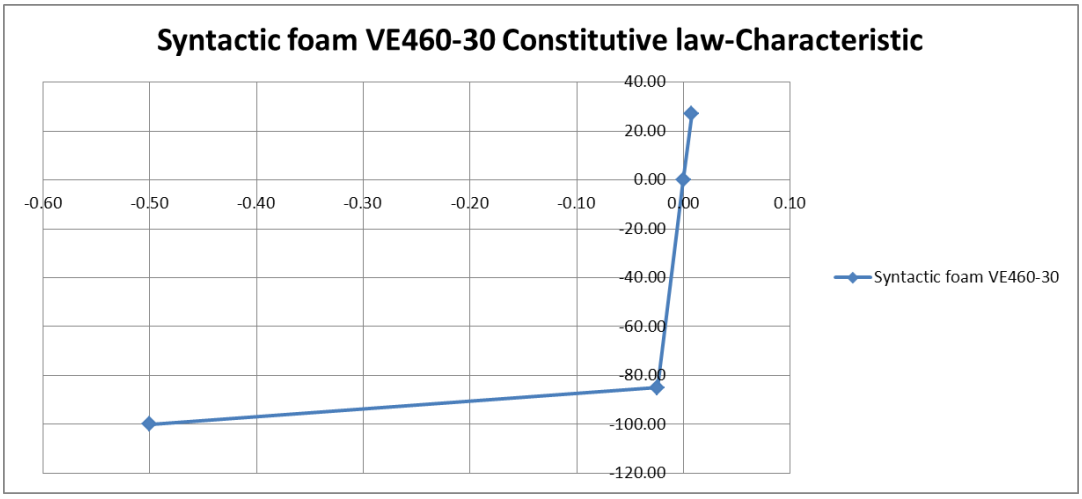

Figure 109 - Syntactic Foam VE460-30 Characteristic Constitutive Law

This is a design procedure again, conservative load increase and material strength factors of 1.5 are considered for the model parameter, thus:

Syntactic Foam	
Strain	**Stress**
-0.5000	-66.6667
-0.0162	-56.6667
0.0000	0.0000
0.0075	18.0000

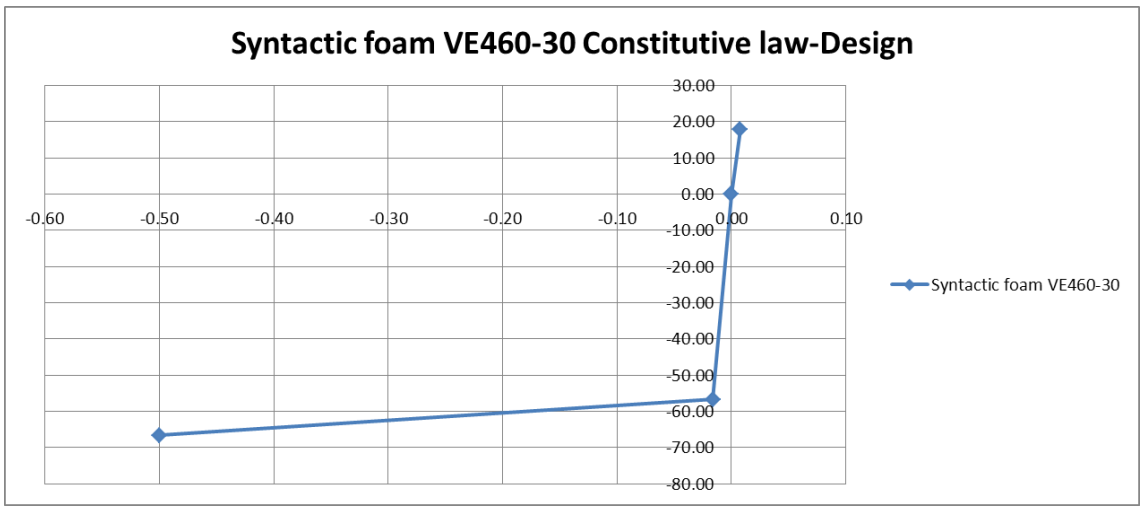

Figure 110 - Syntactic Foam VE460-30 Design Constitutive Law

Comparing FRC and VE460-30, there is one significant difference that the syntactic foam has a very large ultimate compressive strain, but in the case of slabs subjected to blast the defining parameter for determining ULS is the ultimate tensile strain, for which both materials are from the same order (0.0075 for VE460-60 and 0.02 for FRC). Using the same trend for sake of deriving the ultimate limit state index, gives such results:

ULS is defined through the maximum displacement of the slab mid-point.

For VE460-30 material:

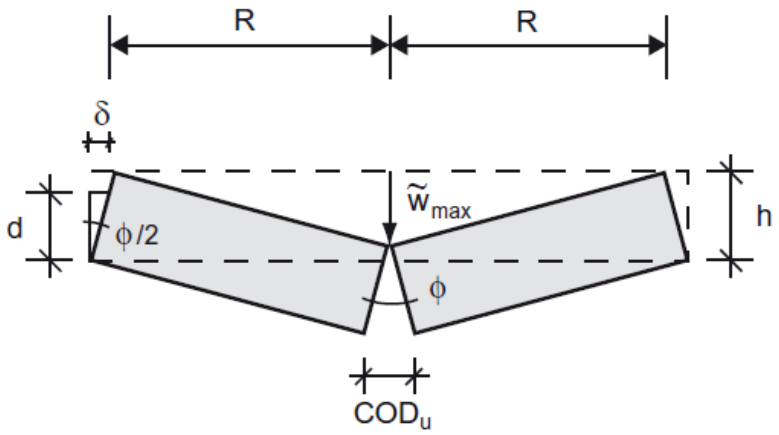

Figure 111 - Ultimate Limit State of the slab

COD_u is an assumption for the ultimate crack opening diameter.

Figure-109 shows the ultimate limit state of the slab.

It's clear from the geometry that:

$$COD = h \times \varphi$$

And from the geometry again:

$$Wmax = R \times \varphi/2$$

Therefore, by substituting:

$$Wmax = R/2 \times COD/(h)$$

We know COD_u as an assumption:

$$COD_u = \min(3\,\text{mm}, \varepsilon_{Ftu}\, l_{cs}).$$

The structural characteristic length l_{cs} is equal to the slab thickness

$$l_{cs} = h$$

and the ultimate tensile strain of the FRC is equal to:

$$\varepsilon_{Ftu} = 2\%.$$

$COD_u = 0.0075 \times 100 = 0.75$

$Wmax = R/2 \times COD/(h)$

W_{max} for R= 290 mm ------> **1.0875 mm** (approximately 1.1mm)

Therefore any blast load (Impulsive, Dynamic and Quasi-Static) that results in such a displacement of the slab mid-node is an asymptotic point on Pressure – Impulse diagrams. Despite the FRC models, where there were a series of benchmarks from the Colombo-Martinelli [29] as for the pressure and its time duration, finding the P-I diagram of VE460-30 is through a full-scale trial and error procedure.

5.2. Computational Results

After a series of trial and errors the ULS is reached:
For Quasi-Static zone:

PI-1

P-I-1	Dynamic			
P(MPa)	I(MPa.s)	t-final	increment	P-design (Mpa)
2.33E-01	0.0018	1.54E-02	1.54E-03	3.50E-01

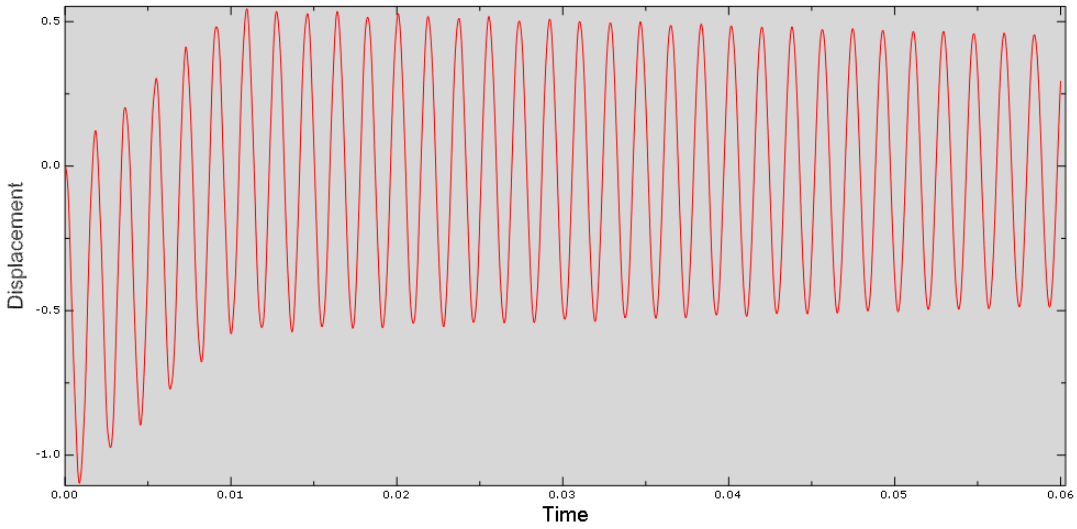

For Impulsive zone:

PI-2

P-I-2	Impulsive			
P(MPa)	I(MPa.s)	t-final	increment	P-design (Mpa)
3.25E-01	0.0011	6.77E-03	6.77E-04	4.88E-01

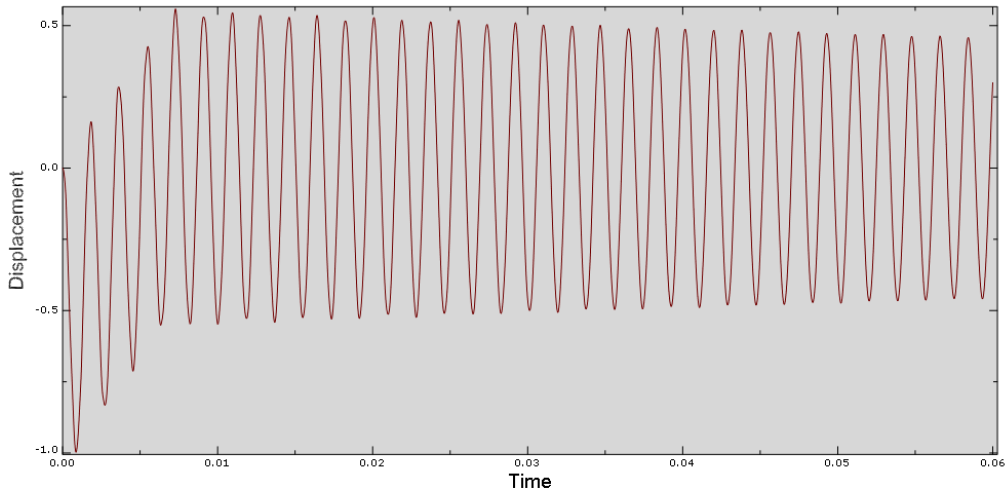

Continuing the trial and error procedure for all other couples of Pressure and Impulse:

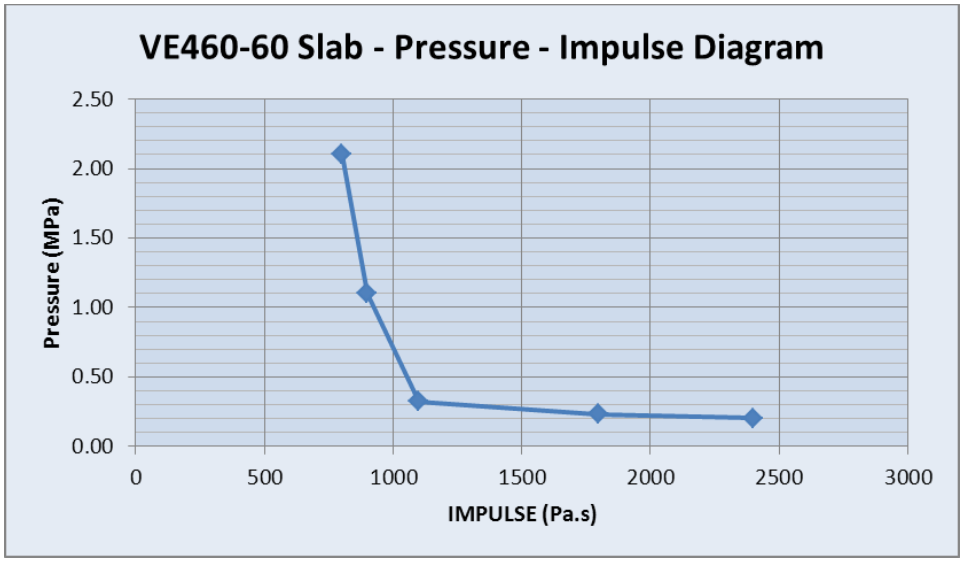

Comparing two materials P-I diagrams:

Blue: FRC

Red: Syntactic Foam

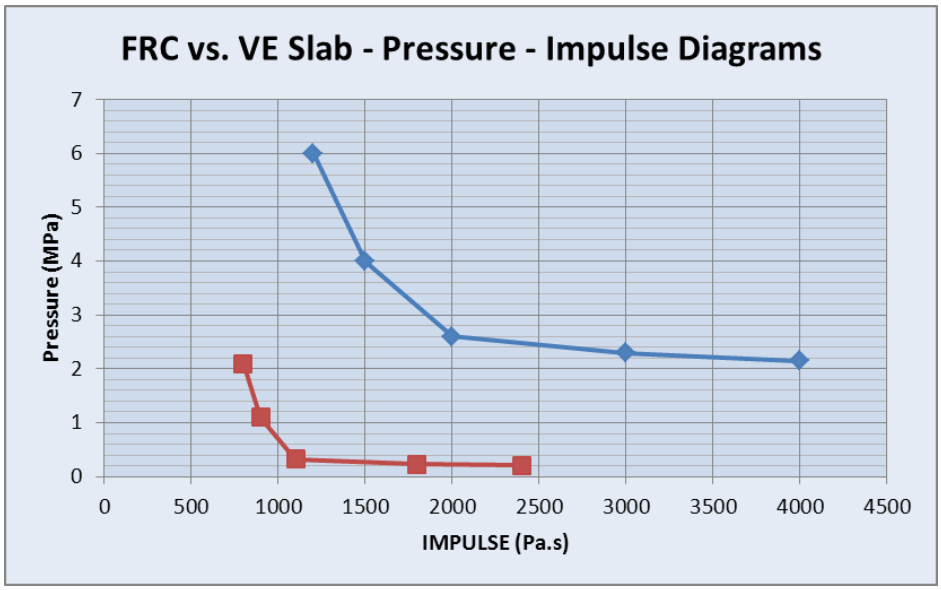

6. Conclusions

6.1. Outline of Main Results

In the current research the capacity of Syntactic Foams to confront extreme loads (blast load) is investigated through computational models.

First the capacity of the Abaqus Explcit in modeling the blast phenomena for circular slabs has been approved through section 4. Then the same modeling technique was repeated for the Syntactic Foams, considering VE460-30 properties.

Reviewing the results and comparing the nature of FRC and syntactic foam being considered (VE460-30), the achieved results are logically acceptable; Comparing FRC and VE460-30, there is one significant difference that the syntactic foam has a very large ultimate compressive strain, but in the case of slabs subjected to blast the defining parameter for determining ULS is the ultimate tensile strain, for which both materials are from the same order (0.0075 for VE460-60 and 0.02 for FRC), however Syntactic foam is about three times weaker. This has led to the generation of the P-I diagram for the composite material which cover a smaller area as the safe region, especially for the impulsive region, with respect to FRC. Anyhow seeing the available capacity of Syntactic Foam in blast calls for a possible practical use of the composite material (syntactic foam in general including VE460-30) as a blast dissipater. Moreover, due to extensive use of such syntactic foams in aerospace and naval industry fields, the material potential to dissipate energy in case of blast could be of primary concern for sake of structural risk analysis of the members with syntactic foam as their main or cover material.

Appendix – A: The Concept of Voigt-Reuss Bounds for Syntactic Foams

Considering a plane stress problem for the 2D model of an arbitrary square RVE and by using standard notation (Nemat-Nasser and Hori, 1993), we define the in-plane macroscopic (i.e., overall) stress vector as follows:

$$\boldsymbol{\Sigma} = \{\Sigma_{11} \;\; \Sigma_{22} \;\; \Sigma_{12}\}^{\mathrm{T}}$$

And the plane macroscopic (i.e., overall) strain vector as stated below:

$$\boldsymbol{E} = \{E_{11} \;\; E_{22} \;\; E_{12}\}^{\mathrm{T}}$$

These are known as volume averages of the relevant microscopic (i.e., local) fields σ and ε, namely:

$$\boldsymbol{\Sigma} = \frac{1}{V}\int_{V} \boldsymbol{\sigma} dV$$

$$\boldsymbol{E} = \frac{1}{V}\int_{V} \boldsymbol{\varepsilon} dV$$

Where V is here used also to denote the measure of the RVE volume, the elastic response of each RVE phases elements at its microscopic scale is described by the following stress-strain relationship:

$$\boldsymbol{\sigma} = \boldsymbol{c}\boldsymbol{\varepsilon}$$

And the macroscopic constitutive relation is assumed to be as follows:

$$\boldsymbol{\Sigma} = \boldsymbol{C}\boldsymbol{E}$$

Which is in fact a relation between volume averages of the relevant microscopic (i.e., local) fields σ and ε. The matrix "C" is the entity that shows the constitutive behavior of the RVE or in other words the macroscopic behavior of the composite material.

Voigt Bound

Assuming that the value of the microscopic strain is equal to the macroscopic one at every point (x) the following equation is valid:

$$\boldsymbol{\varepsilon}(\boldsymbol{x}) = \boldsymbol{E}$$

Considering the following equation:

$$\boldsymbol{\Sigma} = \frac{1}{V}\int_{V} \boldsymbol{\sigma} dV$$

Following could be resulted:

$$\boldsymbol{C} = \frac{\boldsymbol{1}}{\boldsymbol{V}} \times \int \boldsymbol{c}(\boldsymbol{x}) \times \boldsymbol{dv}$$

This is in fact the relation between microscopic constitutive matrices of different phases with the overall Voigt constitutive matrix.

Reuss Bound

Assuming that the value of the microscopic stress is equal to the macroscopic one at every point (x) the following equation is valid:

$$\boldsymbol{\sigma}(\boldsymbol{x}) = \boldsymbol{\Sigma}$$

Considering the relation below:

$$\boldsymbol{E} = \frac{1}{V}\int_{V} \varepsilon dV$$

The following equation could be derived:

$$\boldsymbol{C^{-1}} = \frac{\boldsymbol{1}}{\boldsymbol{V}} \times \int \boldsymbol{c^{-1}}(\boldsymbol{x}) \times \boldsymbol{dv}$$

This is in fact the relation between microscopic constitutive matrices of different phases with the overall Reuss constitutive matrix.

For syntactic foams, having three phases:

1. Vinyl Ester (Matrix)
2. Spherical Glass (Inclusion)
3. Void

$$V = V_{matrix} + V_{Inclusion} + V_{Void}$$

Defining each phase volume fraction:

$$f_{matrix} = \frac{V_{matrix}}{V}$$

$$f_{inclusion} = \frac{V_{inclusion}}{V}$$

$$f_{void} = \frac{V_{void}}{V}$$

For the Voigt bound:

$$C = c_{matrix} \times f_{matrix} + c_{inclusion} \times f_{inclusion}$$

For the Reuss bound:

$$C^{-1} = c^{-1}{}_{matrix} \times f_{matrix} + c^{-1}{}_{inclusion} \times f_{inclusion}$$

c_{matrix} = Plane stress constitutive matrix of the matrix material (Vinyl Ester)

$c_{inclusion}$ = Plane stress constitutive matrix of the inclusion material (spherical glass)

Appendix – B: The text of the MATLAB code Voigt-Reuss Bounds

```
function voigt_reuss_plane_stress_s
%voigt and reuss bounds for plane stress%



[Phase_Property,RVE_Index,RVE_size_parameter]=input_file;
%number of RVEs with different volume fractions
m=size(Phase_Property,3);
%number of phases in the matrix material%
n=size(Phase_Property,1);
Constitutive_Matrix=zeros(3,3,n);
Constitutive_Matrix_1=zeros(3,3,n);

%Young Voigt (Young modulus for each RVE size)
Young_Voigt=zeros(m,2);
%Poisson Voigt (Poisson's Ratio for each RVE size)
Poisson_Voigt=zeros(m,2);
%Shear Voigt (Shear Coefficient for each RVE size)
Shear_Voigt=zeros(m,2);


%Young Reuss (Young modulus for each RVE size)
Young_Reuss=zeros(m,2);
%Poisson Reuss (Poisson's Ratio for each RVE size)
Poisson_Reuss=zeros(m,2);
%Shear Reuss (Shear Coefficient for each RVE size)
Shear_Reuss=zeros(m,2);


for g=1:m
for i=1:n
    coeff =1/Phase_Property(i,2,g);
    Constitutive_Matrix_1(:,:,i)= ...
    coeff*[1,-Phase_Property(i,3,g),0; -
Phase_Property(i,3,g),1,0;0,0,2*(1+Phase_Property(i,3,g))];
    Constitutive_Matrix(:,:,i)=Constitutive_Matrix_1(:,:,i)^(-1);
end
%Voigt bound%
Voigt_C_C=zeros(3,3,n);

%Voigt_Constitutive Matrix
Voigt_C=zeros(3,3,1);


Young_Voigt(g,1)=g;
Poisson_Voigt(g,1)=g;
Shear_Voigt(g,1)=g;
```

```
for i=1:n
%Multiplying Each Phase Area Fraction By Its Constitutive Matrix
    Voigt_C_C(:,:,i)= Phase_Property(i,4,g)* Constitutive_Matrix(:,:,i);
%Adding up Phases Fractional Constitutive Matrices
    Voigt_C = Voigt_C+Voigt_C_C(:,:,i);

end


Voigt_C_1=Voigt_C^(-1);
Young_Voigt(g,2)=1/Voigt_C_1(1,1);
Poisson_Voigt(g,2)=(-1)*Young_Voigt(g,2)*Voigt_C_1(1,2);
Shear_Voigt(g,2)=Young_Voigt(g,2)/(2*(1+Poisson_Voigt(g,2)));


 %Reuss Bound
 Reuss_C_C=zeros(3,3,n);

 %Inverse of Voigt_Constitutive Matrix%
 Reuss_C_1=zeros(3,3,1);
 %Voigt_Constitutive Matrix%
 Reuss_C=zeros(3,3,1);


Young_Reuss(g,1)=g;
Poisson_Reuss(g,1)=g;
Shear_Reuss(g,1)=g;

for i=1:n

    Reuss_C_C(:,:,i)= Phase_Property(i,4,g)* Constitutive_Matrix(:,:,i)^(-1);
    Reuss_C_1 = Reuss_C_1+Reuss_C_C(:,:,i);

end
Reuss_C= Reuss_C_1^(-1);


Young_Reuss(g,2)=1/Reuss_C_1(1,1);
Poisson_Reuss(g,2)=(-1)*Young_Reuss(g,2)*Reuss_C_1(1,2);
Shear_Reuss(g,2)=Young_Reuss(g,2)/(2*(1+Poisson_Reuss(g,2)));


end


disp('Young Modulus from Voigt Bound')
disp(Young_Voigt)
disp('Poissons ratio from Voigt Bound')
disp(Poisson_Voigt)
disp('Shear Modulus from Voigt Bound')
disp(Shear_Voigt)

disp('Young Modulus from Reuss Bound')
```

```
disp(Young_Reuss)
disp('Poissons ratio from Reuss Bound')
disp(Poisson_Reuss)
disp('Shear Modulus from Reuss Bound')
disp(Shear_Reuss)




%Introducing the referrance RVE parameter
disp('RVE Size/Volume Fraction Referrence Parameter')
if RVE_size_parameter ==1
    disp('Inclusion Area Fraction')
elseif RVE_size_parameter ==2
    disp('Inclusion Volume Fraction')
elseif RVE_size_parameter ==3
    disp('RVE size ratio')
end
disp('     ')

disp('press enter rigorously to proceed with the next step')



%Voigt Bound Plots
input('Voigt Young Modulus for RVE sizes')
plot(RVE_Index(:,2),Young_Voigt(:,2));

input('Voigt Poisson Ratio for RVE sizes')
plot(RVE_Index(:,2),Poisson_Voigt(:,2));

%Reuss Bound Plots
input('Reuss Young Modulus for RVE sizes')
plot(RVE_Index(:,2),Young_Reuss(:,2));

input('Reuss Poisson Ratio for RVE sizes')
plot(RVE_Index(:,2),Poisson_Reuss(:,2));

%Young Modulus plots
input('Young Modulus Bounds for RVE index number')
plot(Young_Voigt(:,1),Young_Voigt(:,2),Young_Reuss(:,1),Young_Reuss(:,2));
input('Young Modulus Bounds for RVE index parameter')
plot(RVE_Index(:,2),Young_Voigt(:,2),RVE_Index(:,2),Young_Reuss(:,2));
%Poisson's Ration Plots
input('Poisson Ratio Bounds for RVE index number')
plot(Poisson_Voigt(:,1),Poisson_Voigt(:,2),Poisson_Reuss(:,1),Poisson_Reuss(:
,2));
input('Poisson Ratio Bounds for RVE index parameter')
plot(RVE_Index(:,2),Poisson_Voigt(:,2),RVE_Index(:,2),Poisson_Reuss(:,2));
end
```

Bibliography

[1] Mills N. Polymer foams handbook: engineering and biomechanics applications and design guide. Burlington, MA: Butterworth-Heinemann; 2007.

[2] Sauvant-Moynot V, Gimenez N, Sautereau H. Hydrolytic ageing of syntactic foams for thermal insulation in deep water: degradation mechanisms and water uptake model. J Mater Sci 2006;41(13):4047–54.

[3] Gupta N, Woldesenbet E. Hydrothermal studies on syntactic foams and compressive strength determination. Composite Struct 2003;61(4):311–20.

[4] Gupta N, Priya S, Islam R, Ricci W. Characterization of mechanical and electrical properties of epoxy–glass microballoon syntactic composites 2006;345:1–12.

[5] Woldesenbet E, Peter S. Volume fraction effect on high strain rate properties of syntactic foam composites 2009.

[6] OVERALL ELASTIC PROPERTIES OF POLYSILICON FILMS: A STATISTICAL INVESTIGATION OF THE EFFECTS OF POLYCRYSTAL MORPHOLOGY. Stefano Mariani, Roberto Martini, Aldo Ghisi, Alberto Corigliano And Marco Beghi, Journal for Multiscale Computational Engineering, 9 (3): 327–346 (2011)

[7] Effect of volume fraction and wall thickness on the elastic properties of hollow particle filled composites. Maurizio Porfiri And Nikhil Gupta. Composites: Part B 40 (2009) 166–173

[8] Effect of polydispersivity and porosity on the elastic properties of hollow particle filled composites. M. Aureli, M. Porfiri And N. Gupta. Mechanics of Materials 42 (2010) 726–739

[9] Comparison of tensile and compressive characteristics of vinyl ester/glass microballoon syntactic foams. Nikhil Gupta , Raymond Ye And Maurizio Porfiri. Composites: Part B 41 (2010) 236–245

[10] Analysis of flexural properties of hollow-particle filled composites. G. Tagliavia, M. Porfiri And N. Gupta: Composites: Part B 41 (2010) 86–93

[11] Pal R. New models for effective young's modulus of particulate composites.

Compos B: Eng 2005;36(6-7):513–23.

[12] Torquato S. Random heterogeneous materials: microstructure and macroscopic properties. New York: Springer; 2001.

[13] Lee KJ, Westmann RA. Elastic properties of hollow-sphere-reinforced composites. J Compos Mater 1970;4:242–52.

[14] Huang JS, Gibson LJ. Elastic moduli of a composite of hollow spheres in a matrix. J Mech Phys Solids 1993;41(1):55–75.

[15] Homogenization methods for multi-phase elastic composites: Comparisons and benchmarks. B. Klusemann And B. Svendsen. TECHNISCHE MECHANIK, 30, 4, (2010), 374 – 386

[16] B. Harris, Engineering Composite Materials, The institute of Materials, London, Maney Materials Science; 2nd edition, 1999

[17] www.Composite.about.com

[18] www.Boeing.com

[19] W. Watt, B. V. Perov, Handbook of Composites, Strong Fibers. Amsterdam: North-Holland, 1985

[20] S. W. Tsai, Composites Design, Dayton, Think Composites, 1986

[21] G. Tagliavia, M. Porfiri , N. Gupta, Analysis of hollow inclusion–matrix debonding in particulate composites, International Journal of Solids and Structures 47 (2010) 2164–2177

[22] Sia Nemat-Nasser, Muneo Hori. Micromechanics: overall properties of heterogeneous materials

[23] Lorenzo Bardella. Mechanical behavior of glass-filled epoxy resins: experiments, homogenization methods for syntactic foams, and applications. Tesi presentata per il conseguimento del titolo di Dottore di Ricerca, Universita degli Studi di Brescia.

[24] Eshelby J. D. (1957) The determination of the elastic field of an ellipsoidal inclusion, and related problems Proceedings of the Royal Society, London A241, 376–396.

[25] Voigt W. (1889) Ueber die Beziehung zwischen den beiden Elasticit¨ats-constanten isotroper K¨orper Annalen der Physik (Leipzig) 38 (3), 573–587.

[26] Hashin Z. and Shtrikman S. (1962) On some variational principles in anisotropic and nonhomogeneous elasticity Journal of the Mechanics and Physics of Solids 10, 335–342.

[27]Hashin Z. and Shtrikman S. (1963) A variational approach to the theory of the elastic behaviour of multiphase materials Journal of the Mechanics and Physics of Solids 11, 127–140.

[28] Bardella L. and Genna F. On the Elastic Behavior of Syntactic Foams. International Journal of Solids and Structures. 38(2001) 7235-7260

[29] Colombo M. and Martinelli P. Pressure-Impulse diagrams for RC and FRC circular plates under blast loads. European Journal of Environmental and Civil Engineering DOI:10.1080/19648189.2012.675149

[30] Abaqus User's Manual – Property Module – Materials – Drucker Pruger

[31] Abaqus User's Manual – Property Module – Materials – Concrete Damaged Plasticity

[32] Krauthammer T. Modern Protective Structures. 2008 Taylor & Francis

[33] Shock tube

[34] Abaqus User's Manual – General

[35] EuroCode -8

[36] Abaqus User's Manual – Step Module – Dynamic Explicit

[37] Abaqus User's Manual – Load Module – Pressure

[38] Abaqus User's Manual – Mesh Module